

Combining Human Expertise with Artificial Intelligence: Experimental Evidence from Radiology*

Nikhil Agarwal, Alex Moehring, Pranav Rajpurkar, Tobias Salz[†]

June 26, 2023

Abstract

While Artificial Intelligence (AI) algorithms have achieved performance levels comparable to human experts on various predictive tasks, human experts can still access valuable contextual information not yet incorporated into AI predictions. Humans assisted by AI predictions could outperform both human-alone or AI-alone. We conduct an experiment with professional radiologists that varies the availability of AI assistance and contextual information to study the effectiveness of human-AI collaboration and to investigate how to optimize it. Our findings reveal that (i) providing AI predictions does not uniformly increase diagnostic quality, and (ii) providing contextual information does increase quality. Radiologists do not fully capitalize on the potential gains from AI assistance because of large deviations from the benchmark Bayesian model with correct belief updating. The observed errors in belief updating can be explained by radiologists' partially underweighting the AI's information relative to their own and not accounting for the correlation between their own information and AI predictions. In light of these biases, we design a collaborative system between radiologists and AI. Our results demonstrate that, unless the documented mistakes can be corrected, the optimal solution involves assigning cases either to humans or to AI, but rarely to a human assisted by AI.

JEL: C50, C90, D83, D47

Keywords: Artificial Intelligence, Belief Updating, Radiology

*We are grateful to Stanford University Hospital for facilitating data access. The authors acknowledge support from the Alfred P. Sloan Foundation (2022-17182), JPAL Healthcare Delivery Initiative, and MIT SHASS. The experiment was pre-registered on the AEA registry, number AEARCTR-0009620. The preanalysis plans are available at [SSR Registration 9620](#) and [SSR registration 8799](#).

[†]Agarwal: Department of Economics, MIT and NBER, email: agarwaln@mit.edu. Moehring: MIT Sloan School of Management, email: moehring@mit.edu. Rajpurkar: Department of Biomedical Informatics, Harvard Medical School, email: pranav_rajpurkar@hms.harvard.edu. Salz: Department of Economics, MIT and NBER, email: tsalz@mit.edu. The project benefitted from collaboration with several radiologists, including Drs. Matthew Lungren, Curtis Langlotz, and Anuj Pareek of Stanford, Drs. Etan Dayan and Adam Jacobi of Mt. Sinai Hospital, Steven Truong of VinBrain and several radiologists at VINMEC, and teleradiologists at USARAD, Vesta Teleradiology, and Advanced Teleded. We thank Daron Acemoglu, David Autor, David Chan, Glenn Ellison, Amy Finkelstein, Drew Fudenberg, Paul Joskow, Whitney Newey, Pietro Ortoleva, Paul Oyer, Ariel Pakes, Alex Rees-Jones, Frank Schilbach, Chad Syverson, and Alex Wolitzky for helpful conversations, comments and suggestions. Oishi Banerjee, Andrew Komo, Manasi Kutwal, Angelo Marino and Jett Pettus provided invaluable research assistance.

“We should stop training radiologists now. Its just completely obvious that within five years, deep learning is going to do better than radiologists.”

– Geoffrey Hinton (in 2016)

1 Introduction

Artificial intelligence (AI) is a general-purpose technology with transformative potential similar to that of the steam engine and electricity (Brynjolfsson and Mitchell, 2017; Brynjolfsson et al., 2017; Agrawal et al., 2018; Acemoglu and Johnson, 2023; Goldfarb et al., 2023; Frank et al., 2019). But, in contrast to the transformation during the industrial revolutions, AI can potentially displace humans from tasks that require complex reasoning (Webb, 2019; Felten et al., 2019; Brynjolfsson and Mitchell, 2017). Advances in AI have therefore caused concern about the role of human work, even in highly skilled occupations (Ford, 2015). Indeed, a growing literature shows that AI tools based on machine learning can outperform humans on a host of predictive tasks, including those typically performed by experts (Liu et al. 2019; Lai et al. 2021; Mullainathan and Obermeyer 2019; Kleinberg et al. 2017).

However, Hinton’s prediction about radiology — an iconic example in machine learning — may have been premature.¹ Many argue that instead of being replaced by AI, it is optimal to have human radiologists use AI assistance, at least for the foreseeable future (Langlotz, 2019; Agrawal et al., 2019). In addition to considerable legal and regulatory challenges that stand in the way of full automation, there may be potential gains from combining human expertise with AI input that cannot be realized by exclusively relying on one or the other. For example, radiologists may correct mistaken AI predictions or may have access to information about the clinical context that has not yet been systematized and built into AI tools. Current regulatory practice is consistent with these arguments – approved AI tools for clinical decision-making typically play a supporting role rather than operating autonomously (see Norden and Shah, 2022; Harvey and Gowda, 2020, for example). Similar reasons are likely to result in partial task automation or collaboration between human experts and AI being optimal in other contexts.

We run an experiment to examine how radiologists use AI predictions, whether AI assistance improves their performance, estimate a model of (potentially biased) belief updating, and analyze what this model implies about the optimal form of collaboration between AI and humans.² If humans correctly combine AI predictions with their own information, then AI

¹A more nuanced but qualitatively similar prediction that machine learning tools will displace radiologists is conveyed in Obermeyer and Emanuel (2016).

²We will use the terms ‘humans,’ ‘radiologists,’ and ‘participants’ interchangeably.

assistance unambiguously improves prediction and decision quality. Unless the costs in terms of human effort outweigh these benefits, it is optimal to provide AI assistance to humans. However, substantial literature in economics suggests that humans may err when making probabilistic judgments by deviating from the benchmark model of Bayesian updating with correct beliefs (see [Benjamin et al., 2019](#), for a review). The optimal approach for combining human and AI information in the presence of these mistakes is non-trivial.

The experiment employs professional radiologists whom we recruit through teleradiology companies to diagnose retrospective patient cases. We experimentally manipulate the information set radiologists have access to when making decisions in a two-by-two factorial design. In the minimal information environment, we provide only the chest X-ray image to which we add either AI predictions or contextual information, or both. The AI information treatment provides probabilities that a patient case is positive for a potential chest pathology generated using an algorithm trained on over 250,000 X-rays with corresponding disease labels ([Irvin et al., 2019](#)). This algorithm was shown to perform comparably to board-certified radiologists. The contextual information treatment provides clinical history information that radiologists typically have available but, for privacy reasons, was not available to train the AI. This information includes the treating doctors' indications, the patient's vitals, and the patient's labs.

We first estimate the treatment effects of those informational interventions on radiologists' prediction accuracy and the probability of making a correct decision. We then test alternative models of biased belief updating to investigate whether radiologists exhibit systematic deviations from a Bayesian benchmark when incorporating AI predictions. For example, humans may suffer from automation bias, a tendency to place more weight on machine-provided predictions than on one's own information.³ Additionally, humans may treat AI predictions as independent of their own information ([Enke and Zimmermann, 2019](#)). Finally, we evaluate various forms of human-AI collaboration – in terms of diagnostic performance and costs of expert time – that decide, as a function of the AI prediction, to use only the AI input, only the human input, or the human input with access to AI.

Diagnostic radiology is an ideal laboratory for investigating human-AI interaction for various reasons. Deep learning has made significant advances in radiology, surpassing human decision-making in many cases, and such algorithms are already clinically deployed [Rajpurkar and Lungren \(2023\)](#). It, therefore, serves as a useful leading indicator for other professions

³This terminology is borrowed from the literature that dates to the proliferation of computerized automated support systems in aviation, which raised concerns about human complacency or automation bias (see [Alberdi et al., 2009](#), for an overview).

where similar developments will follow. Moreover, radiology is a highly-paid medical specialty, which means that the potential benefits from productivity enhancements through AI are large. Radiology is also ideal from a research perspective. Unlike other physicians, radiologists do not have direct contact with patients, allowing us to run a decision experiment that resembles their normal workflow through a remote interface that we developed. To aid quantitative analysis, instead of obtaining a free-text report, we collect radiologist’s assessed probability that a given chest pathology is present and a binary clinical recommendation of whether to treat or follow up for that pathology. For our experiment, we hired 180 radiologists through teleradiology companies that serve US hospitals and offer the services of both US-based and non-US-based radiologists.

Analyzing the quality of our participants’ assessments requires establishing, for each patient case, a standard or ground truth. An important challenge in our setting is that definitive diagnostic tests do not exist for most thoracic pathologies and, even when they do exist, are selectively performed depending on a radiologist’s recommendation. We therefore follow the machine learning literature (Sheng et al., 2008) and construct a diagnostic standard by aggregating the assessments of five board-certified radiologists at Mt. Sinai Hospital with at least ten years of experience and chest radiology as a sub-specialty. We assess the robustness of all our results by constructing a (leave-one-out) ground truth using the assessments of our experimental participants and by varying the aggregation method.

There are two important challenges in designing the experiment, which we address using a combination of experimental designs. First, while teleradiology firms allow us to recruit radiologists for our experiment we need to compensate them at the market rate, making data collection expensive. An across-participant design would therefore be cost-prohibitive except for extremely large effect sizes. In the first design, we, therefore, randomize each participant into an order in which they are exposed to the four informational environments but do not encounter cases repeatedly. Thus, this design allows for within-participant comparisons in addition to an initial pure across-participant comparison. The second challenge is that, to estimate a model of belief updating, we need to observe radiologists’ assessments of a given case both with and without AI assistance. Moreover, the assessment without AI assistance is required to estimate the Bayesian benchmark, which we can compare to the assessment that incorporates AI assistance. Our second design addresses this issue by asking each participant to diagnose each patient case once in each of the four information environments in random order while ensuring at least a two-week wash-out period between two encounters of a given case. This wash-out period is intended to eliminate the memory of prior information and

anchoring effects.⁴ Most of our treatment effect analysis pools data from the different designs whereas our model estimates of belief updating only uses data where a radiologist reads the same case both with and without AI assistance.

We find that AI assistance does not improve humans’ diagnostic quality on average even though the AI predictions are more accurate than almost two-thirds of the participants in our experiment. Moreover, the zero average effect cannot be explained by the participants ignoring these predictions – we observe that radiologists’ reported probabilities move significantly towards the AI’s predictions with AI assistance. Instead, the zero effect of AI assistance is driven by heterogeneous treatment effects – diagnostic quality increases when the AI is confident (e.g. the predicted probability is close to zero or one) but decreases when the AI is uncertain. In parallel, AI assistance improves diagnostic quality for patient cases in which our participants are uncertain, but decreases quality for patient cases in which our participants are certain. In contrast, providing clinical history does improve diagnostic quality suggesting that humans have additional valuable information that has not yet been incorporated into AI predictions.

An upshot of the results is that information available only to radiologists is useful, but human experts do not correctly combine their information with AI predictions. Specifically, the result that AI assistance can reduce predictive performance cannot be rationalized if our participants are Bayesians with correct beliefs because the AI assistance provides weakly more information to the decision-maker.

Motivated by these results, we analyze two types of deviations from the benchmark model with correct updating to link errors in probabilistic judgement and optimal deployment of AI assistance.⁵ The first type of deviation occurs when agents do not put correct weights on their own information and AI information. We describe this deviation using the approach introduced in Grether (1980; 1992) (see Benjamin, 2019, for a review) to define biases in belief updating. We say that an agent exhibits own-information bias if they over-weights their baseline information when provided with AI assistance and own-information neglect if they under-weights it. Analogously, an agent exhibits automation bias if they over-weights the AI information relative to their own and automation neglect if they under-weights it. The second type of deviation occurs if agents utilize an incorrect joint distribution of their

⁴To ensure that our results do not rely on the wash-out being successful, a third design obtains an assessment with AI assistance only after assessments without AI assistance have been obtained. However, this third treatment is subject to order effects. We find no evidence of order effects on diagnostic quality although there is evidence that familiarity with the interface increases the speed with which participants go through patient cases.

⁵We will remain agnostic about whether the deviations we consider are due to non-Bayesian updating or can be explained by Bayesian updating with incorrect prior beliefs.

own information and AI information – an example of such a deviation is correlation neglect (Enke and Zimmermann, 2019). Our theoretical analysis shows that if agents exhibit only automation neglect, then AI assistance unambiguously increases diagnostic quality. All other forms of biases we consider result in AI assistance reducing diagnostic quality for certain realizations of AI and own information.

We then use the data from our experiment to estimate empirical analogs of the deviations described above and select the model that best describes the treatment effects we document. This exercise requires us to solve several challenges unique to a naturalistic setting where the experimenter does not control the information structure. We find that in the model that best describes our data, agents exhibit automation neglect and act as if their own information and AI predictions are independent (conditional on the truth), even though this is not the case. Interestingly, we do not find evidence of substantial own-information bias or neglect.

Finally, we take our data to estimate the trade-off between diagnostic quality and radiologist time when AI predictions can be selectively utilized, and design an optimal human-AI collaborative system. For each pathology and conditional on the AI prediction for that pathology, our experiment allows us to compute both the diagnostic quality and time taken if a patient case is diagnosed by the AI, a randomly chosen radiologist without AI assistance, and a radiologist assisted with the AI prediction. We use these data to train a classification algorithm that yields the frontier of diagnostic quality and total radiologist time. The results from this exercise mirror our treatment effect analysis – because radiologists take more time with AI and do not correctly incorporate the AI’s information, the majority of cases are optimally decided either by the radiologist or the AI alone but not by the radiologist with access to AI.

Related Literature

A growing body of literature in computer science has explored the predictive performance of humans versus machine learning algorithms, with radiology often serving as a key area of application (Rajpurkar et al., 2018, 2017). Additionally, the study of human-AI collaboration has become an increasingly important facet of medical AI research (Tschandl et al., 2020; Reverberi et al., 2022). For comprehensive overviews of these areas, see Rajpurkar et al. (2022); Hosny et al. (2018); Zhou et al. (2021); Lai et al. (2021). Research on the effectiveness of human-AI collaboration is evolving, with notable studies in radiology including Rajpurkar et al. (2020); Kim et al. (2020); Park et al. (2019); Seah et al. (2021); Fogliato et al. (2022). An active literature studies whether AI assistance benefits radiologists, and which radiologists benefit the most (Rajpurkar et al., 2020; Seah et al., 2021; Ahn et al., 2022; Sim et al., 2020; Gaube et al., 2023). In contrast to prior studies, we recruit a large group of high-

skilled experts from teleradiology companies under contracts that allow us to incentivize our participants. A key differentiating factor of our research is that, unlike previous studies which mainly concentrated on performance, our work emphasizes behavioral biases and their impact on human-AI interaction.

An emerging literature in economics also compares human and AI performance. Within economics, these studies tend to rely on observational approaches, with examples addressing issues in medicine (Ribers and Ullrich, 2022; Mullainathan and Obermeyer, 2019) and bail decisions (Kleinberg et al., 2015; Angelova et al., 2022). However, analyses based on observational data face critical identification challenges, such as the selective labels problem (see Kleinberg et al., 2017; Mullainathan and Obermeyer, 2019; Rambachan, 2021)). A limited set of studies use quasi-experimental approaches (e.g., Stevenson and Doleac, 2019; Angelova et al., 2022) or randomized controlled trials (e.g., Imai et al. (2020); Noy and Zhang (2023); Grimon et al. (2022)) to investigate human use of AI tools, typically focusing on overall performance or variability in participant response. We add to this literature by developing an experimental approach that manipulates the information environment that calculates and compares behavior with a Bayesian benchmark to document systematic biases and demonstrate that these biases lead to a non-trivial delegation problem.⁶

While several studies in behavioral economics have documented errors in probabilistic judgment and belief formation, they do not focus on the issues surrounding human-AI interaction (c.f. Tversky and Kahneman, 1974; Benjamin et al., 2019; Enke and Zimmermann, 2019; Conlon et al., 2022, for example). Our definitions of own-information and automation bias build on the framework in Grether (1980). We contribute to this literature in two ways. First, we develop an approach to estimate the parameters of the model in Grether (1992) in an environment where the joint distribution of the signals cannot be controlled (or partialled out) by the researcher.⁷ This approach is necessary because we cannot modify the signal within medical images. Second, we link the design of AI information provision to the (biased) updating rule that humans use. This link shows that the use of AI information by humans is an important and practical application of the ideas in this literature.

⁶Our finding that radiologists exhibit automation neglect is related to those in Dietvorst et al. (2015), which shows that humans are averse to following algorithmic recommendations as compared to human recommendations. This aversion can be reduced if humans are allowed to modify the algorithm’s recommendation (Dietvorst et al., 2018).

⁷Most applications that we are aware of rely on one of two experimental approaches. In the first approach, the researcher can partial out either the prior information or the likelihood ratio of the signal provided, for example in the classic bookbag-and-poker-chip experiments (see Benjamin et al. 2019; Benjamin 2019, for reviews). In the second approach, the researcher directly provides signals from a known joint distribution (e.g. Conlon et al., 2022).

Our analysis of optimal human-AI collaboration is related to papers that build delegation algorithms to predict the types of cases for which human performance exceeds machine performance (e.g. [Mozannar and Sontag, 2020](#); [Raghu et al., 2019](#); [Bansal et al., 2021](#)). Relative to this work, our analysis uses a decision-theoretic model and specific human biases to trace their consequences for optimal AI deployment.

Finally, our work also adds to the literature on decision-making in the health care context (e.g. [Abaluck et al., 2016](#); [Currie and MacLeod, 2017](#); [Gruber et al., 2021](#); [Chan et al., 2022](#); [Chandra and Staiger, 2020](#)). This work aims to understand predictions and payoffs from observational data on medical decisions, objectives that are achievable under less stringent functional form restrictions in our experimental approach. An important distinguishing feature is that none of these papers consider the effects of AI predictions on medical decision-making.

Overview

The rest of the paper is organized in the following way. Section 2 introduces our model of a decision-maker in a diagnostic setting. Section 3 describes the necessary details of the setting and our experimental design. Section 4 discusses the treatment effects. Section 5 estimates a descriptive model of deviations from Bayesian updating. Section 6 shows the gains achievable under the optimal collaboration between radiologists and AI.

2 Conceptual Model

Our study focuses on classification problems and, specifically machine learning algorithms within the domain of AI tools. These algorithms are designed to predict the appropriate classification for a given case and may assist a human decision-maker. This decision-maker, indexed by r , must take a binary action $a_{ir} \in \{0, 1\}$ on case i based on a prediction of a binary state $\omega_i \in \{0, 1\}$. The realized payoff $u_r(a_{ir}, \omega_i)$ from an action depends both on the state and the action. The expert does not know ω_i but observes, depending on the information environment, a subset of two signals that are potentially informative about the state. The first signal is generated by a prediction algorithm (AI), with realizations $s_i^A \in S^A$. The second signal is directly obtained by the expert, with a realization $s_{ir}^E \in S^E$. These signals are of arbitrary dimension. The joint distributions of the signals conditional on the state is given by $\pi_r(\cdot|\omega) \in \Delta(S^A, S^E)$, with prior probabilities over the state $\pi(\omega)$. We do not place any restrictions on $\pi_r(\cdot|\omega)$. The signals need not be independent conditional on the state of the world, and the signal distribution may depend on the expert, capturing skill ([Chan et al., 2022](#)). We also allow for cases when one of the signals is more informative than

the other (Blackwell, 1953).

Assume that the human's objective is to match the action to the state. Thus, the human faces a classification problem. It is without loss of generality to normalize the payoff from taking the action that matches the state to zero. Let $c_{FP,r}$ be the disutility of human r if she takes the action $a = 1$ when the state is $\omega = 0$ (false positive) and $c_{FN,r}$ be the disutility if she takes the action $a = 0$ when the state is $\omega = 1$ (false negative). The payoff of the human is therefore

$$u_r(a, \omega) = -1 \cdot \{a = 1, \omega = 0\} \cdot c_{FP,r} - 1 \cdot \{a = 0, \omega = 1\} \cdot c_{FN,r}. \quad (1)$$

We allow the human's posterior belief given the observed signals to deviate from those implied by the true probability law $\pi_r(\cdot|\omega)$. Specifically, let $s_{ir} \subset \{s_r^A, s_{ir}^E\}$ be the subset of signal realizations observed by the human r and $p_r(\omega | s_{ir}) \in [0, 1]$ be the human's posterior belief that the state is $\omega \in \{0, 1\}$ when she observes s_{ir} . Suppressing the dependence of signals on the pair (i, r) , the human's action given the signal s is

$$a_r^*(s; p_r) = 1 \cdot \left\{ \frac{p_r(\omega = 1 | s)}{p_r(\omega = 0 | s)} > c_{rel,r} \equiv \frac{c_{FP,r}}{c_{FN,r}} \right\}. \quad (2)$$

The expected payoff from following $a^*(s)$ is

$$V_r(s; p_r) = E[u_r(a_r^*(s; p_r), \omega) | s] = \sum_{\omega} u(a_r^*(s; p_r), \omega) \pi_r(\omega | s),$$

where decisions are based on the human's belief p_r , but are evaluated according to the true law π_r . Because we allow for p_r to differ from π_r , the odds ratio $\frac{p_r(\omega=1|s)}{p_r(\omega=0|s)}$ may differ from the analogous quantity constructed using π_r . Thus, the action $a_r^*(s; p_r)$ can deviate from the optimal action $a_r^*(s; \pi_r)$ given the signal $s = (s^A, s^E)$. Except in knife-edge cases, $V_r(s; p_r)$ is lower than $V(s; \pi_r)$ whenever $a^*(s; p_r) \neq a^*(s; \pi_r)$.

A key objective is to analyze deviations in humans' use of AI signals from the benchmark model of Bayesian updating with correct beliefs (about the joint distribution of the signals and the state). Bayes' rule implies that, given the signals (s_i^A, s_{ir}^E) , the log-odds of $\omega = 1$ to $\omega = 0$ —the key decision-relevant quantity—is given by

$$\log \frac{\pi_r(\omega_i = 1 | s_i^A, s_{ir}^E)}{\pi_r(\omega_i = 0 | s_i^A, s_{ir}^E)} = \log \frac{\pi_r(s_i^A | \omega_i = 1, s_{ir}^E)}{\pi_r(s_i^A | \omega_i = 0, s_{ir}^E)} + \log \frac{\pi_r(\omega_i = 1 | s_{ir}^E)}{\pi_r(\omega_i = 0 | s_{ir}^E)}. \quad (3)$$

The second term on the right-hand side is the posterior log-odds ratio for the two states

$\omega_i = 1$ to $\omega_i = 0$ given that the human’s signal is s_{ir}^E . The first term is positive if, given the realization s_{ir}^E , the signal s_i^A is more likely if $\omega_i = 1$ as compared to $\omega_i = 0$. In this case, the posterior odds shift in favor of the state $\omega_i = 1$. Analogously, the odds shift away from $\omega_i = 1$ if, given s_{ir}^E , the signal s_i^A is more likely if the state were $\omega_i = 0$.

The task of empirically analyzing deviations in participants’ beliefs from the benchmark in equation (3) is challenging because the signals differ across cases i and humans may, due to differences in skill, have heterogeneous signal distributions $\pi_r(\cdot)$. The ideal dataset would elicit $p_r(\omega_i = 1 | s_i^A, s_{ir}^E)$ and $\pi_r(\omega_i = 1 | s_{ir}^E)$ for the same case and the same human to keep the signals (s_i^A, s_{ir}^E) , and human-specific parameters fixed, and use the latter to estimate $\pi_r(\omega_i = 1 | s_i^A, s_{ir}^E)$ using equation (3).

However, empirically implementing this strategy requires us to confront several experimental and methodological challenges. First, the experiment needs to be sensitive to anchoring and order effects when eliciting $p_r(\omega_i = 1 | s_i^A, s_{ir}^E)$ and $\pi_r(\omega_i = 1 | s_{ir}^E)$ from participants. Second, the potential for measurement error and the dependence of the first term in equation (3) on a latent signal s_{ir}^E complicates the exercise. We defer our approach to this second challenge to section 5, and turn our attention to the experimental design.

3 Setting and Experiment

Our experiment elicits the probability of a pathology’s presence $p_r(\omega = 1 | s)$ and a recommended treatment/follow-up decision a under varying information treatments. There are four information treatments in the experiment, with only the chest X-ray in the minimal information case, to which we add AI assistance, contextual information, or both. Next, we describe the experimental context and interface before presenting the design of our experiments.

3.1 Experimental Context

3.1.1 Radiology

Radiologists diagnose the presence of a given pathology at the request of a treating physician. The information available to a radiologist consists of diagnostic images (e.g. chest X-rays), any relevant medical history (e.g. laboratory results), and clinical indication notes of the treating physician.⁸ The treating physician’s notes are of varying detail levels – they may provide no clinical information or guidance, request the analysis of a specific pathology, or

⁸Radiologists are rarely in direct contact with the patient or the treating physician, except via the formal information exchange outlined here.

only list the patient’s primary symptom (see appendix B.2 for examples). Irrespective of the pathology suspected by the treating physicians, radiologists are expected to report all pathological findings.

Because image-based classification is a core task performed by radiologists, a high-paying profession, it is not surprising that AI tools have made significant inroads in the field in the last decade. Recent advances in deep learning methods for image recognition have yielded algorithms that can match or surpass the performance of human radiologists (Obermeyer and Emanuel, 2016; Langlotz, 2019). As of 2020, 55 companies offered a total of 119 algorithmic products of which 46 have FDA approval (Tadavarthi et al., 2020). Most products related to clinical decision-making are marketed as support tools as opposed to autonomous tools, partly due to regulatory and liability issues (Harvey and Gowda, 2020).

3.1.2 *CheXpert*

We provide AI assistance using the CheXpert model, which is a deep learning prediction algorithm for chest X-ray interpretation (Irvin et al., 2019). This model is trained on a dataset of 224,316 chest radiographs of 65,240 patients labeled for the presence of fourteen common chest radiographic pathologies.⁹ The algorithm does not use any other patient information, such as the clinical history or vitals.¹⁰ Nonetheless, a prior version of this algorithm was shown to match or surpass the performance of board-certified radiologists from Stanford Hospital on five pathologies (Patel et al., 2019). These study results are also presented to our participants when introducing the AI tool. Section 4 confirms that the algorithm outperforms a majority of radiologists in our experiment. We relegate additional details about the algorithm to appendix B.3. The algorithm assistance to our participants will be in the form of a vector of probabilities for the presence of every pathology.¹¹

⁹The term artificial intelligence is typically reserved for a system of different prediction tasks to mimic a more complex set of behaviors, whereas machine learning is concerned with one specific prediction task. For a detailed discussion of this distinction see, for instance, (Taddy, 2018).

¹⁰While large datasets of images are increasingly available (e.g. Kramer et al. 2011, Johnson et al. 2016, Irvin et al. 2019) it is significantly more difficult to construct such datasets for other patient information due to the compulsory manual review of textual data for HIPPA compliance.

¹¹Some algorithms attempt to make their predictions explainable to a human by highlighting the parts of the image that drive a specific prediction. However, prior studies show that providing such localization in addition to the numeric output does not improve the accuracy of radiologists (Gaube et al., 2022). A quantitative output allows us to compute a Bayesian benchmark to the radiologist’s prediction, which is otherwise difficult.

3.2 Experimental Designs

Our experiment varies the information available to diagnose patient cases—participants may or may not receive AI assistance and access to the clinical history. The X-ray is shown under all information conditions. We expose our participants to all four possible information conditions: X-ray only, henceforth XO ; clinical history without AI, henceforth CH ; AI without clinical history, henceforth AI ; and both clinical history and AI, henceforth $AI+CH$.

There are two objectives of our experiment. The first is to compute the treatment effects of AI and CH on diagnostic quality and radiologist time. The second is to analyze systematic deviations from the Bayesian benchmark.

Both these objectives are complicated by the likely heterogeneity in radiologist skills. For estimating treatment effects, radiologist heterogeneity implies that a design that randomizes treatments only across radiologists will require a large participant pool except for extremely large effect sizes. Our participants are highly paid experts, making this approach expensive. And, as explained in section 2, across-radiologist variation in information treatments is not tailored for the second objective. We would ideally know how a given radiologist changes her assessment for the same case under a different information condition.

Our approach to address these challenges is to use a combination of three different experimental designs, each with certain advantages and disadvantages. Appendix B.1 illustrates the three design variations.

3.2.1 Design 1 (Figure B.1)

In the first design, participants are assigned to a random sequence of the four information treatments. Each information condition is assigned fifteen cases at random without repetition. Participants read all 15 cases in one information environment before moving to the next one.

This design builds in both across- and within-participant variation in information treatments. The within-participant variation has greater power because it controls for participant heterogeneity at the potential cost of order effects. The concern of order effects is both testable and mitigated by the randomization of treatment sequence across subjects.

This first design is well-suited to estimate treatment effects of our information environments. However, as mentioned earlier, it is not ideal for estimating an empirical analog to equation (5) because no case is encountered twice.

3.2.2 Design 2 (Figure B.2)

Radiologists diagnose each patient case in each of the four information environments in the second design. For the moment, set aside concerns arising from the feature that the same radiologist encounters the same case multiple times. This design will allow us to estimate an empirical analog to equation (5). It also has the added benefit of controlling for both case-radiologist heterogeneity because, unlike in the previous design, we can conduct within-case-radiologist comparisons across treatments.

Because radiologists repeatedly encounter cases, we need to address the potential for order effects due to memory. For example, radiologists might anchor on their previous assessment using AI predictions or contextual information and might remember this information the next time the same case is encountered. We, therefore, limit radiologists’ ability to remember either their diagnosis or previously provided information by using a “washout” interval between two encounters of the same case.¹² Specifically, radiologists complete the experiment in four sessions that are separated by at least two weeks. Each session is similar to the first design: radiologists diagnose fifteen cases in each of the four information environments with no case repeated within a session. Across sessions, the information environment under which a given case is diagnosed is permuted. Thus, by the end of the fourth session, each of the sixty cases is diagnosed exactly once in each information environment. Our results are consistent with the washout being effective – radiologists’ predictions do not move towards the AI prediction if it was provided in a prior session but do if it is provided in the current session (see figure C.28).

3.2.3 Design 3 (Figure B.3)

In the third design, we address residual concerns about the order effects of radiologists diagnosing cases with AI before those without AI—whether due to anchoring, memory, or experimenter demand—by having participants diagnose fifty cases, first without and then with AI assistance. Within each block, clinical history is randomly provided in either the first or second half of images.

This design also allows us to conduct within case-radiologist comparisons. The potential disadvantage of this design is that we cannot distinguish order effects from the effect of providing AI. This issue is unavoidable given the guiding principle that participants receive weakly more information about a case during a repeat encounter. However, we can test for

¹²This principle has been used in computer science (Seah et al., 2021; Conant et al., 2019; Pacilè et al., 2020).

and do rule out order effects on accuracy based on the first two designs.

3.2.4 Participant Recruitment

Participants for the first and third designs, which constitute the majority, were recruited through teleradiology companies. The teleradiology companies allow us to recruit several experts in a relatively liquid spot market, a practice that is now common for decision experiments with non-expert subjects (Hunt and Scheetz, 2019). Most healthcare providers in the US rely on these companies’ services, although many large hospitals have on-call radiologists (Rosenkrantz et al., 2019). We work with teleradiology companies that serve US hospitals and offer the services of both US-based and non-US-based radiologists. Our contracts with teleradiology companies specify a piece-rate, and the companies, in turn, compensate the participants with a piece-rate.¹³ In addition, we provided monetary incentives for accuracy to a subset of radiologists, as described in the next section.

The second design required us to work with a partner who could guarantee subjects’ participation over several months. We collaborated with VinMac healthcare system in Vietnam to recruit their staff radiologists to ensure continued participation. VinMac is in the process of developing its own in-house AI capabilities and was willing to assist with our experiment in exchange for recognition in a publication of the resulting dataset. The VinMac radiologists did not receive any payments to participate in the experiment but we find that their performance is very close to the performance of the tele-radiologists.

In total, 180 radiologists participated in our experiment. Close to 25% of our participants are US-based, 20% have a degree from a US institution, 80% are affiliated with a large clinic, and 61% with an academic institution. As demonstrated in appendix C.3, the quality of the assessments made by the radiologists in our study is comparable to that of the staff radiologists from Stanford University Hospital, who originally diagnosed the patient case.

3.2.5 Incentives

We cross-randomize incentives for accuracy in the first and third designs but not the second because of the specific ways in which our partner’s radiologists are employed.¹⁴ Payments were determined following the binarized scoring rule in Hossain and Okui (2013), where truth

¹³We worked with three companies with piece-rates ranging from \$7.50 to \$13.00.

¹⁴There does not appear to be a consensus in the experimental literature on whether incentives are superior to non-incentivized responses when eliciting beliefs (see Danz, Vesterlund, and Wilson, 2020; Charness, Gneezy, and Rasocho, 2021). A comparison between the incentivized and non-incentivized participants allows us to answer this question in the context of this experiment.

is determined as described in section 3.3.1 below. This incentive scheme uses a loss function of the mean squared prediction error, averaging over patient cases and pathologies, and the respondents earn a fixed bonus of \$120 if a random draw is less than the loss function. This bonus is more than 20% of the base payment to teleradiology firms. We explain to the participants that expected payments are maximized if they provide their best estimates using a non-mathematical description of the payment rule. We specify the distribution so that 30% of pilot participants would earn the bonus, cross-randomized with the other two treatment arms.

3.3 Implementation and Data Collection

3.3.1 Patient Cases and Ground Truth

The experiment uses 324 historical patient cases with potential thoracic pathologies from Stanford University’s healthcare system. For each case, we have access to the chest X-ray and the clinical history in the form of the primary provider’s written notes, the patient vitals, and demographics.¹⁵ The use of retrospective cases allows us to avoid ethical and other issues that would arise when experimenting in high-stakes settings.

Our analysis requires constructing ω_i for each patient case. There are important challenges in using an observational dataset of patient health records to construct this field. One approach would be to use the results from further medical tests. Unfortunately, definitive gold-standard tests do not exist for most thoracic pathologies.¹⁶ Even when follow-up tests are conducted, they are selected on the likely presence of a pathology, an issue referred to as the selective labels problem (e.g. Mullainathan and Obermeyer, 2019). Medical outcomes from patient health records also do not suffice because actions taken by the treating physician in response to the radiology report contaminate these measures. Recent literature has suggested instrumental variables approaches for solving this selective labels problem, but this work targets population quantities and not a “ground truth” on each case (e.g. Chan et al., 2022; Mullainathan and Obermeyer, 2019).

We construct ω_i by aggregating the assessment of a group of expert radiologists, an approach common in computer science (Sheng et al., 2008; Mccluskey et al., 2021). Specifically, we

¹⁵All cases are first encounters with no prior X-ray as a comparison. We started with 500 cases that fit these primary criteria. We omitted pediatric cases from this set. Finally, a radiologist reviewed the cases to remove instances with poor image quality. The clinical history was manually reviewed to remove patient-identifiable information and cleared for public release.

¹⁶Many pathologies do not have commonly used non-imaging-based diagnostic tools. For instance, the presence of cardiomegaly – an enlarged heart – can only be determined using imaging tools, thoracic surgery, or an autopsy.

ask five board certified radiologists from Mount Sinai to read each of the 324 cases using the interface described above with the available X-ray and clinical history. For each case i and expert radiologist r , we, therefore, obtain $\pi_r(\omega_i = 1 | s_{i,r}^E)$ for each pathology, which we aggregate to generate ω_i . Specifically, we classify $\omega_i = 1$ if $\sum_r \pi_r(\omega_i = 1 | s_{i,r}^E) / 5 > 0.5$. This approach immediately addresses the selective labels problem because the availability of assessments is not selected on the likelihood of a pathology being present. Results in [Wallsten and Diederich \(2001\)](#) suggest that, under weak conditions that allow for measurement error in the reports and correlations across reports, the aggregate opinion of several experts is highly diagnostic as long as the experts are median unbiased. To assess robustness, we aggregate $\pi_r(\omega_i = 1 | s_{i,r}^E)$ using both a log-odds average and a leave-one-out mean of the assessments of all the radiologists in our experiment in the clinical history treatment condition.

3.3.2 Experimental Interface and Data Collected

We developed the interface to present the patient cases and to collect radiologists’ predictions and decisions in collaboration with board certified radiologists at Stanford University Hospital and Mt. Sinai Hospital. In contrast to free-text reports, we designed it to generate structured and quantitative data on chest X-ray responses that resemble a typical radiological report. A guiding principle in the design was to mimic clinical practice and to present and obtain all clinically relevant information. We briefly describe this interface and provide images and further details in appendix [B](#).

On the landing page of each case, a high-resolution image of a patient’s X-ray is presented to the radiologist, with the functionality to zoom and adjust brightness and contrast. When the experiment calls to show the clinical history, the interface presents clinical notes, vitals, and laboratory results available at the time the X-ray was originally ordered. If the experiment provides AI assistance, participants are shown AI predictions for fourteen pathologies and a composite prediction for whether or not there are any relevant findings.

The data entry interface collects a radiologist’s assessments of the probability that various thoracic pathologies are present for a given case. The probability that a pathology is present given the available information, i.e. $p_r(\omega = 1 | s)$, is elicited using a continuous slider. We visually subdivide possible responses into five intervals with standard language labels used in written radiological reports to aid the participants.¹⁷ Our radiology collaborators grouped pathologies into eight exclusive parent categories based on their type. Each group has children

¹⁷The specific labels are “*Not present*”, “*Very Likely*”, “*Unlikely*”, “*Possible*”, “*Likely*”, and “*Highly Likely*”. Several radiological publications have suggested such standardized language for radiological reports. See for instance [Panicek and Hricak \(2016\)](#).

that are more specific, which may be further subdivided in some cases. The groups all correspond to a standard class of pathologies. For instance, “airspace opacity” is distinct from a “cardiomediastinal abnormality.” In the main text we focus on the parent categories with AI predictions and drop further subdivisions from the analysis. We refer to those as top-level pathologies. Our results are robust to including the lower-level pathologies in the analysis as we show in appendix C.4. The interface categorizes thoracic pathologies into groups by type to ease data entry. For example, allowing the user to simultaneously set the assessed probability of each disease in a specific category to zero.¹⁸ In addition, we elicited an overall bottom-line assessment of whether the radiologists considers the case normal or not.

We also ask for a binary “treatment/follow-up” recommendation for each pathology that is not definitively ruled out.¹⁹ We will interpret this input as $a_r^*(s)$. In a real clinical setting, a recommendation to follow-up could trigger the treating physician to prescribe additional medical tests or interventions with potential costs and benefits. Thus, an optimal recommendation trades off the cost of false positives and false negatives when recommending an action as in section 2. The probabilistic assessments with the follow-up decision will allow us to estimate radiologists’ relative cost of false positives and false negatives.

In addition to $p_r(\omega = 1 | s)$ and $a_r^*(s)$, we record active time, response times, and any click-stream data that results from the interaction with the interface. The participants are not explicitly informed about this monitoring, and there are no explicit time limits. Our experiment runs remotely, and participants connect to a server, which hosts the interface and records responses. The interface has been extensively tested beforehand on different browsers by conducting pilots with every company we recruited the participants from.²⁰

¹⁸Our radiology collaborators grouped pathologies into eight exclusive parent categories based on their type. Each group has children that are more specific, which may be further subdivided in some cases. The groups all correspond to a standard class of pathologies. For instance, an “airspace opacity” is distinct from a “cardiomediastinal abnormality.” The more specific disease of “bacterial pneumonia” manifests as an airspace opacity. This structure reduced the burden on our participants, and we piloted the interface with several radiologists specializing in the interpretation of chest X-rays. Prior clinical research on AI in chest X-Ray image classification has used similar hierarchies (see Seah et al., 2021, for example).

¹⁹The binary treatment/follow-up decision is only asked for pathologies where a follow-up is clinically relevant. This includes all pathologies with AI assistance.

²⁰This interface is browser-based and built using the o-tree framework Chen et al. (2016). Since we are not directly communicating with our participants we also deploy a device fingerprinting service from fingerprint.com to ensure that there are no repeat participants.

3.3.3 Participant Training

We train the participants using a combination of written instructions and a video. The materials provide an overview of the experimental tasks, the interface, and information about the AI assistance tool. The firms and the participants know that the research study involves retrospective patient cases. To train participants on the AI tool, we provide them with materials that explain the development of the algorithm, present metrics of its performance on various diseases, and summarize the algorithm’s performance relative to radiologists based on prior research. The participants are informed that the algorithm only uses the chest X-ray to form predictions, and this knowledge is later tested in a comprehension question. In addition, we show the participants fifty example cases that show the X-ray and clinical history next to the AI output. After the instructions, they answer eight comprehension questions, which the participants must answer correctly before proceeding to the experiment. We also include an endline survey. We do not directly interact with the subjects except to field questions about the experiment or provide tech support.²¹ The complete set of instructions is provided in appendix B.2.

4 Estimated Treatment Effects

4.1 Overall Performance of AI and Radiologists

This section’s analysis focuses on measures of performance (deviation from ground truth, incorrect decision), deviation from AI prediction, and measures of effort. Table 1 summarizes the data on these measures and sample sizes from our experiment. The main text focuses on top-level pathologies with AI with robustness to other pathology groups relegated to appendix C.4.

Radiologists make the correct follow-up/treatment recommendation on approximately 70% of case-pathologies on average and spend ~2.8 minutes per case with large variability across cases. All summary statistics are very similar across the three experimental designs (tables C.7 and C.9). For instance, the average deviation from the ground truth for the three designs ranges from 0.191 to 0.232, and average active time ranges from 2.58 to 3.03 minutes.

²¹We are blinded to the participants’ treatment status while the experiment is in progress.

Table 1: Summary Statistics

	All Designs		Design 1	
	Mean	SD	Mean	SD
	(1)	(2)	(3)	(4)
Reported Probability	0.233	0.290	0.214	0.287
Decision	0.322	0.467	0.277	0.448
Deviation from Ground Truth	0.223	0.281	0.218	0.290
Deviation from AI	0.191	0.169	0.201	0.171
Correct Decision	0.695	0.460	0.736	0.441
Active time	2.82	2.63	3.03	3.17
Observations	36,280		13,440	
Radiologists	180		112	

Note: This table presents summary statistics of the experimental data. Columns (1) and (2) present the mean and standard deviation for all designs while Columns (3) and (4) present the same for design 1 only. Decision is an indicator for whether treatment/follow-up is recommended, correct decision is an indicator for whether the decision matches the ground truth, deviation from ground truth is the absolute difference between the reported probability and the ground truth, deviation from AI is the absolute difference between the expert’s reported probability and the AI’s reported probability, active time is measured in minutes.

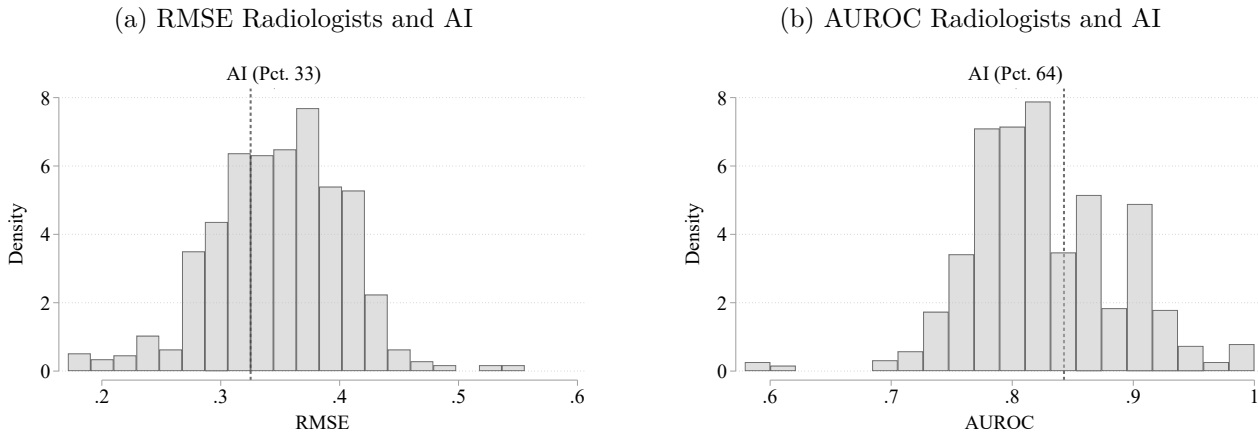
In a comparison study with three radiologists, [Irvin et al. \(2019\)](#) show that the CheXpert model yields a better classifier than two out of three radiologists on five pathologies and all three on a subset of three pathologies. Our results may differ from that because we use a different pool of radiologists, a different sample of cases, and reads with contextual information (clinical history) to construct the ground truth. The latter two differences raise the bar for the AI because they reflect differences in the data-generating process.

To benchmark the quality of AI predictions in our sample and the radiologists in our experiment, we compare our participant pool with the AI input using two performance measures. The first measure is derived from the receiver operating characteristic (ROC) curve, which measures the trade-off between the false positive and the true positive rate of a classifier as the cutoff for classifying a case as positive or negative is varied. It uses only ordinal information about the AI. A classifier that is not better than random has an AUROC value of 0.5 whereas a perfectly predictive classifier has a value of one. The second measure is the root mean squared error (RMSE), that utilizes cardinal information about the AI prediction. A

lower RMSE indicates higher performance.²² We pool the data for top-level pathologies with AI for each radiologist’s reports and for the AI’s prediction.

Figure 1 shows significant heterogeneity in performance across radiologists as well as the scope for AI assistance to improve radiologist performance. The AUROC shows that the bottom tail of the distribution of radiologists performs worse than the AI, whereas the upper tail predicts close to perfectly. This heterogeneity aligns with findings from observational data based on only treatment decisions (see Chan et al., 2022). The AI is more predictive than approximately two-thirds of radiologists, whether compared using AUROC or RMSE. Thus, there is ample room for AI assistance to improve the performance of radiologists. In fact, a majority of radiologists would do better on average by simply following the AI prediction. We present pathology-specific comparison results in appendix C.2.

Figure 1: Comparing AI performance to radiologists



Note: These histograms show distributions of two different accuracy measures of radiologist assessments alongside the AI’s accuracy. The left graph shows the distribution of the RMSE while the right shows the distribution of the average AUROC. Both distributions are shrunk to the grand mean using empirical Bayes. These measures are for each radiologist and include the top-level pathologies. The dotted line is the average measure of the AI algorithm for the corresponding distribution. Only the assessments where contextual history information is available for the radiologists but not the AI prediction are considered. Robustness by design and ground truth definition can be found in sections C.4.1 & C.4.2.

We also compare the performances of our participants and the radiologist who originally diagnosed each patient case in appendix C.3.²³ There is no discernible difference between

²²An important distinction between the two measures is that the AUROC is ordinal whereas RMSE is cardinal.

²³We classified the original free text radiology reports associated with each case as positive, negative, or uncertain for each pathology using the CheXbert algorithm described in Smit et al. (2020). To facilitate comparisons, we also discretized the probability assessments elicited during the experiment into these three categories. Then, we compared the accuracy of the original reads against the radiologists participating in the experiment.

the two groups, which is consistent with the hypothesis that radiologists participating in the study were of similar skill and exerted similar effort as the radiologists completing the original reads.

4.2 How do Radiologists Respond to AI and Contextual Information?

We now describe the effects of our information treatments estimated using the following specification:

$$Y_{irt} = \gamma_{h_i} + \gamma_{CH} \cdot d_{CH}(t) + \gamma_{AI} \cdot d_{AI}(t) + \gamma_{AI \times CH} \cdot d_{CH}(t) \cdot d_{AI}(t) + \varepsilon_{irt},$$

where Y_{rit} is an outcome variable of interest for radiologist r diagnosing patient case-pathology i and treatment t , and γ_{h_i} are pathology fixed effects since there are multiple pathologies h_i for each case in this pooled analysis. Treatments t vary by whether or not clinical history is provided $d_{CH}(t) \in \{0, 1\}$ and whether or not AI information is provided $d_{AI}(t) \in \{0, 1\}$. We report two-way clustered standard errors at the radiologist and patient-case level. The specification omits radiologist-specific fixed effects because the treatments are balanced within radiologists. Cases are also balanced across treatments (see appendix C.1), which suggests that case randomization was successful. We will also compute conditional treatment effects given ranges of the AI signal s_i^A that are grouped based on $\pi(\omega_i = 1 | s_i^A)$.

Table 2: Average treatment effects

Treatment	Deviation from AI		Deviation from Ground Truth		Effort Measures			
	All Designs	Design 1	All Designs	Design 1	All Designs		Design 1	
	(1)	(2)	(3)	(4)	Active Time	Clicks	Active Time	Clicks
AI × CH	0.001 (0.003)	−0.001 (0.006)	0.004 (0.005)	0.003 (0.012)	−0.86 (3.68)	0.22 (0.82)	0.04 (6.94)	0.32 (1.63)
AI	−0.038 (0.004)	−0.036 (0.006)	0.002 (0.004)	0.002 (0.008)	6.75 (2.47)	1.34 (0.56)	6.26 (4.71)	1.53 (1.05)
CH	−0.001 (0.002)	−0.004 (0.004)	−0.011 (0.004)	−0.015 (0.008)	7.37 (2.53)	0.16 (0.55)	6.53 (4.78)	0.09 (1.08)
CONTROL MEAN	0.211 (0.007)	0.221 (0.008)	0.227 (0.010)	0.224 (0.011)	157.57 (4.46)	44.25 (1.21)	161.56 (7.05)	40.71 (1.53)
PATHOLOGY FE OBSERVATIONS	Yes 36280	Yes 13440	Yes 36280	Yes 13440	- 14635	- 14635	- 6718	- 6718

Note: This table summarizes the average treatment effects (ATE) of different information environments on the absolute value of the difference between the radiologist probability and AI probability (column (1) and (2)); absolute value of the difference between the radiologist probability and the ground truth (columns (3) and (4)); and radiologists' effort measured in terms of active time and clicks (columns (5), (6), (7) and (8)). We either pool across all designs (All Designs) or condition on only design 1. Results on effort measure excludes five patient-cases with unaccounted time measure, and observations from design 3 because of learning effects in this set-up. The results are for the two top-level pathologies, airspace opacity and cardiomeastinal abnormality. Standard errors are two-way clustered at the radiologist and patient-case level in parenthesis. Robustness by design can be found in section C.4.1.

The above analysis focuses on the effects on the marginal distributions of the outcome variables Y_{irt} for each pathology. Thus, the specification abstracts away from interactions between pathologies in the effects on information provision, for example due to potential dependence between the predictions and decisions. In section 5, we will present evidence showing that the best fitting model has radiologists updating their beliefs as-if they do not account for dependence between pathologies.

The treatment effect analysis in the main text pools the three experimental designs and does not condition on the sequence in which subjects encounter information treatments. Appendix C.4.5 shows that our results are robust to including controls for order effects. The estimates from all three designs are similar to each other. They are also statistically indistinguishable from those that use only an across participant comparison from the first treatment encountered in design 1 (appendix C.4.3).

4.2.1 Do Radiologists Utilize AI Predictions?

We begin by testing whether radiologists respond to the information that the AI provides. The left panel in table 2 shows how the different information environments affect the disagreement of the radiologists' report with the AI's assessment, which is defined as $Y_{irt} = |p_r(\omega_i = 1 | s_{irt}) - \pi(\omega_i = 1 | s_i^A)|$. The term $p_r(\omega_i = 1 | s_{irt})$ is elicited whereas $\pi(\omega_i = 1 | s_i^A)$ is the AI's predicted probability that $\omega_i = 1$. When t indicates that AI assistance is provided, then $s_{irt} = (s_{ir}^E, s_i^A)$, and when t indicates that AI assistance is not provided, then $s_{irt} = s_{ir}^E$. The signal s^E also depends on whether contextual information is provided.

The results show that radiologists utilize AI assistance: their predictions are closer to the AI predictions when provided with assistance. To see this, observe that the control means for the deviation from the AI are approximately 0.21 for both when we pool designs and for design 1 only. Treatments where AI is provided reduce this baseline average deviation by 18% (all designs) and 16% (design 1). ($p < 0.01$).

4.2.2 Treatment Effects on Diagnostic Performance

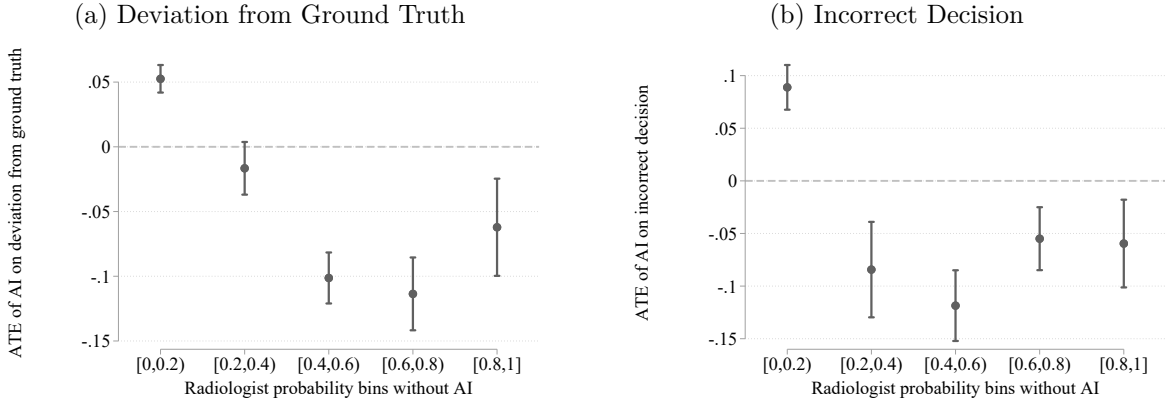
We next ask whether the information treatments affect radiologists' diagnostic performance. As a measure, we consider the absolute deviation of the radiologist's probability report from the binary ground truth, $Y_{irt} = |p_r(\omega_i = 1 | s_{irt}) - \omega_i|$ where lower values implies better performance. Appendix C.4.2 contains results that use a continuous ground truth, which are

qualitatively similar. The middle panel of table 2 shows the average treatment effects on performance.

Our results indicate that while access to contextual information improves performance on average, AI assistance does not. We find that access to clinical history reduces the deviation from the ground truth by 4.8% ($p < 0.05$) of the control mean if we pool designs and by 6.7% in design 1 ($p < 0.05$). In contrast, the effects for AI are close to zero and not statistically significant. In light of the findings in the previous two sections — that the AI is more accurate than most radiologists and that radiologists move their assessments toward the AI—it is puzzling that the AI information does not improve accuracy.

This contradiction occurs because the average treatment effects mask significant heterogeneity in treatment effects. Our within-participant designs—designs 2 and 3—allow us to estimate conditional treatment effects given radiologists’ predictions without AI assistance. Specifically, we partition cases based on the expert’s signal into five equally spaced bins of $\pi_r(\omega_i = 1 | s_{ir}^E)$. Figure 2 shows the conditional treatment effects of providing AI assistance on diagnostic performance. Panel (a) shows the deviation from the ground truth and panel (b) shows the probability of incorrect decision. We find that providing AI assistance in cases when the radiologist is uncertain improves performance on both metrics, whereas AI assistance is harmful when the radiologist is close to certain that the pathology is not present for a given case. Given an average reported probability of 25% or less, the vast majority of cases fall in the first bin yielding a small average treatment effect that masks important heterogeneity. The result that AI assistance can decrease performance rejects a model in which radiologists are Bayesians with correct beliefs.

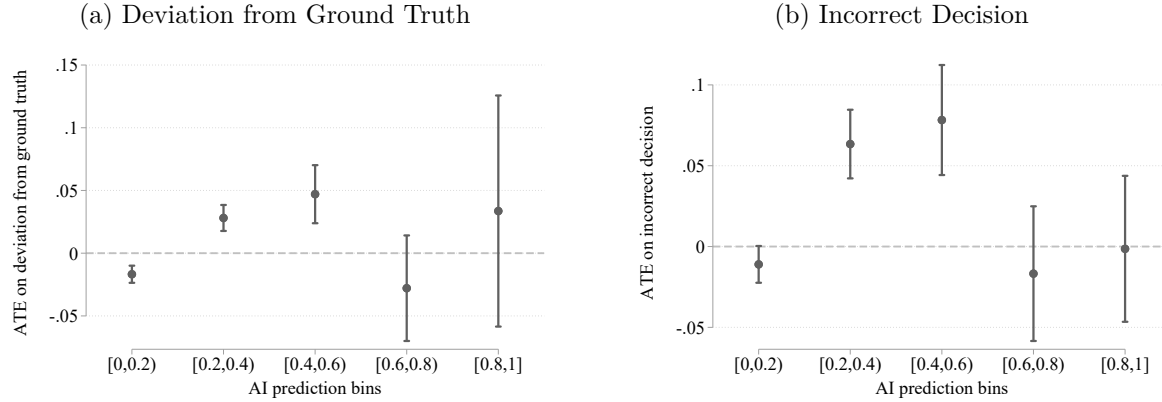
Figure 2: Conditional treatment effect given radiologist prediction



Note: Panel (a) shows the conditional average treatment effect of providing AI information on the absolute value of difference between the radiologist probability and the ground truth. Panel (b) shows analogous treatment effects on incorrect diagnosis, where a correct diagnosis is defined as the treatment recommendation matching the ground truth. Both these treatment effects are conditional on the ranges of the expert’s prediction constructed using the no AI assistance. Standard errors are two-way clustered at the radiologist and patient-case level. The error bars depict 95% confidence intervals. Robustness to experimental design is in appendix C.4.1.

While AI assistance can help uncertain experts, we find that providing uncertain AI predictions reduces performance. As with the analysis of conditional treatment effects given expert predictions, we estimate conditional treatment effects given AI predictions by partitioning cases into five bins based on $\pi(\omega_i = 1 | s_i^A)$. Figure 3 presents the estimates, pooling data from all three experimental designs. When the AI provides a confident prediction (e.g. either close to zero or close to one) performance is significantly improved. We see that in the lowest bins of AI signals, the deviation from the ground truth is reduced. In the second highest bin we also see a marked, though not statistically significant, improvement in performance. However, in the middle range of signals, where the confidence of the AI is low, radiologists’ diagnostic performance and probability of making a correct decision is lower when AI information is provided. This result reinforces the conclusion that radiologists err when updating their beliefs.

Figure 3: Conditional treatment effect given AI prediction



Note: Panel (a) shows the conditional average treatment effect of providing AI information on the absolute value of difference between the radiologist probability and the ground truth. Panel (b) shows analogous treatment effects on incorrect diagnosis, where a correct diagnosis is defined as the treatment recommendation matching the ground truth. Both these treatment effects are conditional on the ranges of AI prediction. Standard errors are two-way clustered at the radiologist and patient-case level. The error bars depict 95% confidence intervals. Robustness to experimental design is in appendix C.4.1 and C.4.2.

4.2.3 Treatment Effects on Time Per Case and Proxies of Effort

Finally, we turn our attention to the effects of AI assistance on time taken and the number of unique interaction (clicks) as a proxy for effort. One hypothesis is that AI assistance could economize on costly human effort without sacrificing overall performance by enabling quicker assessments. At the polar opposite, it is possible that humans take more time because they are provided with more information to process. Which of these effects dominate determines the effect on labor costs when humans use AI assistance, and therefore the optimality of delegating cases versus a collaborative setup.

Our results indicate that radiologists are slower when provided with AI assistance. The last panel of table 2 shows the treatment effects on time spent per case and clicks. These outcomes are measured at the case level. In the X-Ray Only treatment, radiologists spend about 2.6 minutes per case. Both AI and CH increase the time spend per case by a statistically significant amount of approximately 4%. The interaction effect $\gamma_{AI \times CH}$ is not significant for either of the two outcome variables. These effects suggest that decisions where both radiologists and the AI are involved come at a non trivial increase in time spent per case. This result further undercuts the potential benefits in performance from including humans assisted with AI predictions “in the loop.”

4.3 Discussion

We find that AI assistance does not improve the performance of our participants on average, even though the AI predictions are more accurate than the majority of radiologists, and that radiologists respond to this assistance. However, the average treatment effects mask important heterogeneity – AI assistance improves performance for a large set of cases, but also decreases performance in many instances. These results point to biases in the use of AI predictions which we will further investigate in section 5.

We also find that humans have access to valuable contextual information, suggesting that full automation has its drawbacks. But, the biases above – especially in conjunction with our finding that radiologists take longer when given AI assistance – undercut this potential information advantage in a setup that involves AI assistance. Thus, the problem of how best to deploy AI assistance may be non-trivial and the optimal solution may involve selective automation and/or AI assistance. Section 6 analyzes this problem.

Appendix C.4 shows that the results are qualitatively robust to a variety of alternative analyses. The results are similar when we split the analysis by experimental design and when we only focus on the initial across-comparison (using design 1 and 2), although the latter leads to estimates that are imprecise. Alternative ground-truth measures – including a leave-one-out ground truth based on the assessments of our experimental participants and a continuous ground truth, which simply averages the assessments of the ground-truth labelers – also yield similar conclusions. The qualitative patterns of the treatment effects are unchanged if we calibrate each radiologists’ assessments to the ground-truth before conducting the analysis. Finally, incentives for accuracy, which are cross-randomized in designs 1 and 3, do not have significant effects either.

5 Automation/Own-Information Bias/Neglect

An upshot of the results in section 4 is that our participants deviate from the baseline of a Bayesian with correct beliefs about the joint distribution of their own information and the AI signal. In this section, we model and estimate systematic deviations from this benchmark – which we will refer to as Bayesian²⁴ for short – and determine the implications of these deviations on utilizing human expertise and AI predictions.

²⁴The omission of the qualifier “with correct beliefs” slightly abuses terminology because a possible explanation of the deviations we have documented is that our participants are Bayesians but update their beliefs using an incorrect model for the joint distribution of s^A , s^E and ω . We will entertain this possibility below.

5.1 A Model of Deviations from Bayesian Updating

The framework in section 2 shows that a key question is whether the odds-ratios

$$\frac{p_r(\omega_i = 1 | s_i^A, s_{ir}^E)}{p_r(\omega_i = 0 | s_i^A, s_{ir}^E)} \quad \text{and} \quad \frac{\pi_r(\omega_i = 1 | s_i^A, s_{ir}^E)}{\pi_r(\omega_i = 0 | s_i^A, s_{ir}^E)}$$

differ from each other. Recall that Bayes' rule implies that

$$\ln \frac{\pi_r(\omega_i = 1 | s_i^A, s_{ir}^E)}{\pi_r(\omega_i = 0 | s_i^A, s_{ir}^E)} = \ln \frac{\pi_r(s_i^A | \omega_i = 1, s_{ir}^E)}{\pi_r(s_i^A | \omega_i = 0, s_{ir}^E)} + \ln \frac{\pi_r(\omega_i = 1 | s_{ir}^E)}{\pi_r(\omega_i = 0 | s_{ir}^E)}. \quad (4)$$

We now consider a set of models of belief updating to describe systematic deviations from this benchmark. In our model, the human correctly interprets their own signal when AI assistance is not available but errs when both s_i^A and s_{ir}^E are observed. As we will show below, AI assistance nonetheless unambiguously improves performance for a subset of parameters within this family.

The first class of biases that we consider, arises when the two terms on the right-hand side of equation (4) are incorrectly weighted. Following Grether (1980; 1992), we parametrize this type of error using the following parsimonious functional form:

$$\log \frac{p_r(\omega_i = 1 | s_i^A, s_{ir}^E)}{p_r(\omega_i = 0 | s_i^A, s_{ir}^E)} = b_r \log \frac{\pi_r(s_i^A | \omega_i = 1, s_{ir}^E)}{\pi_r(s_i^A | \omega_i = 0, s_{ir}^E)} + d_r \log \frac{\pi_r(\omega_i = 1 | s_{ir}^E)}{\pi_r(\omega_i = 0 | s_{ir}^E)}, \quad (5)$$

where $b_r, d_r \geq 0$. The Bayesian (with correct beliefs) is a special case with $b_r = d_r = 1$. While this linear form is restrictive, it has been useful for documenting several empirical regularities showing deviations from Bayesian updating like base-rate neglect and under inference (see Benjamin, 2019, for a review).

We will say that the human exhibits *automation bias* if $b_r > d_r$, and *automation neglect* if $b_r < d_r$. As a motivation for this nomenclature, observe that when $b_r > d_r$, the human over-weights the AI signal relative to their own. In the specific case when $d_r = 1$, the agent overshoots when updating the posterior odds relative to a Bayesian. Analogously, if $b_r < d_r$, then the human under-weights the AI signal relative to their own. We say that the human exhibits *own-information neglect* if $d_r < 1$ and *own-information bias* if $d_r > 1$, where the cutoff value of one is based on the Bayesian benchmark. Own-information biases are similar to base-rate biases, but apply to beliefs given the expert's signals instead of unconditional population rates (see Griffin and Tversky, 1992; Kahneman and Tversky, 1973).

A second class of deviations we consider will allow for models in which decision-makers do

not correctly account for the dependence between s_i^A and s_{ir}^E , which we call *signal dependence neglect*. For example, if humans act as-if s_i^A and s_{ir}^E are independent conditional on ω_i even if they are not, then their posterior beliefs can be written as

$$\log \frac{p_r(\omega_i = 1 | s_i^A, s_{ir}^E)}{p_r(\omega_i = 0 | s_i^A, s_{ir}^E)} = b_r \log \frac{\pi_r(s_i^A | \omega_i = 1)}{\pi_r(s_i^A | \omega_i = 0)} + d_r \log \frac{\pi_r(\omega_i = 1 | s_{ir}^E)}{\pi_r(\omega_i = 0 | s_{ir}^E)}, \quad (6)$$

where b_r and d_r are allowed to differ from 1 as above. In the case when the signals are jointly multivariate normal and $b_r = d_r = 1$, signal dependence neglect yields correlation neglect as defined in (Enke and Zimmermann, 2019).²⁵ More generally, we will consider models that vary the conditioning set in the first term on the right-hand side and the dimension of s_i^A in the first term on the right-hand side. The specific examples are motivated and discussed further in section 5.3 below.

We intend the functional form above as descriptions of humans' updating rules and will remain agnostic about underlying mechanisms and micro-foundations. In particular, we remain silent on whether our participants are Bayesians that are utilizing the incorrect joint distribution of $(\omega_i, s_i^A, s_{ir}^E)$ when updating their beliefs or if they are non-Bayesians. The former type of model, known as a quasi-Bayesian model,²⁶ can generate automation bias or neglect as well as correlation biases.²⁷ An implicit assumption in our model, and likely other micro-foundations for the functional forms above as well, is that the signal acquired by the human is invariant to the provision of AI assistance. Whether additional training, or experience with the AI can correct deviations from the benchmark model is therefore something that we leave for future work.

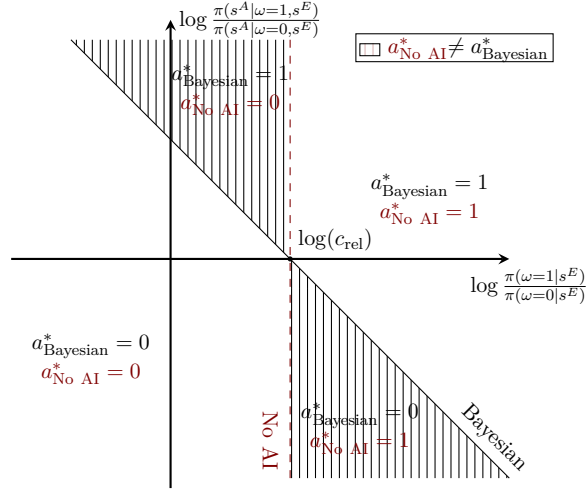
Nonetheless, the models above will prove useful for our purposes. From a theoretical perspective, they will help outline the types of deviations that potentially decrease decision quality. From an empirical perspective, they help understand the drivers of the treatment effects documented earlier and turn out to be a good approximation to the data from the experiment.

²⁵If s_i^A and s_{ir}^E are unidimensional with $(s_i^A, s_{ir}^E) \sim N(0, \Sigma_r)$, then the covariance matrix Σ_r is a sufficient statistic for the posterior probability that $\omega_i = 1$ given the signals if $\omega_i = 1 \{s_i^A + s_{ir}^E \geq \varepsilon_i\}$ and ε_i is independent of (s_i^A, s_{ir}^E) .

²⁶See Rabin (2013) for a definition and Barberis et al. (1998); Rabin (2002); Rabin and Vayanos (2010) for examples.

²⁷To see this, assume that $p_r(s_i^A | \omega_i, s_{ir}^E) = \pi(s_i^A | \omega_i, s_{ir}^E)^b$ and $p_r(s_{ir}^E, \omega_i) = \pi(s_{ir}^E, \omega_i)$ to generate the functional form in equation (5) for any b_r as long as $d_r = 1$. The derivation of equation (6) is similar. In contrast to automation bias/neglect and correlation biases, own-information bias/neglect cannot be derived in a quasi-Bayesian model because we assume that $p_r(\omega_i | s_{ir}^E) = \pi_r(\omega_i | s_{ir}^E)$.

Figure 4: Comparing decisions with and without AI assistance – Bayesian with correct beliefs



Note: The figure shows the decision criterion of a Bayesian with and without AI assistance and where their decisions agree and disagree. Shaded regions show the regions in which AI improves or worsens decision making.

5.2 Implications for Human-AI Collaboration

We now show that the types of deviations described above have implications for when AI assistance unambiguously improves human performance. The results will also illustrate the utility of the simple functional forms in equations (5) and (6). This subsection drops the i and r indices for simplicity of notation.

It is useful to start by considering the decisions with and without AI assistance for a Bayesian decision maker. Figure 4 illustrates the realizations of s^A for which the optimal decision with AI assistance differs from the the decision without AI assistance for a fixed c_{rel} . The horizontal and vertical axes respectively represent $\log \frac{\pi(\omega=1|s^E)}{\pi(\omega=0|s^E)}$ and $\log \frac{\pi(s^A|\omega=1,s^E)}{\pi(s^A|\omega=0,s^E)}$. As shown by the vertical dashed line, the decision-maker would take the action 1 if and only if $\log \frac{\pi(\omega=1|s^E)}{\pi(\omega=0|s^E)}$ exceeds $\log c_{rel}$. The solid line represents the analogous boundary for a Bayesian who has access to AI assistance. Observe that the decisions a Bayesian makes as a function of the signals s^A and s^E cannot be improved without additional information. Thus, a Bayesian with correct beliefs and access to both signals improves upon the no AI action in the vertically shaded region.

Now consider humans that may deviate from this benchmark model. A human who takes a given action without AI assistance $a_{No AI}^* = a^*(s^E; p_r)$, but a different action with AI assistance (so that $a_{No AI}^* \neq a_{AI}^*$) makes a worse decision if $a_{AI}^* = a^*(s^A, s^E; p_r)$ disagrees with

the Bayesian's decision $a_{\text{Bayesian}}^* = a^*(s^A, s^E; \pi_r)$ with AI assistance. This follows because, in the binary action setup, only one of the decisions can agree with the Bayesian decision. In all other cases, the human's decision is weakly improved for the signal realization (s^A, s^E) . In other words, a human whose decision changes upon receiving the AI signal s^A is better off with AI assistance only if the change agrees with the Bayesian decision. The human is unambiguously better off if this property holds for all signals.

Our first result states that a human who deviates from the benchmark model because they only exhibits automation neglect is unambiguously better off with AI assistance.

Proposition 1. *Suppose that the human's posterior is described by equation (5).*

(i) *If the human only exhibits automation neglect ($b < 1, d = 1$), then for all pairs of signal realizations (s^A, s^E) , and any c_{rel} , the human attains weakly higher expected payoff $V(s)$ with AI assistance.*

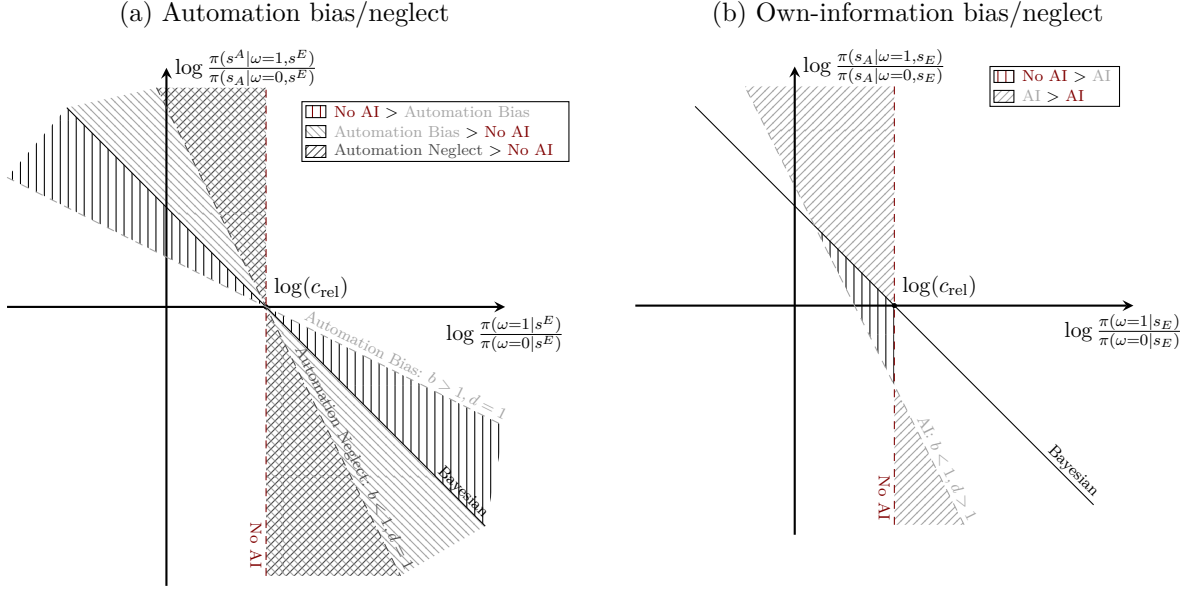
(ii) *In all other cases ($b > 1$ or $d \neq 1$), for any c_{rel} , there exist log-likelihood ratios $\log \frac{\pi(s^A|\omega=1, s^E)}{\pi(s^A|\omega=0, s^E)}$ and $\log \frac{\pi(\omega=1|s^E)}{\pi(\omega=0|s^E)}$ such that the human attains lower expected payoff $V(s)$ with AI assistance.*

See appendix A for the proof.

Figure 5a illustrates the case without own-information bias or neglect by setting $d = 1$ but allows for either automation bias or neglect by setting $b \neq 1$. The two dashed lines represent cutoffs analogous to those in figure 4 for humans with automation bias and automation neglect. Although a human that only exhibits automation neglect under-responds to the AI information, their beliefs move towards a Bayesian decision-makers but does not overshoot it. Whenever her decision changes, it agrees with the Bayesian's. In contrast, if the human exhibits automation bias, they errs for moderately informative AI signals with intermediate values of $\log \frac{\pi(s^A|\omega=1, s^E)}{\pi(s^A|\omega=0, s^E)}$ because they over-reacts. At high enough values of this log-likelihood ratio, both the Bayesian and the human exhibiting automation bias would take the same action.

In the case when there is either own-information bias or neglect ($d \neq 1$), it is always possible for the payoff with AI to be lower than the payoff without AI assistance. In our model, this occurs because providing the AI signal generates a bias in how the expert uses their own information. Figure 5b illustrates the result (for $d > 1$ and $b < 1$). Relative to the analogous line in figure 5a, the intercept of the dashed line is not equal to $\log c_{rel}$. The vertically striped triangle depicts combinations of the log-likelihood ratios above in which the biased expert achieves a higher payoff without AI. In these cases, the expert takes the correct action without AI assistance but incorrectly uses their own information with AI assistance, resulting in an

Figure 5: Comparison with Bayesian decisions



Note: This figure shows the where the decisions of an expert as a function of the signals disagree with the Bayesian in cases with and without AI assistance. Panel (a) shows automation bias and neglect (absent own-information bias and neglect). Panel (b) shows a decision maker who exhibits both automation neglect and own-information bias.

error. Hence, in the presence of own-information bias or neglect, AI assistance can result in worse decision for some signals.

We next consider a decision-maker with a different type of bias, namely, one in which the decision-maker exhibits signal dependence neglect. Perhaps not surprisingly, our next result shows that this type of bias on its own can result in worse decisions with AI assistance:

Proposition 2. *Suppose that the human exhibits signal dependence neglect so that the posterior belief is described by equation (6). For any value of $b > 0$, $d > 0$, and $c_{rel} > 0$, there exist log-likelihood ratios $\log \frac{\pi(s^A|\omega=1,s^E)}{\pi(s^A|\omega=0,s^E)}$ and $\log \frac{\pi(s^A|\omega=1)}{\pi(s^A|\omega=0)}$ such that the human attains lower expected payoff $V(s)$ with AI assistance.*

Compared to the models of only automation/own-information bias/neglect, signal dependence neglect adds another dimension of potential mistakes to those illustrated in the figures above. The result bears resemblance to those in [Enke and Zimmermann \(2019\)](#), which showed that in a multivariate normal model with positively correlated signals, correlation neglect results in over-reaction to signals and verified this hypothesis in lab experiments. Proposition 2 differs in that it allows for general signal distributions and for signal dependence neglect to co-exist with automation and own-information bias/neglect. This extension is essential for a naturalistic environment like ours because the experimenter does not have full control over

the signal structure. The general signal structure makes it difficult to characterize mistakes in terms of over or under-updating, unlike in the case of a multivariate normal model. Even when $b = d = 1$ so that automation or own-information bias/neglect are not relevant, an examination of equations (4) and (5) reveals that whether or not a decision-maker exhibits under- or over-updating depends on the difference between $\log \frac{\pi(s^A|\omega=1,s^E)}{\pi(s^A|\omega=0,s^E)}$ and $\log \frac{\pi(s^A|\omega=1)}{\pi(s^A|\omega=0)}$. The propositions above have important implications for the design of human-AI collaboration, which we consider in section 6. Specifically, we study an AI designer who only has access to the AI signal s^A and must decide on one of the three modes of delegation – utilize only the AI prediction, delegate the case to the human, or provide AI assistance to a human expert. The results show that other than in the case when automation neglect is the only relevant bias, the designer must learn the types of biases as well as the distribution of $\pi(s^A, s^E|\omega)$ to determine which delegation modality yields the best decision.

5.3 Estimating Deviations from Bayesian Updating

We now turn to an empirical implementation of the model above. The analysis in this section will be based on designs 2 and 3 because they allow us to observe the same participant make decisions under all information-conditions on a given case. Start by considering an empirical analog to equation (5):

$$\log \frac{p_r(\omega_i = 1 | s_{ir}^A, s_{ir}^E)}{p_r(\omega_i = 0 | s_{ir}^A, s_{ir}^E)} = a + b \cdot \log \frac{\pi_r(s_{ir}^A | \omega_i = 1, s_{ir}^E)}{\pi_r(s_{ir}^A | \omega_i = 0, s_{ir}^E)} + d \cdot \log \frac{\pi_r(\omega_i = 1 | s_{ir}^E)}{\pi_r(\omega_i = 0 | s_{ir}^E)} + \varepsilon_{ir}, \quad (7)$$

where we have omitted heterogeneity across radiologists in b_r and d_r . Appendix C.5.6 discusses radiologist heterogeneity in our estimates. Two of the terms in this equation are directly elicited in the experiment: the probability in the second term on the right-hand side, $\pi_r(\omega_i = 1 | s_{ir}^E)$, is equal to the radiologists' assessment in the treatment arm where the subjects read cases without AI assistance and the term $p_r(\omega = 1 | s_{ir}^A, s_{ir}^E)$ in the dependent variable is the assessment in the treatment arm with AI. The “update term,” given by $\log \frac{\pi_r(s_{ir}^A | \omega_i = 1, s_{ir}^E)}{\pi_r(s_{ir}^A | \omega_i = 0, s_{ir}^E)}$ will be estimated and substituted into the equation above.

There are three challenges in estimating the update term. The first challenge is that it is a ratio of conditional densities. We address this issue by rewriting it using Bayes' rule as

follows:

$$\log \frac{\pi_r \left(s_{ir}^A | \omega_i = 1, s_{ir}^E \right)}{\pi_r \left(s_{ir}^A | \omega_i = 0, s_{ir}^E \right)} = \log \frac{\pi_r \left(\omega_i = 1 | s_{ir}^A, s_{ir}^E \right)}{\pi_r \left(\omega_i = 0 | s_{ir}^A, s_{ir}^E \right)} - \log \frac{\pi_r \left(\omega_i = 1 | s_{ir}^E \right)}{\pi_r \left(\omega_i = 0 | s_{ir}^E \right)}.$$

If s_{ir}^E can be constructed or controlled for, then we can estimate the first term on the right-hand side using data on ω_i and s_{ir}^A via a binary response model. This estimation is possible because the signal from the AI that the humans receive is isomorphic to the vector of predicted probabilities for the various diseases observed. The second term in this equation has been elicited.

This brings us to the second challenge – constructing s_{ir}^E when estimating $\pi_r \left(\omega_i = 1 | s_{ir}^A, s_{ir}^E \right)$ because we do not observe it directly. Let c_i be the patient case associated with case-pathology i and $I(c_i)$ be the set of case-pathologies associated with case c_i . If s_{ir}^E is unidimensional and $\pi_r \left(\omega_i | s_{ir}^E \right)$ is monotonic in s_{ir}^E , then $\pi_r \left(\omega_i | s_{ir}^E \right)$ is a valid control variable. However, we want to allow for the possibility that the radiologist evaluates a case holistically and uses signals across pathologies. Under the assumption that $s_i^A \perp s_{ir}^E | \omega_i, \left(\pi_r \left(\omega_{i'} | s_{i'r}^E \right) \right)_{i' \in I(c_i)}$, the vector of probabilities for all pathologies reported by r for case i , denoted $\left(\pi_r \left(\omega_{i'} | s_{i'r}^E \right) \right)_{i' \in I(c_i)}$, is a valid control variable. In this multi-dimensional case, a sufficient condition is that s_{ir}^E is invertible in $\left(\pi_r \left(\omega_{i'} | s_{i'r}^E \right) \right)_{i' \in I(c_i)}$. Our empirical specifications will therefore employ multi-variate proxy controls for s_{ir}^E using elicited probability assessments for multiple pathologies.

To allow for flexible interactions between s_i^A and s_{ir}^E while avoiding over-fitting, we estimate $\pi_r \left(\omega_i = 1 | s_{ir}^A, s_{ir}^E \right)$ using a pathology-specific random forest that predicts ω_i using the vector of predicted probabilities for all pathologies for case c_i reported by radiologist r without AI assistance, the vector of predicted probabilities for case c_i the AI algorithm produces, and summaries of the patient clinical history when made available to the radiologist, and participant-specific fixed-effects. The hyper-parameters of the random forest are chosen by grouped k-fold cross-validation, where we ensure that each patient case appears in only one fold to avoid overfitting to the patient case. Further details of the training procedure are described in appendix C.5.2.

The third challenge is the potential for measurement error, particularly in the form that radiologists' signal s_{ir}^E when elicited without AI might differ from their signal when given AI assistance. Classical measurement error arising from this source would lead to attenuation bias in the coefficient estimates. To address this issue, we will construct instruments s_{ir}^E using the reported probabilities of the other radiologists in our experiment.

With these solutions in hand, we would like to assess whether humans exhibit signal depen-

dence neglect when updating beliefs. As prefaced earlier, although the humans' and AI's signals are not conditionally independent given the ground truth, humans may act as-if they are. We will therefore estimate and select between models that vary the set of signals conditioned on in the update term. For example, in the case when radiologists behave as if s_i^A and s_{ir}^E are independent conditional on ω_i , the update term drops the conditioning on s_{ir}^E . We can vary the pathologies across the set of models considered when constructing $I(c_i)$.²⁸ Including these models in our selection approach will also tell us whether radiologists' assessments are separable across different pathologies.

The correct model of behavior satisfies the conditional moment restriction $E[\varepsilon_{irt} | s_{i,-r}^E, s_i^A] = 0$, where $s_{i,-r}^E$ collects the signals of the radiologists other than r in our experiment. For estimation, we utilize unconditional moment restrictions based on functions of $s_{i,-r}^E$ and s_i^A that closely mimic the terms in equation (7). Our instruments include $\log \frac{\pi(\omega_i=1|s_i^A)}{\pi(\omega_i=0|s_i^A)}$, and leave-one-out averages of $\log \frac{\pi(\omega_i=1|s_i^A, s_{ir'}^E)}{\pi(\omega_i=0|s_i^A, s_{ir'}^E)}$ for radiologists other than r that use various proxies for $s_{ir'}^E$, based on different sets of pathologies $I(c_i)$ that are conditioned on.²⁹ Empirical analogs of the resulting moment conditions are used to estimate the model using GMM.

We will employ the model-selection procedure proposed in [Andrews and Lu \(2001\)](#) to select between non-nested models. This method utilizes the J-statistic of the GMM objective function, which is adjusted for the number of moments and parameters that are included in the model. The selection criterion, MMSC-BIC, penalizes models that reject a greater number of moment restrictions.

5.4 Results

Table 3 presents estimates from six models, which is a subset of the models we consider.³⁰ The first three models do not utilize clinical history when made available to the participants to construct the proxy for s_{ir}^E whereas the last three models do. We consider three models in each of these two sets by varying $I(c_i)$. The first corresponds to the case when the signal s_i^A only includes the focal pathology and is conditionally independent of s_{ir}^E given ω_i . The

²⁸The conditionally independent case corresponds to the extreme case in which $I(c_i) = \emptyset$, whereas the Bayesian model includes all pathologies.

²⁹Specifically, we construct fourteen instruments. The first is a constant and the second is the average of $\log \frac{\pi(\omega_i=1|s_{ir'}^E)}{\pi(\omega_i=0|s_{ir'}^E)}$ for all $r' \neq r$. The remaining twelve construct the average of $\log \frac{\pi(\omega_i=1|s_{ir'}^E)}{\pi(\omega_i=0|s_{ir'}^E)}$ for all $r' \neq r$ by varying the conditioning variables $s_{ir'}$. The different sets of conditioning variables in $s_{ir'}$ are presented in the second panel of appendix table C.21. These sets are used because they are the relevant terms in at least one of the models that we consider in the testing procedure.

³⁰See table C.20 in the appendix for the results from all models. Results from all pathologies with AI are qualitatively similar (see table C.21).

second allows for dependence between s_i^A and s_{ir}^E given ω_i , but only through $\pi(\omega_i | s_{ir}^E)$ for the focal pathology and potentially clinical history. The third utilizes the correct update term constructed using all available AI predictions and the vector of probabilities $\pi(\omega_i | s_{ir}^E)$ for all pathologies. Setting $b = d = 1$ and the constant to 0 in this last case corresponds to Bayesian updating with correct beliefs.

The results from this exercise point to two types of errors in radiologists' use of AI signals. The first type of error is that radiologists neglect signal dependence even though AI predictions and radiologists' signals are highly correlated after conditioning on the ground truth (see appendix table C.18). This conclusion follows because we select the model in column 1, which uses an update term based on equation (6) and therefore does not control for s^E . Another implication of the selected model is that radiologists do not incorporate information across different pathologies since only the focal pathology is relevant. This result validates our previous analysis that analyzes each pathology separately.

Second, across different models, including all models that are not selected, we estimate that radiologists exhibit automation neglect. However, radiologists do not exhibit substantial own-information bias or neglect since the estimated value of d is close to 1 in all specifications. Accounting for measurement error in estimating this model is important, as versions that do not do so estimate d significantly less than 1 (appendix C.5.3).

Connecting these observations back to our theoretical discussion in section 2, the parameters are such that radiologists will not benefit unambiguously from access to the AI signal, primarily because of signal dependence neglect.

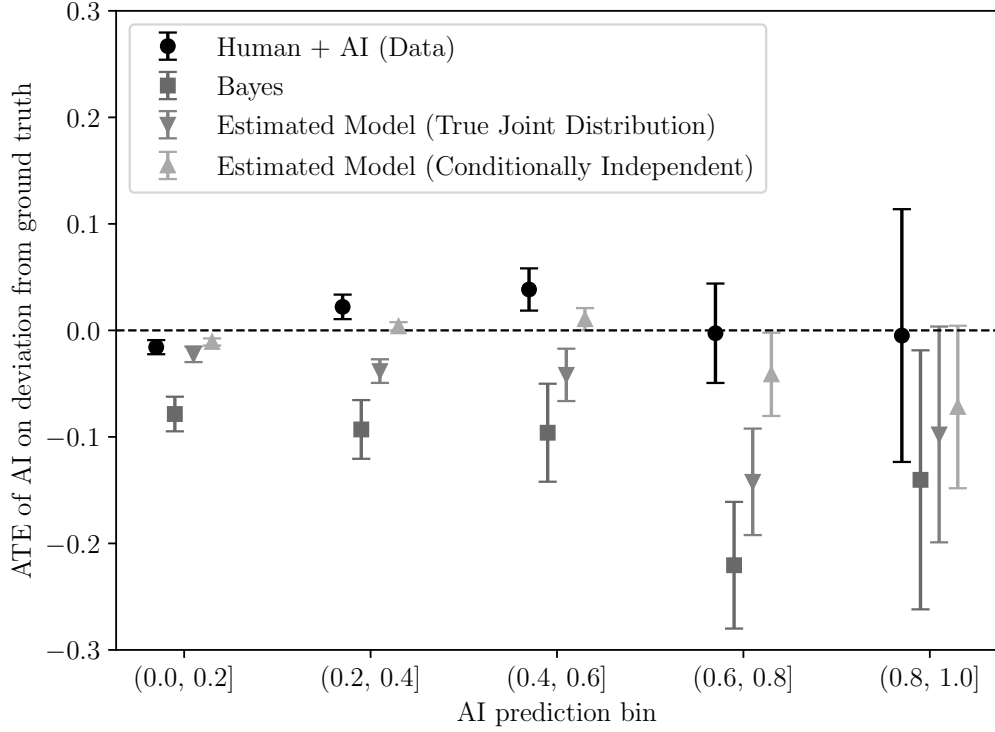
Table 3: Model Selection: Top Level with AI – IVGMM

	(1)	(2)	(3)	(4)	(5)	(6)
AUTOMATION BIAS (b)	0.29 (0.02)	0.34 (0.03)	0.35 (0.03)	0.19 (0.02)	0.27 (0.02)	0.35 (0.03)
OWN INFO BIAS (d)	1.10 (0.01)	1.08 (0.01)	1.05 (0.01)	1.07 (0.01)	1.06 (0.01)	1.05 (0.01)
CONSTANT	0.40 (0.03)	0.40 (0.04)	0.37 (0.04)	0.31 (0.03)	0.33 (0.03)	0.36 (0.04)
FOCAL s_A	✓	✓	✓	✓	✓	✓
OTHER s_A			✓			✓
FOCAL s_E		✓	✓		✓	✓
OTHER s_E			✓			✓
CLINICAL HISTORY s_E				✓	✓	✓
J-STATISTIC	18.23	16.86	0.17	4.3	10.7	0.09
MMSC-BIC	-23.96	-21.12	-8.27	-12.57	-10.39	-8.35
NUMBER OF MOMENTS	13	12	5	7	8	5
Observations	11420	11420	11420	11420	11420	11420
R-SQUARED	0.50	0.49	0.52	0.46	0.48	0.52

Note: This table summarizes estimates of b and d for different specifications of the update term. The models differ by whether the update term conditions on the signal s_E of the pathology at hand, the AI’s and the radiologist’s signal of other pathologies as well as the information that is provided in the clinical history of a patient. Each model is estimated via GMM. The reported MMSC-BIC statistic adjusts the J-statistic for the number of included parameters, awarding bonus terms for models with fewer parameters (see [Andrews and Lu \(2001\)](#) for details). This table presents a subset of the models that we select from. The full set of models included in the selection procedure are presented in [table C.20](#). The update term is estimated via random forest as described in [appendix section C.5.2](#). Standard errors are clustered at the radiologist level.

These deviations also explain the heterogeneous conditional average treatment effects documented in [section 4](#). [Figure 6](#) shows the treatment effect of AI on the deviation from ground truth of our radiologists along with three different models under which we compute the same treatment effects: the Bayesian benchmark, the model in [equation \(5\)](#) where radiologists use the correct updating term, and the selected model from [table 3](#). As expected, the Bayesian would benefit significantly from gaining access to the AI signal. In fact, as indicated by the large reductions in the deviation from the ground truth, there is significant potential value in combining the human and the AI signal. Imposing the model in [equation \(5\)](#) with the correct updating term – [column \(6\)](#) – reduces these improvements and moves the implied treatment effects closer to the data. However, we see that throughout the entire signal range of s_A , such a decision-maker would still unambiguously benefit from gaining access to the AI. Only when we impose the selected update term, under which radiologists do not account for the dependence of signals, does the model generate the observed negative treatment effect

Figure 6: Model Treatment Effects



Note: This graph shows the observed conditional treatment effects of providing radiologists access to AI (Human+AI) and compares those to three different model-implied treatment effects: giving AI access to a Bayesian decision maker, giving AI access to a decision maker who acts according to the empirical version of equation 5, both under the correct updating term and when the decision maker treats the AI signal as conditionally independent.

conditional on intermediate AI predictions as in our treatment effect analysis. We see that such a model closes even more of the gap between the Bayesian treatment effects and the observed treatment effects.

It is significant that the model presented above is able to replicate the pattern of conditional treatment effects even though it is restrictive – it imposes linearity in log-odds and does not allow for heterogeneity in b and d across radiologists. Appendix C.5.5 investigates the linearity restriction in equation (7). We estimate a boosted tree that predicts the dependent variable in the equation using the same two independent variables in the equation. We find that the empirical analog to the relevant boundary of the decision-regions depicted in figure 5 is well-approximated using a linear model. Appendix C.5.6 investigates heterogeneity – it presents estimates that allow for b and d to vary with radiologists. We find that the estimated distributions of b_r and d_r are centered close to the point estimates above, with most of the estimated distributions of b_r and d_r in the range $[0.1, 0.4]$ and $[1.0, 1.2]$ respectively.

Thus, consistent with the conclusions above, we find evidence for automation neglect, but no meaningful own-information bias or neglect. These results suggest that the estimated model represents a good approximation to the experimental data.

Taken together, the results indicate that while there are large potential gains from combining radiologists' assessments with AI predictions, biases in radiologists' use of AI assistance undercuts these gains. We find that radiologists exhibit both automation-neglect and signal dependence neglect. These mistakes lead to no better diagnostic performance when provided with AI assistance. One approach for addressing this issue is to provide radiologists with better training, an avenue we leave for future research. A second approach is to design better collaborative systems that are built on predicting the types of cases in which human experts outperform AI predictions and vice-versa, and the types of cases in which AI-assisted humans do best, an issue we turn to next.

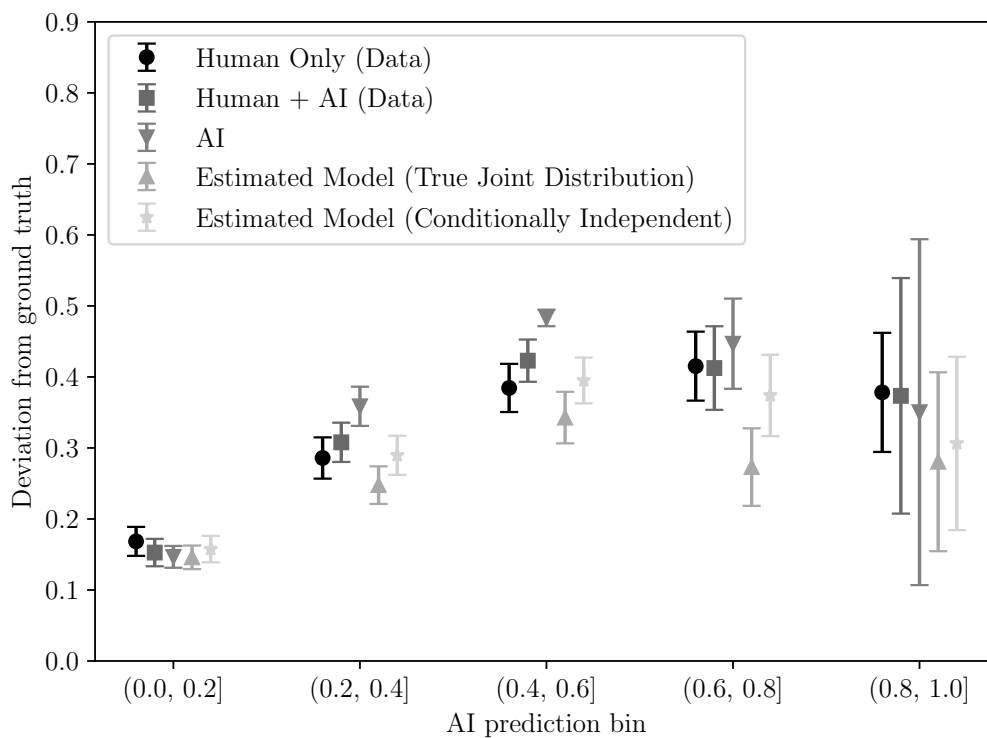
6 Designing Human-AI Collaboration

We now consider the design of collaborative systems between AI and radiologists. The designs we consider restrict attention to systems that use the AI signal to delegate a case to one of three modalities – radiologists alone, the AI alone, or the radiologist with access to the AI. As a warm-up for this exercise, it is useful to examine the predictive performance of the different modalities, conditional on s^A (see figure 7). Recall from the conditional treatment effect analysis, radiologists' assessments improve with AI in the lowest and the two highest bins of AI signals. Figure 7 also shows that in two out of three ranges in which the AI improves radiologists' decision-making that its own performance is even better than the performance of the radiologists with AI.

However, this figure misses the differences in the human time costs across modalities. Our analysis of the estimated treatment effects shows that radiologists take more time when provided with AI predictions. Moreover, using AI predictions alone saves on costly human effort. This points to the conclusion that in most cases where AI improves decision-making, one is at least as well off by relying exclusively on AI prediction. But using only AI or never assisting humans with AI predictions may come at the cost of performance in cases when using the human alone is superior.

Motivated by these observations, we now examine if there is a trade-off between the marginal costs of human effort and diagnostic performance.

Figure 7: Model Deviation from Ground Truth



Note: This figure shows the performance of the different modalities that we consider for the optimal collaborative system. Cases are either decided by only the radiologist, only the AI, or the radiologist with access to the AI. The performance measures for Human Only and Human + AI are constructed from our treatment effect analysis.

6.1 Computing the Trade-off Between Decision Loss and Costs of Human Effort

Consider a policy $\tau(\cdot)$ that chooses between full automation (AI), radiologist with access to AI ($E + AI$), or radiologist without access to AI (E), as a function of the AI signal s_i^A . The optimal policy which minimizes the sum of the expected decision-loss (costs of false positives and false negatives) and the monetized time cost of using human radiologists solves:

$$\tau^*(s_i^A) = \arg \min_{\tau \in \{E, E+AI, AI\}} -m \cdot V_{i\tau}(s_i^A) + w \cdot C_{i\tau}(s_i^A). \quad (8)$$

The first term contains the expected decision-loss from a modality given by $V_{i\tau}(s_i^A) = E \left[V_{ir\tau}(s_i^A) \middle| s_i^A \right]$, which is the expected diagnostic quality averaging over radiologists and cases given the modality, preferences for false positives and false negatives, and the AI signal. Preferences for false positives and false negatives are allowed to vary by pathology but are the same across modalities. We estimate these preferences using data on the binary treatment recommendations of the radiologists in our experiment, given their probability assessments. Details of this preference estimation step are available in appendix C.6. The average cost of false negatives across pathologies is three times the cost of a false positive. Since we do not know the dollar cost of a false negative (m), we will present results for varying values of m .

The second term in the objective function contains $C_{i\tau}(s_i^A) = \left[C_{ir\tau}(s_i^A) \middle| s_i^A \right]$, which is the expected radiologist time for a given modality. If the case is fully automated, this time cost is zero and otherwise those time costs are based on our experimental estimates, which show that radiologists spend more time on cases when presented with AI predictions. For the interpretation of the magnitudes, we translate both radiologists' expected time cost and the expected decision loss into dollars. For the costs of radiologist time, we set $w = \$4$ per minute based on a payment of \$10 per case and an average time per read of 2.5 minutes.

We solve this problem by training a classification tree that assigns the case to a modality conditional on the AI signal $s_{A,i}$. We use 55% of cases as training data for the decision tree, 20% of cases for validation, and 25% in the test set. For this exercise, we focus on two top-level pathologies, cardiomedial abnormality, and airspace opacity. Finally, to quantify the drawbacks of biased humans, we will contrast the solution from such a system when the decisions under $E + AI$ are as observed in the data with the system that uses the Bayesian assessments for $E + AI$.

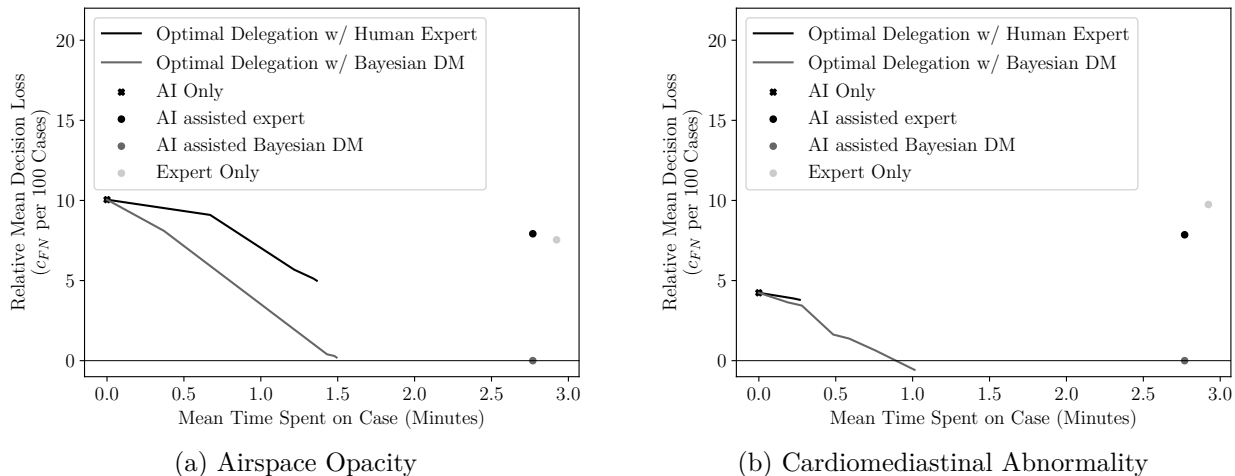
An important restriction in this formulation of the delegation problem is that the signal received by the expert is exogenous and does not respond to the availability of AI. This assumption rules out models of endogenous information acquisition, for example, rational

inattention as in Sims (2003). A potentially interesting aspect is whether a designer can leverage such endogenous responses by designing an information revelation policy that induces effort. We leave such extensions that leverage insights from information design (Kamenica and Gentzkow, 2011; Bergemann and Morris, 2019) to future work, but measure the total amount of time taken by the experts in our experiment with and without AI assistance.

6.2 Results

Figure 8 shows a possibilities frontier for the trade-off between diagnostic quality against decision time for the two top-level pathologies with AI, calculated by varying m . It also shows the corner solutions where all cases are assigned to each of the modalities. The results suggest that there are potential gains from the optimal delegation of cases. An unassisted radiologist takes 2.7 minutes per case, or about \$11, and incurs a relative decision loss of approximately seven for both of the top level pathologies with AI assistance. By moving to a solution on the frontier with a human expert – one whose assessments are as in our experiment – the designer can reduce both decision loss and the time taken per case by delegating many cases to the AI. The frontier with a Bayesian expert, as expected, is much more favorable. Moreover, the frontier for both a Human and a Bayesian expert coincide when the dollar cost of incorrect decisions (m) is small because the vast majority of cases are assigned to the AI.

Figure 8: Loss-Time Frontier

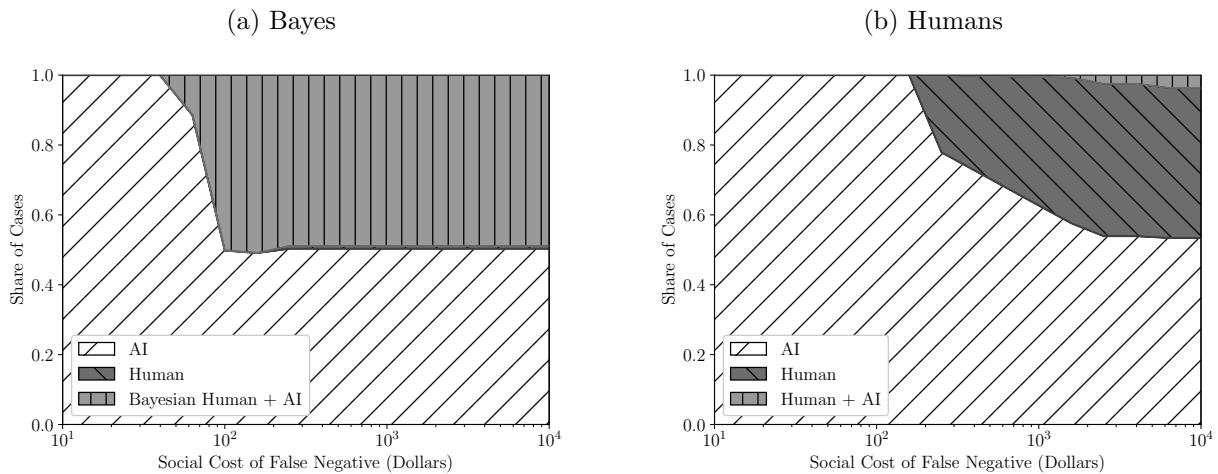


Note: This graph shows how radiologists and the AI perform relative to delegation systems on the frontier of the cost of human time versus decision loss. Panel (a) focuses on airspace opacity. Panel (b) focuses on cardiomedial abnormality.

Next, we investigate the proportion of decisions assigned to the three modalities as we vary

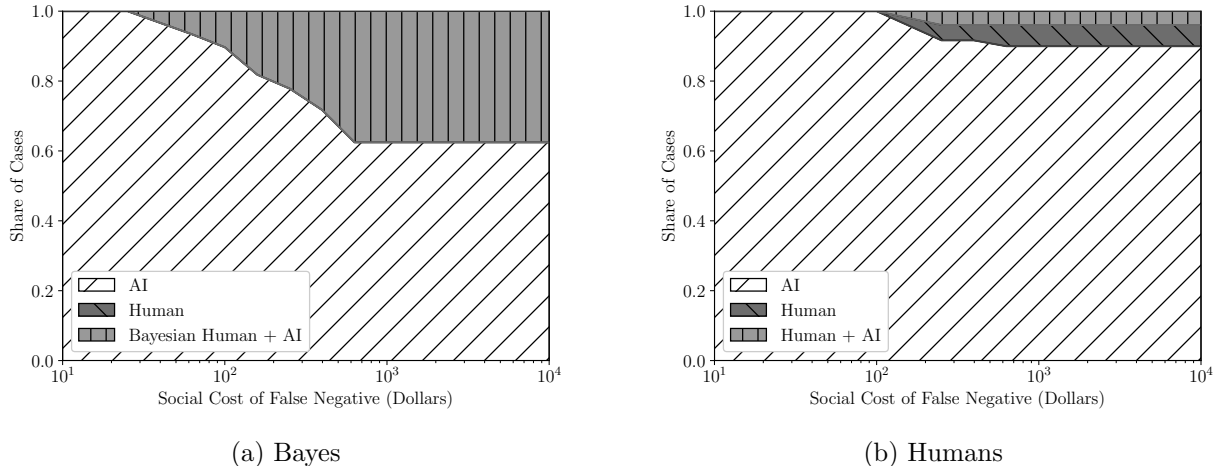
m (figures 9 and 10). Both for the case where radiologists are Bayesian and the observed behavior in our experiment, we find that the AI decides almost all cases if the cost of a false negative – a missed diagnosis – is less than \$100 per case. If radiologists acted as Bayesians with correct beliefs, the share of cases that involve human-AI collaboration rises markedly above a cost of \$100, but even for costs as high as \$10,000, this share does not exceed 50% for airspace opacity and does not exceed 40% for cardiomediastinal abnormality. Moreover, under Bayesian decision-making, the share of cases where only the radiologist decides is negligible for both pathologies and the only reason for using an unassisted radiologist is to save on time costs. When we conduct the same exercise and use the observed behavior of radiologists, we find that humans are involved in approximately 50% of cases for airspace opacity if the cost of a false positive is sufficiently large. For cardiomediastinal abnormality, the share of cases with humans involved only reaches 10% for very large costs of false positives. Moreover, the majority of cases where a radiologist is involved have the radiologist make decisions without AI for both pathologies. A more complete assessment of the optimal combination of human and machine decisions, therefore, confirms the intuition from above that cases are either decided by the radiologist or the AI but not by both of them together.

Figure 9: Airspace Opacity Modality Shares



Note: The graphs show the share of cases decided by each modality (humans, AI, humans+AI) conditional on the cost of a false negative in dollars, denoted m in the text, for airspace opacity. Panel (a) focuses on a Bayesian decision maker. Panel (b) focuses on a human decision-maker with decisions and time-taken as in our experiment.

Figure 10: Cardiomeastinal Abnormality Modality Shares



Note: The graphs show the share of cases decided by each modality (humans, AI, humans+AI) conditional on the cost of a false negative in dollars, denoted m in the text, for cardiomeastinal abnormality. Panel (a) focuses on a Bayesian decision maker. Panel (b) focuses on a human decision-maker with decisions and time-taken as in our experiment.

6.3 Caveats

There are several caveats to the analysis here. The first is that any collaborative system may change radiologists' expectations about the difficulty of cases and adjust strategically to those changing expectations. For example, if radiologists are only handed the most difficult cases, they may exert more effort. We leave such strategic adjustments to a collaborative system for future work. We also have not considered alternative mechanisms to elicit radiologists' signals that may be less prone to errors. For instance, one may want to ask the radiologist to submit their assessment before seeing the AI's assessment and then combine both assessments optimally ex-post. Finally, the solutions presented here treat pathologies as separable. This case is relevant if there is a single pathology of interest.

7 Conclusion

AI is predicted to profoundly reshape the nature of work (see [Felten et al., 2023](#)). Humans are likely to use AI as decision aids for many tasks not only in the long run but also in the medium run for tasks that will ultimately be fully automated. A central question is therefore how humans use AI tools and how tasks should be assigned. To understand the benefits and pitfalls of human-machine collaboration, we conduct an experiment in which radiologists are provided with AI assistance. Besides serving as an iconic example of a

highly-skilled profession that is being transformed by AI, radiology also represents a large class of professionals whose main job is a high-stakes classification task. Since we can simulate radiologists' normal workflow, this is an ideal setting for conducting such an experiment.

While the potential benefits of deploying AI assistance are large in our setting, biases in humans' use of AI assistance eliminate these potential gains. Even though the AI tool in our experiment performs better than two thirds of radiologists, optimally combining their predictions could substantially improve performance. Yet, we find that giving radiologists access to AI predictions does not, on average, lead to higher performance. This average treatment effect, however, masks systematic heterogeneity: providing AI does improve radiologists' predictions and decisions for cases where the AI is certain, but not when uncertain. This latter result – that prediction quality can be reduced for some range of AI signals – rejects Bayesian updating with correct beliefs. We also describe systematic errors in belief updating – namely radiologists exhibit automation neglect (e.g. radiologists weight the AI prediction relative to their own) and treat the AI prediction and their own signals as independent even though they are not. Moreover, radiologists take significantly more time to make a decision when AI information is provided.

Together, these results have important implications for how to design the collaboration between humans and machines. Increased time costs and sub-optimal use of AI information both work against having radiologists make decisions with AI assistance. In fact, an optimal delegation policy that utilizes heterogeneity in treatment effects given the AI prediction suggests that cases should either be decided by the AI alone or by the radiologist alone. Only a small share of cases are optimally delegated to radiologists with access to AI. In other words, we find that radiologists should work *next to* as opposed to *with* AI. To the extent that expert decision makers generally under-respond to information other than their own (Conlon et al., 2022) and incorporating additional information is cognitively costly, these insights may hold in other settings where experts' main job is a classification task.

There are several important considerations that are outside the scope of this work. One question motivated by the unrealized potential gains of AI assistance we find is whether the benefits from AI-specific training for radiologists and/or experience with AI are large. Answering these questions requires different experimental designs or longer-run studies. Another important consideration is that the organization of human-AI collaboration may influence experts' incentives, to which they may respond strategically. Finally, any interaction with AI will be mediated by organizational and regulatory incentives. Organizations may set guidelines on how to use AI or provide feedback, and regulations may influence liability implications. These issues are interesting avenues for future work.

AI continues to evolve rapidly. This development is increasingly driven by large corporate labs (Heston and Zwetsloot, 2020), which have resources that are unaffordable to academic institutions. For these and other reasons, economists are unlikely to have a major role in the technical development of AI tools. Our comparative advantage lies in studying how humans interact with these tools and thereby help shape the institutions that guide their use to ensure that this development is beneficial to society. Empirical analysis is a particularly useful tool in this endeavor, especially if the algorithms themselves are a black-box and cannot be understood from first principles.

References

- Jason Abaluck, Leila Agha, Chris Kabrhel, Ali Raja, and Arjun Venkatesh. The determinants of productivity in medical testing: Intensity and allocation of care. *Am. Econ. Rev.*, 106(12):3730–3764, December 2016.
- Daron Acemoglu and Simon Johnson. Power and progress: Our Thousand-Year struggle over technology and prosperity. *Public Affairs, New York*, 2023.
- Ajay Agrawal, Joshua Gans, and Avi Goldfarb. *Prediction Machines: The Simple Economics of Artificial Intelligence*. Harvard Business Press, April 2018.
- Ajay Agrawal, Joshua S Gans, and Avi Goldfarb. Artificial intelligence: The ambiguous labor market impact of automating prediction. *J. Econ. Perspect.*, 33(2):31–50, May 2019.
- Jong Seok Ahn, Shadi Ebrahimian, Shaunagh McDermott, Sanghyup Lee, Laura Naccarato, John F Di Capua, Markus Y Wu, Eric W Zhang, Victorine Muse, Benjamin Miller, Farid Sabzalipour, Bernardo C Bizzo, Keith J Dreyer, Parisa Kaviani, Subba R Digumarthy, and Mannudeep K Kalra. Association of artificial Intelligence–Aided chest radiograph interpretation with reader performance and efficiency. *JAMA Netw Open*, 5(8):e2229289–e2229289, August 2022.
- Eugenio Alberdi, Lorenzo Strigini, Andrey A Povyakalo, and Peter Ayton. Why are people’s decisions sometimes worse with computer support? In *Lecture Notes in Computer Science*, Lecture notes in computer science, pages 18–31. Springer Berlin Heidelberg, Berlin, Heidelberg, 2009.
- Donald W K Andrews and Biao Lu. Consistent model and moment selection procedures for GMM estimation with application to dynamic panel data models. *J. Econom.*, 101(1):123–164, March 2001.
- Victoria Angelova, Will Dobbie, and Crystal Yang. Algorithmic recommendations and human discretion, 2022.
- Gagan Bansal, Besmira Nushi, Ece Kamar, Eric Horvitz, and Daniel S Weld. Is the most accurate AI the best teammate? optimizing AI for teamwork. *AAAI*, 35(13):11405–11414, May 2021.
- Nicholas Barberis, Andrei Shleifer, and Robert Vishny. A model of investor sentiment. *J. financ. econ.*, 49(3):307–343, September 1998.
- Dan Benjamin, Aaron Bodoh-Creed, and Matthew Rabin. Base-Rate neglect: Foundations and implications, 2019.
- Daniel J Benjamin. Chapter 2 - errors in probabilistic reasoning and judgment biases. In *Handbook of Behavioral Economics: Applications and Foundations 1*, volume 2, pages 69–186. January 2019.

- Dirk Bergemann and Stephen Morris. Information design: A unified perspective. *J. Econ. Lit.*, 57(1):44–95, March 2019.
- David Blackwell. Equivalent comparisons of experiments. *Ann. Math. Stat.*, 24(2):265–272, 1953.
- Erik Brynjolfsson and Tom Mitchell. What can machine learning do? workforce implications. 358(6370):1530–, 2017.
- Erik Brynjolfsson, Daniel Rock, and Chad Syverson. Artificial intelligence and the modern productivity paradox: A clash of expectations and statistics. November 2017.
- David C Chan, Matthew Gentzkow, and Chuan Yu. Selection with variation in diagnostic skill: Evidence from radiologists. *Q. J. Econ.*, 137(2):729–783, May 2022.
- Amitabh Chandra and Douglas O Staiger. Identifying sources of inefficiency in healthcare. *Q. J. Econ.*, 135(2):785–843, May 2020.
- Gary Charness, Uri Gneezy, and Vlastimil Rasocho. Experimental methods: Eliciting beliefs. *J. Econ. Behav. Organ.*, 189:234–256, September 2021.
- Daniel L Chen, Martin Schonger, and Chris Wickens. oTree—An open-source platform for laboratory, online, and field experiments. *Journal of Behavioral and Experimental Finance*, 9:88–97, March 2016.
- Emily F Conant, Alicia Y Toledano, Senthil Periaswamy, Sergei V Fotin, Jonathan Go, Justin E Boatsman, and Jeffrey W Hoffmeister. Improving accuracy and efficiency with concurrent use of artificial intelligence for digital breast tomosynthesis. *Radiol Artif Intell*, 1(4):e180096, July 2019.
- John J Conlon, Malavika Mani, Gautam Rao, Matthew W Ridley, and Frank Schilbach. Not learning from others. August 2022.
- Janet Currie and W Bentley MacLeod. Diagnosing expertise: Human capital, decision making, and performance among physicians. *J. Labor Econ.*, 35(1), 2017.
- David Danz, Lise Vesterlund, and Alistair J Wilson. Belief elicitation: Limiting truth telling with information on incentives. June 2020.
- Berkeley J Dietvorst, Joseph P Simmons, and Cade Massey. Algorithm aversion: people erroneously avoid algorithms after seeing them err. *J. Exp. Psychol. Gen.*, 144(1):114–126, February 2015.
- Berkeley J Dietvorst, Joseph P Simmons, and Cade Massey. Overcoming algorithm aversion: People will use imperfect algorithms if they can (even slightly) modify them. *Manage. Sci.*, 64(3):1155–1170, March 2018.
- Enke and Zimmermann. Correlation neglect in belief formation. *Rev. Econ. Stud.*, 2019.

- Ed Felten, Manav Raj, and Robert Seamans. How will language modelers like ChatGPT affect occupations and industries? March 2023.
- Edward W Felten, Manav Raj, and Robert Seamans. The occupational impact of artificial intelligence: Labor, skills, and polarization. September 2019.
- Riccardo Fogliato, Shreya Chappidi, Matthew Lungren, Paul Fisher, Diane Wilson, Michael Fitzke, Mark Parkinson, Eric Horvitz, Kori Inkpen, and Besmira Nushi. Who goes first? influences of Human-AI workflow on decision making in clinical imaging. In *Proceedings of the 2022 ACM Conference on Fairness, Accountability, and Transparency, FAccT '22*, pages 1362–1374. Association for Computing Machinery, June 2022.
- Martin Ford. *Rise of the Robots: Technology and the Threat of a Jobless Future*. Basic Books, May 2015.
- Morgan R Frank, David Autor, James E Bessen, Erik Brynjolfsson, Manuel Cebrian, David J Deming, Maryann Feldman, Matthew Groh, José Lobo, Esteban Moro, Dashun Wang, Hyejin Youn, and Iyad Rahwan. Toward understanding the impact of artificial intelligence on labor. *Proc. Natl. Acad. Sci. U. S. A.*, 116(14):6531–6539, April 2019.
- Susanne Gaube, Harini Suresh, Martina Raue, Eva Lermer, Timo Koch, Matthias Hudecek, Alun D Ackery, Samir C Grover, Joseph F Coughlin, Dieter Frey, Felipe Kitamura, Marzyeh Ghassemi, and Errol Colak. Who should do as AI say? only non-task expert physicians benefit from correct explainable AI advice. June 2022.
- Susanne Gaube, Harini Suresh, Martina Raue, Eva Lermer, Timo K Koch, Matthias F C Hudecek, Alun D Ackery, Samir C Grover, Joseph F Coughlin, Dieter Frey, Felipe C Kitamura, Marzyeh Ghassemi, and Errol Colak. Non-task expert physicians benefit from correct explainable AI advice when reviewing x-rays. *Sci. Rep.*, 13(1):1383, January 2023.
- Avi Goldfarb, Bledi Taska, and Florenta Teodoridis. Could machine learning be a general purpose technology? a comparison of emerging technologies using data from online job postings. *Res. Policy*, 52(1):104653, January 2023.
- David M Grether. Bayes rule as a descriptive model: The representativeness heuristic. *Q. J. Econ.*, 95(3):537–557, November 1980.
- David M Grether. Testing bayes rule and the representativeness heuristic: Some experimental evidence. *J. Econ. Behav. Organ.*, 17(1):31–57, January 1992.
- Dale Griffin and Amos Tversky. The weighing of evidence and the determinants of confidence. *Cogn. Psychol.*, 24(3):411–435, July 1992.
- Grimon, Marie-Pascale, and Christopher Mills. The impact of algorithmic tools on child protection: Evidence from a randomized controlled trial. 2022.
- Jonathan Gruber, Benjamin R Handel, Samuel H Kina, and Jonathan T Kolstad. Managing intelligence: Skilled experts and decision support in markets for complex products. 2021.

- H Benjamin Harvey and Vrushab Gowda. How the FDA regulates AI. *Acad. Radiol.*, 27(1): 58–61, January 2020.
- Roxanne Heston and Remco Zwetsloot. Mapping u.s. multinationals’ global AI R&D activity, 2020.
- Ahmed Hosny, Chintan Parmar, John Quackenbush, Lawrence H Schwartz, and Hugo J W L Aerts. Artificial intelligence in radiology. *Nat. Rev. Cancer*, 18(8):500–510, August 2018.
- Tanjim Hossain and Ryo Okui. The binarized scoring rule. *Rev. Econ. Stud.*, 80(3):984–1001, February 2013.
- Nicholas C Hunt and Andrea M Scheetz. Using MTurk to distribute a survey or experiment: Methodological considerations. *Journal of Information Systems*, 33(1):43–65, March 2019.
- Kosuke Imai, Zhichao Jiang, James Greiner, Ryan Halen, and Sooahn Shin. Experimental evaluation of Algorithm-Assisted human Decision-Making: Application to pretrial public safety assessment. December 2020.
- Jeremy Irvin, Pranav Rajpurkar, Michael Ko, Yifan Yu, Silvana Ciurea-Ilcus, Chris Chute, Henrik Marklund, Behzad Haghgoo, Robyn Ball, Katie Shpanskaya, Jayne Seekins, David A Mong, Safwan S Halabi, Jesse K Sandberg, Ricky Jones, David B Larson, Curtis P Langlotz, Bhavik N Patel, Matthew P Lungren, and Andrew Y Ng. CheXpert: A large chest radiograph dataset with uncertainty labels and expert comparison. In *Proceedings of the AAAI Conference on Artificial Intelligence*, volume 33, pages 590–597, July 2019.
- Alistair E W Johnson, Tom J Pollard, Lu Shen, Li-Wei H Lehman, Mengling Feng, Mohammad Ghassemi, Benjamin Moody, Peter Szolovits, Leo Anthony Celi, and Roger G Mark. MIMIC-III, a freely accessible critical care database. *Sci Data*, 3:160035, May 2016.
- Daniel Kahneman and Amos Tversky. On the psychology of prediction. *Psychol. Rev.*, 80(4):237–251, July 1973.
- Emir Kamenica and Matthew Gentzkow. Bayesian persuasion. *Am. Econ. Rev.*, 101(6): 2590–2615, October 2011.
- Hyo Eun Kim, Hak Hee Kim, Boo Kyung Han, Ki Hwan Kim, Kyunghwa Han, Hyeonseob Nam, Eun Hye Lee, and Eun Kyung Kim. Changes in cancer detection and False-Positive recall in mammography using artificial intelligence: a retrospective, multireader study. *The Lancet Digital Health*, 2(3):e138–e148, March 2020.
- Jon Kleinberg, Jens Ludwig, Sendhil Mullainathan, and Ziad Obermeyer. Prediction policy problems. *Am. Econ. Rev.*, 105(5):491–495, May 2015.
- Jon Kleinberg, Himabindu Lakkaraju, Jure Leskovec, Jens Ludwig, and Sendhil Mullainathan. Human decisions and machine predictions. *Q. J. Econ.*, 133(1):237–293, August 2017.

- Barnett S Kramer, Christine D Berg, Denise R Aberle, and Philip C Prorok. Lung cancer screening with low-dose helical CT: results from the national lung screening trial (NLST). *J. Med. Screen.*, 18(3):109–111, 2011.
- Vivian Lai, Chacha Chen, Q Vera Liao, Alison Smith-Renner, and Chenhao Tan. Towards a science of Human-AI decision making: A survey of empirical studies. December 2021.
- Curtis P Langlotz. Will artificial intelligence replace radiologists? *Radiology: Artificial Intelligence*, 1(3):e190058, May 2019.
- Xiaoxuan Liu, Livia Faes, Aditya U Kale, Siegfried K Wagner, Dun Jack Fu, Alice Bruynseels, Thushika Mahendiran, Gabriella Moraes, Mohith Shamdas, Christoph Kern, Joseph R Ledsam, Martin K Schmid, Konstantinos Balaskas, Eric J Topol, Lucas M Bachmann, Pearse A Keane, and Alastair K Denniston. A comparison of deep learning performance against health-care professionals in detecting diseases from medical imaging: a systematic review and meta-analysis. *The Lancet Digital Health*, 1(6):e271–e297, October 2019.
- Robert McCluskey, A Enshaei, and B A S Hasan. Finding the Ground-Truth from multiple labellers: Why parameters of the task matter. *ArXiv*, 2021.
- Hussein Mozannar and David Sontag. Consistent estimators for learning to defer to an expert. In *Proceedings of the 37th International Conference on Machine Learning*, volume 119 of *Proceedings of Machine Learning Research*, pages 7076–7087. PMLR, 2020.
- S Mullainathan and Z Obermeyer. A machine learning approach to low-value health care: wasted tests, missed heart attacks and mis-predictions, 2019.
- Justin G Norden and Nirav R Shah. What AI in health care can learn from the long road to autonomous vehicles. *NEJM Catalyst Innovations in Care Delivery*, 3(2), 2022.
- Shakked Noy and Whitney Zhang. Experimental evidence on the productivity effects of generative artificial intelligence. March 2023.
- Ziad Obermeyer and Ezekiel J Emanuel. Predicting the future — big data, machine learning, and clinical medicine. *N. Engl. J. Med.*, 375(13):1216–1219, September 2016.
- Serena Pacilè, January Lopez, Pauline Chone, Thomas Bertinotti, Jean Marie Grouin, and Pierre Fillard. Improving breast cancer detection accuracy of mammography with the concurrent use of an artificial intelligence tool. *Radiol Artif Intell*, 2(6):e190208, November 2020.
- David M Panicek and Hedvig Hricak. How sure are you, doctor? a standardized lexicon to describe the radiologist’s level of certainty. *AJR Am. J. Roentgenol.*, 207(1):2–3, July 2016.
- Allison Park, Chris Chute, Pranav Rajpurkar, Joe Lou, Robyn L Ball, Katie Shpanskaya, Rashad Jabarkheel, Lily H Kim, Emily McKenna, Joe Tseng, Jason Ni, Fidaa Wishah, Fred Wittber, David S Hong, Thomas J Wilson, Safwan Halabi, Sanjay Basu, Bhavik N

- Patel, Matthew P Lungren, Andrew Y Ng, and Kristen W Yeom. Deep Learning-Assisted diagnosis of cerebral aneurysms using the HeadXNet model. *JAMA network open*, 2(6): e195600, June 2019.
- Bhavik N Patel, Louis Rosenberg, Gregg Willcox, David Baltaxe, Mimi Lyons, Jeremy Irvin, Pranav Rajpurkar, Timothy Amrhein, Rajan Gupta, Safwan Halabi, Curtis Langlotz, Edward Lo, Joseph Mammarrappallil, A J Mariano, Geoffrey Riley, Jayne Seekins, Luyao Shen, Evan Zucker, and Matthew Lungren. Human–Machine partnership with artificial intelligence for chest radiograph diagnosis. *npj Digital Medicine*, 2(1):111, December 2019.
- M Rabin. Inference by believers in the law of small numbers. *Q. J. Econ.*, 2002.
- M Rabin and D Vayanos. The gambler’s and hot-hand fallacies: Theory and applications. *Rev. Econ. Stud.*, 2010.
- Matthew Rabin. Incorporating limited rationality into economics. *J. Econ. Lit.*, 51(2): 528–543, June 2013.
- Maithra Raghu, Katy Blumer, Greg Corrado, Jon Kleinberg, Ziad Obermeyer, and Sendhil Mullainathan. The algorithmic automation problem: Prediction, triage, and human effort. *arXiv*, March 2019.
- Pranav Rajpurkar and Matthew P Lungren. The current and future state of AI interpretation of medical images. *N. Engl. J. Med.*, 388(21):1981–1990, May 2023.
- Pranav Rajpurkar, Jeremy Irvin, Kaylie Zhu, Brandon Yang, Hershel Mehta, Tony Duan, Daisy Ding, Aarti Bagul, Curtis Langlotz, Katie Shpanskaya, Matthew P Lungren, and Andrew Y Ng. CheXNet: Radiologist-Level pneumonia detection on chest X-Rays with deep learning. (1711.05225), December 2017.
- Pranav Rajpurkar, Jeremy Irvin, Robyn L Ball, Kaylie Zhu, Brandon Yang, Hershel Mehta, Tony Duan, Daisy Ding, Aarti Bagul, Curtis P Langlotz, Bhavik N Patel, Kristen W Yeom, Katie Shpanskaya, Francis G Blankenberg, Jayne Seekins, Timothy J Amrhein, David A Mong, Safwan S Halabi, Evan J Zucker, Andrew Y Ng, and Matthew P Lungren. Deep learning for chest radiograph diagnosis: A retrospective comparison of the CheXNeXt algorithm to practicing radiologists. *PLoS Med.*, 15(11):e1002686, November 2018.
- Pranav Rajpurkar, Chloe O’Connell, Amit Schechter, Nishit Asnani, Jason Li, Amirhossein Kiani, Robyn L Ball, Marc Mendelson, Gary Maartens, Daniël J van Hoving, Rulan Griesel, Andrew Y Ng, Tom H Boyles, and Matthew P Lungren. CheXaid: Deep learning assistance for physician diagnosis of tuberculosis using chest X-Rays in patients with HIV. *npj Digital Medicine*, 3:115, December 2020.
- Pranav Rajpurkar, Emma Chen, Oishi Banerjee, and Eric J Topol. AI in health and medicine. *Nat. Med.*, 28(1):31–38, January 2022.
- Ashesh Rambachan. Identifying prediction mistakes in observational data, 2021.

- Carlo Reverberi, Tommaso Rigon, Aldo Solari, Cesare Hassan, Paolo Cherubini, and Andrea Cherubini. Experimental evidence of effective human–AI collaboration in medical decision-making. *Sci. Rep.*, 12(1):1–10, September 2022.
- Michael Allan Ribers and Hannes Ullrich. Machine predictions and human decisions with variation in payoff and skills: the case of antibiotic prescribing, 2022.
- Andrew B Rosenkrantz, Tarek N Hanna, Scott D Steenburg, Mary Jo Tarrant, Robert S Pyatt, and Eric B Friedberg. The current state of teleradiology across the united states: A national survey of radiologists’ habits, attitudes, and perceptions on teleradiology practice. *J. Am. Coll. Radiol.*, 16(12):1677–1687, December 2019.
- Jarrel C Y Seah, Cyril H M Tang, Quinlan D Buchlak, Xavier G Holt, Jeffrey B Wardman, Anuar Aimoldin, Nazanin Esmaili, Hassan Ahmad, Hung Pham, John F Lambert, Ben Hachey, Stephen J F Hogg, Benjamin P Johnston, Christine Bennett, Luke Oakden-Rayner, Peter Brotchie, and Catherine M Jones. Effect of a comprehensive deep-learning model on the accuracy of chest x-ray interpretation by radiologists: a retrospective, multireader multicase study. *Lancet Digit Health*, 3(8):e496–e506, August 2021.
- Victor S Sheng, Foster Provost, and Panagiotis G Ipeirotis. Get another label? improving data quality and data mining using multiple, noisy labelers. In *Proceedings of the 14th ACM SIGKDD international conference on Knowledge discovery and data mining*, KDD ’08, pages 614–622, New York, NY, USA, August 2008. Association for Computing Machinery.
- Yongsik Sim, Myung Jin Chung, Elmar Kotter, Sehyo Yune, Myeongchan Kim, Synho Do, Kyunghwa Han, Hanmyoung Kim, Seungwook Yang, Dong-Jae Lee, and Byoung Wook Choi. Deep convolutional neural network–based software improves radiologist detection of malignant lung nodules on chest radiographs. *Radiology*, 294(1):199–209, January 2020.
- Christopher A Sims. Implications of rational inattention. *J. Monet. Econ.*, 50(3):665–690, April 2003.
- Akshay Smit, Saahil Jain, Pranav Rajpurkar, Anuj Pareek, Andrew Y Ng, and Matthew P Lungren. CheXbert: Combining automatic labelers and expert annotations for accurate radiology report labeling using BERT. April 2020.
- Megan Stevenson and Jennifer L Doleac. Algorithmic risk assessment in the hands of humans. December 2019.
- Yasasvi Tadavarthi, Brianna Vey, Elizabeth Krupinski, Adam Prater, Judy Gichoya, Nabile Safdar, and Hari Trivedi. The state of radiology AI: Considerations for purchase decisions and current market offerings. *Radiol Artif Intell*, 2(6):e200004, November 2020.
- Matt Taddy. The technological elements of artificial intelligence. February 2018.
- Philipp Tschandl, Christoph Rinner, Zoe Apalla, Giuseppe Argenziano, Noel Codella, Allan Halpern, Monika Janda, Aimilios Lallas, Caterina Longo, Josep Malvehy, John Paoli,

- Susana Puig, Cliff Rosendahl, H Peter Soyer, Iris Zalaudek, and Harald Kittler. Human–computer collaboration for skin cancer recognition. *Nat. Med.*, 26(8):1229–1234, June 2020.
- A Tversky and D Kahneman. Judgment under uncertainty: Heuristics and biases. *Science*, 185(4157):1124–1131, September 1974.
- Thomas S Wallsten and Adele Diederich. Understanding pooled subjective probability estimates. *Math. Soc. Sci.*, 41(1):1–18, January 2001.
- Michael Webb. The impact of artificial intelligence on the labor market. 158713(November), 2019.
- S Kevin Zhou, Hayit Greenspan, Christos Davatzikos, James S Duncan, Bram Van Ginneken, Anant Madabhushi, Jerry L Prince, Daniel Rueckert, and Ronald M Summers. A review of deep learning in medical imaging: Imaging traits, technology trends, case studies with progress highlights, and future promises. *Proc. IEEE*, 109(5):820–838, May 2021.

Appendix

A Appendix of Proofs

A.1 Proof of Proposition 1

Case $b < 1$ and $d = 1$: Suppose $a^*(s^E; p) = 0$ and $a^*(s^A, s^E; p) = 1$. Equivalently, $\log c_{rel} > \log \frac{\pi(\omega=1|s^E)}{\pi(\omega=0|s^E)}$ and $\log c_{rel} \leq b \log \frac{\pi(s^A|\omega=1, s^E)}{\pi(s^A|\omega=0, s^E)} + \log \frac{\pi(\omega=1|s^E)}{\pi(\omega=0|s^E)}$. Since $b \in (0, 1)$, it must be that $\log \frac{\pi(s^A|\omega=1, s^E)}{\pi(s^A|\omega=0, s^E)} > 0$ and $\log c_{rel} < \log \frac{\pi(s^A|\omega=1, s^E)}{\pi(s^A|\omega=0, s^E)} + \log \frac{\pi(\omega=1|s^E)}{\pi(\omega=0|s^E)}$ so that $a^*(s^A, s^E; \pi) = 1$. Hence, if $0 = a^*(s^E; p) \neq a^*(s^A, s^E; p)$ then $a^*(s^A, s^E; p) = a^*(s^A, s^E; \pi)$ and $V(s^E; p) \leq V(s^A, s^E; \pi) = V(s^A, s^E; p)$, with strict inequality if the measure on (s^A, s^E) under $\pi(\cdot)$ such that $0 = a^*(s^E; p) \neq a^*(s^A, s^E; \pi)$ is strictly positive. The proof of the case when $a^*(s^E; p) = 1$ and $a^*(s^A, s^E; p) = 0$ is analogous. If $a^*(s^E; p) = a^*(s^A, s^E; p)$ then $V(s^E; p) = V(s^A, s^E; p)$.

Case $b > 1$ and $d = 1$: If $\log c_{rel} - \log \frac{\pi(\omega=1|s^E)}{\pi(\omega=0|s^E)} > 0$, then for $\log \frac{\pi(s^A|\omega=1, s^E)}{\pi(s^A|\omega=0, s^E)}$ $\in \left(\frac{1}{b} \log c_{rel} - \frac{1}{b} \log \frac{\pi(\omega=1|s^E)}{\pi(\omega=0|s^E)}, \log c_{rel} - \log \frac{\pi(\omega=1|s^E)}{\pi(\omega=0|s^E)} \right)$ we have both $\log c_{rel} > \log \frac{\pi(s^A|\omega=1, s^E)}{\pi(s^A|\omega=0, s^E)}$ $+ \log \frac{\pi(\omega=1|s^E)}{\pi(\omega=0|s^E)}$ and $\log c_{rel} < b \log \frac{\pi(s^A|\omega=1, s^E)}{\pi(s^A|\omega=0, s^E)} + \log \frac{\pi(\omega=1|s^E)}{\pi(\omega=0|s^E)}$. Thus, $0 = a^*(s^E; p) \neq a^*(s^E, s^A; p) \neq a^*(s^E, s^A; \pi)$. An analogous argument for the case when $\log c_{rel} \leq \log \frac{\pi(\omega=1|s^E)}{\pi(\omega=0|s^E)}$ completes this case.

Case $d \neq 1$: We analyze this in two subcases.

- $(1 - d) \log c_{rel} > 0$: We show that there exist values of $\left(\log \frac{\pi(\omega=1|s^E)}{\pi(\omega=0|s^E)}, \log \frac{\pi(s^A|\omega=1, s^E)}{\pi(s^A|\omega=0, s^E)} \right)$ such that $a^*(s^A, s^E; p) = 0$, $a^*(s^E; p) = 1$, and $a^*(s^A, s^E; \pi) = 1$. Equivalently, we need to find values such that $\log c_{rel} > b \log \frac{\pi(s^A|\omega=1, s^E)}{\pi(s^A|\omega=0, s^E)} + d \log \frac{\pi(\omega=1|s^E)}{\pi(\omega=0|s^E)}$, $\log c_{rel} < \log \frac{\pi(\omega=1|s^E)}{\pi(\omega=0|s^E)}$ and $\log c_{rel} < \log \frac{\pi(s^A|\omega=1, s^E)}{\pi(s^A|\omega=0, s^E)} + \log \frac{\pi(\omega=1|s^E)}{\pi(\omega=0|s^E)}$ if $d \neq 1$. Re-write this system as $y = \log \frac{\pi(\omega=1|s^E)}{\pi(\omega=0|s^E)} - \log c_{rel}$ and $x = \log \frac{\pi(s^A|\omega=1, s^E)}{\pi(s^A|\omega=0, s^E)}$, we need to find a solution to the system $y > 0$, $x + y > 0$ and $bx + dy < (1 - d) \log c_{rel}$. Since $(1 - d) \log c_{rel} > 0$, there exist small enough values of $x, y > 0$ such that the solution exists.
- $(1 - d) \log c_{rel} < 0$: An argument analogous of case 1 shows that there exist values of $\left(\log \frac{\pi(\omega=1|s^E)}{\pi(\omega=0|s^E)}, \log \frac{\pi(s^A|\omega=1, s^E)}{\pi(s^A|\omega=0, s^E)} \right)$ such that $a^*(s^A, s^E; p) = 1$, $a^*(s^E; p) = 0$, and $a^*(s^A, s^E; \pi) = 0$.

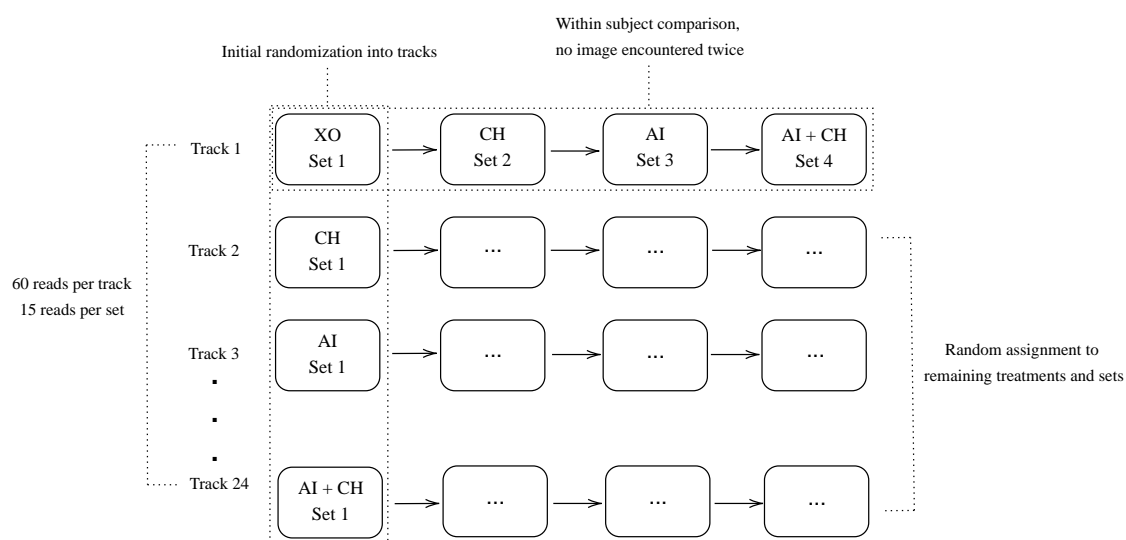
A.2 Proof of Proposition 2

Consider $\log c_{rel} > \log \frac{\pi(\omega=1|s^E)}{\pi(\omega=0|s^E)}$ and $\log c_{rel} < b \log \frac{\pi(s^A|\omega=1)}{\pi(s^A|\omega=0)} + d \log \frac{\pi(\omega=1|s^E)}{\pi(\omega=0|s^E)}$ so that $0 = a^*(s^E; p) \neq a^*(s^A, s^E; p) = 1$. For small enough $\log \frac{\pi(s^A|\omega=1, s^E)}{\pi(s^A|\omega=0, s^E)}$, $\log c_{rel} < \log \frac{\pi(s^A|\omega=1)}{\pi(s^A|\omega=0)} + \log \frac{\pi(\omega=1|s^E)}{\pi(\omega=0|s^E)}$ so that $a^*(s^A, s^E; \pi) = 0$. The case in which $\log c_{rel} < \log \frac{\pi(\omega=1|s^E)}{\pi(\omega=0|s^E)}$ is analagous.

B Appendix of Experimental Interface and Instructions

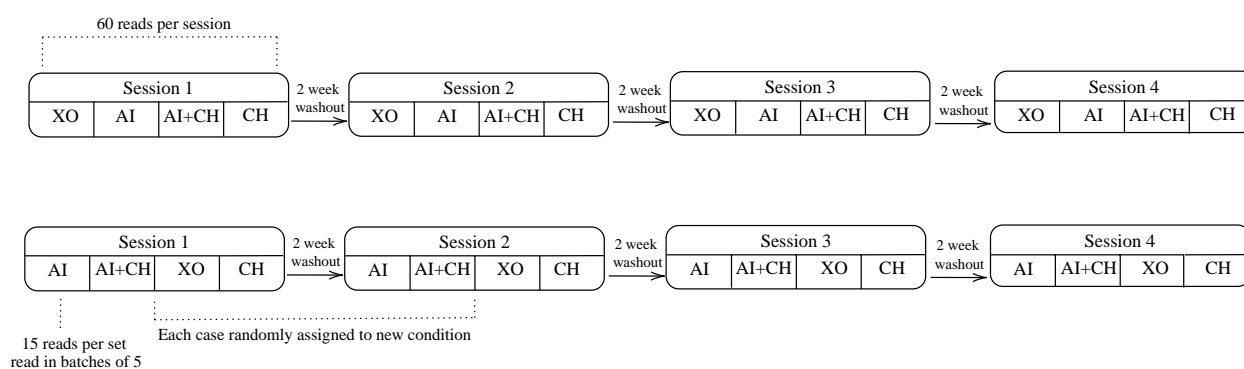
B.1 Design

Figure B.1: Design 1



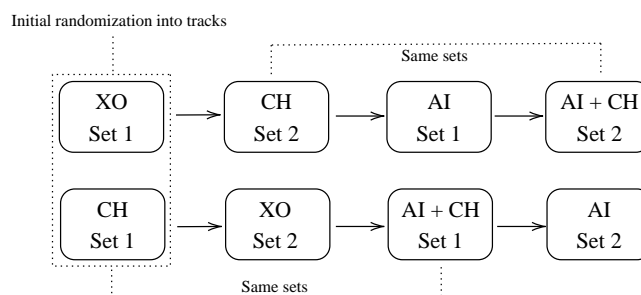
Note: In this design, radiologists are assigned to a randomized sequence of the four information environments., resulting in twenty-four possible tracks. Under each information environment they read fifteen cases. Radiologists encounter each patient case at most once. At the beginning of the experiment every radiologist reads eight practice cases. Furthermore, a random half of the participating radiologists receive incentives for accuracy.

Figure B.2: Design 2



Note: In this design, radiologists diagnose sixty patient cases each under the four information environments. Radiologists read every case under every information environment across four sessions, separated by a washout period. Each case is only encountered once per session and to ensure that radiologists do not recall their/AI predictions from previous reads of the same cases, we ensure a minimum two-week washout period between two subsequent sessions. Within every experimental session they therefore read fifteen under each information environment. The randomization occurs at the track-level where every track has a different sequence of the information environments. (Example tracks shown here.)

Figure B.3: Design 3



Note: In this design, radiologists diagnose fifty cases, first without and then with AI assistance. Clinical history is randomly provided in either the first or second half of images forming the basis of the randomization. The cases diagnosed with and without clinical history are different.

B.2 Instructions

Below you will find the instructions received by the subjects when receiving the interface-based treatment. Comments on the instructions are provided in italics and were not seen by subjects.

Instructions

You are about to participate in a study on medical decision making. You may pause the study at any time. To resume, revisit the link you were given and your progress will have been saved.

We will present you with adult patients with potential thoracic pathologies. These patients will be presented under the following four scenarios:

1. Only a chest X-ray is shown.
2. An X-ray is accompanied with additional information about the clinical history.
3. An X-ray is shown along with Artificial Intelligence (AI) support. This AI tool is described in further detail below.
4. An X-ray is shown along with both additional information on clinical history and the AI support.

The patients are randomly assigned to each of these scenarios. That is, availability of clinical history and/or AI support is unrelated to the patient.

Clinical History: includes available lab results or indications by the treating physician, if any.

AI support: This tool uses only the X-ray image to predict the probability of each potential pathology of interest. The tool is based on state-of-the-art machine learning algorithms developed by a leading team of researchers at Stanford University.

Responses

For each patient and pathology, we will ask for both an assessment and a treatment decision:

1. We will first ask for your assessment of the probability that each condition is present in a patient. **Please consider all pathologies and findings that would be relevant in a radiology report for the patient. You should express your uncertainty about the presence of one or many conditions by appropriately choosing the probability.** Note that it is possible that the patient has multiple such conditions or none of them.
2. If you determine that a pathology may be present, we may ask you to rate the severity and/or extent of the disease on a scale.
3. Finally, when relevant we will ask whether you would recommend treatment or follow up according to the clinical standard of care if you determine that the pathology may be present. The first two responses are diagnostic while the third is a clinical decision. We are aware that a single physician or radiologist typically does not perform both tasks. However, for this study, we ask that you respond to the best of your ability in both of these roles.

Browser Compatibility

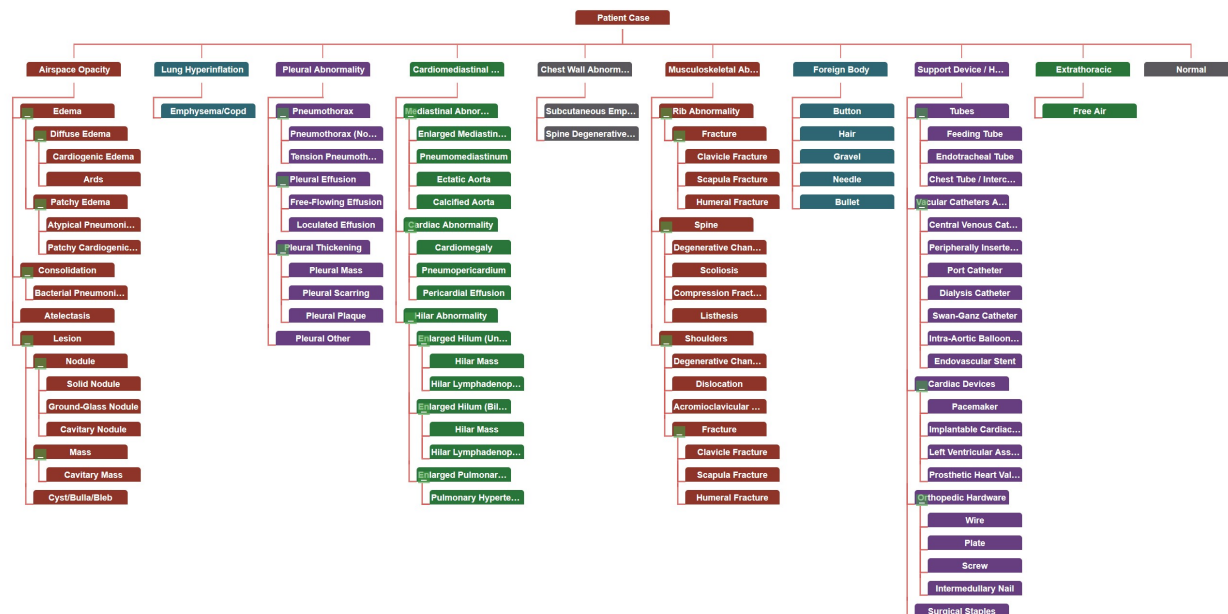
This platform supports desktop versions of Chrome, Firefox, and Edge. Important features on non-supported browsers (including Safari) are missing and we discourage their use for this experiment. In addition, the platform does not support any mobile devices and the platform will perform poorly on mobile. If you encounter any issues during the experiment, please send an email to DiagnosticAI@mit.edu and we will follow-up quickly.

Hierarchy

The interface uses a hierarchy to categorize various thoracic conditions. It will be useful to familiarize yourself with this hierarchy before you start, but you may also revisit the hierarchy at any time throughout the experiment by clicking the help tab in the upper right corner.

[The probability for the sub-pathologies is required only if the parent pathology prevalence is greater than 10%]

Figure B.4: Pathology Hierarchy



AI Support Tool

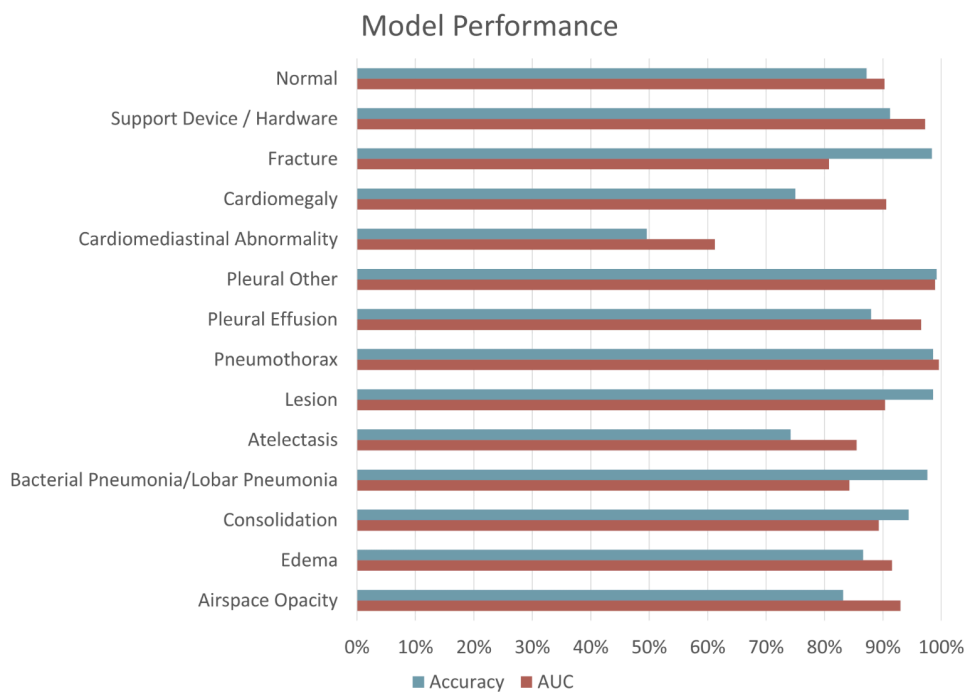
The AI support tool that is provided uses only the X-ray image to predict the probability of each potential pathology of interest. The tool is based on state-of-the-art machine learning algorithms developed by a leading team of researchers at Stanford University. The tool is trained only on X-ray images, meaning it does not incorporate the clinical history of the patients.

Performance of the AI Support

The AI tool is described in Irvin et al. [2019], which showed the AI tool performed at or near expert levels across the pathologies studied. Below we plot two measures of performance of the AI tool. We plot in blue the accuracy of the tool, defined as the share of cases correctly diagnosed when treating false positives and false negatives equally. In red, we plot the Area Under the ROC curve (AUC), which is another measure of AI classification performance.

The AUC is a number between 0 and 100%, with numbers close to 100% representing better algorithm performance. The AUC is equal to the probability that a randomly chosen positive case is ranked higher than a randomly chosen negative case.

Figure B.5: Performance of AI Tool

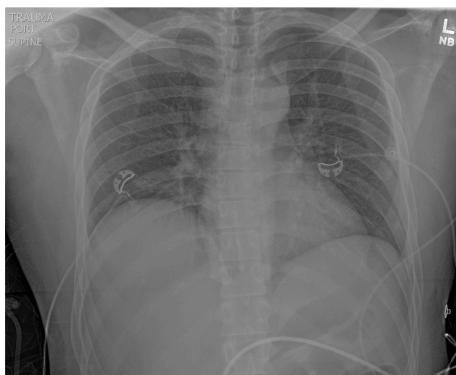


Example Images

Below are 50 example images with the associated AI tool predictions. These images are randomly chosen to allow you to familiarize yourself with the AI support tool and its accuracy *[Here we only provide two out of the fifty images]*.

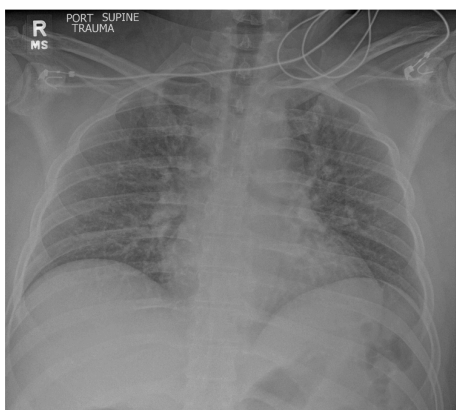
Figure B.6: Example Images

Example 1



Pathology	AI Prediction
Airspace Opacity	16%
• Edema	7%
• Consolidation	3%
◦ Bacterial Pneumonia/Lobar Pneumonia	3%
• Atelectasis	9%
• Lesion	4%
Pleural Abnormality	
• Pneumothorax	7%
• Pleural Effusion	1%
• Pleural Other	0%
Cardiomediastinal Abnormality	14%
◦ Cardiomegaly	1%
Musculoskeletal Abnormality	
◦ Fracture	9%
Support Device / Hardware	12%
Normal	47%

Example 2



Pathology	AI Prediction
Airspace Opacity	42%
• Edema	42%
• Consolidation	14%
◦ Bacterial Pneumonia/Lobar Pneumonia	14%
• Atelectasis	5%
• Lesion	5%
Pleural Abnormality	
• Pneumothorax	3%
• Pleural Effusion	0%
• Pleural Other	1%
Cardiomediastinal Abnormality	16%
◦ Cardiomegaly	5%
Musculoskeletal Abnormality	
◦ Fracture	9%
Support Device / Hardware	3%
Normal	21%

Demonstration

The brief video below walks you through the interface and a few examples. *[At this stage participants saw an instruction video which can be found [here](#)]*

Consent

You have been asked to participate in a study conducted by researchers from the Massachusetts Institute of Technology (M.I.T.) and Harvard University.

The information below provides a summary of the research. Your participation in this research is voluntary and you can withdraw at any time.

1. Study procedure: We will ask you to examine a number of chest x-rays. We will vary both the amount of information provided about the patient and the availability of an AI support tool.
2. Potential Risks & Benefits: There are no foreseeable risks associated with this study and you will receive no direct benefit from participating.

Your participation in this study is completely voluntary and you are free to choose whether to be in it or not. If you choose to be in this study, you may subsequently withdraw from it at any time without penalty or consequences of any kind. The investigator may withdraw you from this research if circumstances arise.

Privacy & Confidentiality

The only people who will know that you are a research subject are members of the research team which might include outside collaborators not affiliated with MIT. No identifiable information about you, or provided by you during the research, will be disclosed to others without your written permission, except: if necessary to protect your rights or welfare, or if required by law. In addition, your information may be reviewed by authorized MIT representatives to ensure compliance with MIT policies and procedures.

When the results of the research are published or discussed in conferences, no information will be included that would reveal your identity.

Questions

If you have any questions or concerns about the research, please feel free to contact us directly at diagnosticAI@mit.edu.

Your Rights

You are not waiving any legal claims, rights or remedies because of your participation in this research study. If you feel you have been treated unfairly, or you have questions regarding

your rights as a research subject, you may contact the Chairman of the Committee on the Use of Humans as Experimental Subjects, M.I.T., Room E25-143B, 77 Massachusetts Ave, Cambridge, MA 02139, phone 1-617-253 6787.

I understand the procedures described above. By clicking next, I am acknowledging my questions have been answered to my satisfaction, and I agree to participate in this study.

Interface questions

[Each of these questions has a true or false response which was entered through a radio button. Participants are not able to start the experiment without answering each question correctly.]

Before beginning the experiment, we would like to confirm a few facts through the following comprehension questions. Please answer True or False to the following questions.

- 1) The algorithm's prediction is based on information from both the X-ray scan as well as the clinical history.
- 2) When the algorithm does not show a prediction, it is because the algorithm thinks the pathology is not present.
- 3) The follow up decision refers to any treatment or additional diagnostic procedures that one would conduct based on the findings of the report.
- 4) Two patients with the same probability score for a condition ought to always receive the same "follow-up" recommendation.
- 5) When a condition at a higher level of the hierarchy receives a less than ten percent chance of being present then all the lower level conditions within this branch automatically receive a zero probability of being present.
- 6) If the algorithm says that the probability of a pathology is present with 80% probability, it means that the AI predicts 80 cases out of 100 have the pathology present.
- 7) Suppose your assessment is that the patient definitely has either edema or consolidation, and you believe that edema is twice as likely as consolidation. Then you would assign 66.67% to edema and 33.33% to consolidation:
- 8) I should only indicate pathologies and findings that would be relevant in a radiology report for the patient.

Interface

Figure B.7 is an example of the clinical history indications available to the participating radiologists under the relevant treatment condition. The thoroughness of the information

varies across available information for every patient. Some examples of varying clinical history information are:

1. 68 years of age, Female, chest pain
2. Unknown age, Unknown, Trauma
3. 55 years of age, Male, Order History: Relevant PMH gastroparesis. Presents with vomiting, retching chest discomfort for a duration of today. Concern for PTX, perforated viscus, pneumomediastinum.
4. 74 years of age, Female, s/p unwitnessed fall, r/o rib fx, pna or effusion
5. Trauma
6. 56 years of age, Male, S/P ICD/ Pacemaker insertion / Complete X-ray without lifting arms above shoulders..


Figure B.7: Clinical History Information

Indication			
30 years of age, Female, history of hypertension, abnormal EKG, abdominal pain, evaluate for cardiomegaly or mediastinal widening.			
Vitals			
Variable	Value		
Weight	170 lbs		
BP	243/166 mmHg		
Temp	99.1F		
Pulse	99.0 bpm		
Age	30		
Abnormal Labs All Labs			
Variable	Value	Unit	Flag
ALT (SGPT), Ser/Plas	38.0	U/L	High
AST (SGOT), Ser/Plas	39.0	U/L	High
Eosinophil, Absolute	0.01	K/uL	Low

Note: The clinical history information environment in the experiment had information on patient indications, vitals and abnormal labs.

Figure B.8: Interface Slider

Airspace Opacity

AI Prediction:  **12% (Very unlikely)**

Highly unlikely	Very unlikely	Unlikely	Possible	Likely	Highly likely
-----------------	---------------	----------	----------	--------	---------------

Probability of Airspace Opacity: 43%

Size Small Medium Large Very Large

Recommend follow up Yes No

Note: The participants use the slider to indicate the probability of a pathology being present for a given patient based on the treatment offered. For prevalence greater than 10% the participants are required to indicate the prevalence of a sub-pathology (if it exists) and whether a follow-up is recommended.

B.3 Additional Details on the AI Algorithm

The training data is a set of tuples of images and labels. These training datasets typically rely on human input to assign the labels, which indicate whether or not a specific pattern or object is present in the image. Training is conducted through stochastic gradient descent. These algorithms build on the nested structure of the neural net to compute gradients computationally efficient via chain rule. Each training step is performed on a small batch of data so that the algorithm does not have to consider the entire dataset for each optimization step. After each round of optimization on the training set, the model performance is assessed through predictions on a hold-out validation sample. Most humans are able to recognize cars, pedestrians, and traffic light, which means that training datasets for common classification tasks are easy to come by. The same is not true for medical imaging. Classifying disease based on X-rays, CT scans, and retina scans requires the input of highly trained experts. Recently, several researchers have released large training datasets of medical images with disease labels that are extracted from written clinical descriptions (Irvin et al., 2019). The neural net has a DenseNet121 architecture. A DenseNet is a type of convolutional neural network that utilizes dense connections between layers through Dense Blocks; in these blocks, we connect all layers with matching feature-map sizes directly with each other. Images are supplied in a standardized format of 320×320 pixels. For optimization the researchers use the Adam optimizer with default β -parameters of $\beta_1 = 0.9$, $\beta_2 = 0.999$ and learning rate 1×10^{-4} . The batch size is fixed at 16 images. The training is performed for 3 epochs. The full training procedure is described in (Irvin et al., 2019).

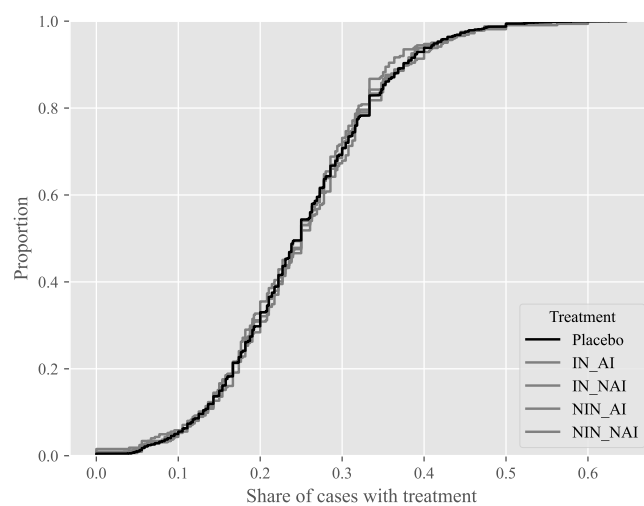
C Data Appendix

C.1 Balance Tests

We verify that the randomization occurred as expected through various balance and randomization tests. Figure C.9 plots the distribution of treatment probabilities by patient-case in Design 1. We also plot a placebo distribution that samples from the null distribution to support the claim that the randomization occurred as expected. To test this formally, we present balance tests for Design 1 and Design 2 in Table C.1 and Table C.2, respectively.³¹ For these balance tests, we calculate the average covariates across the four treatment arms and report p-values from the test of the joint null that the four means are equal. For Design 2, these are done within sessions as patients are balanced by design across all sessions.

³¹Design 3 is balanced by design, as each radiologist reads the same cases with and without AI assistance.

Figure C.9: Distribution of Patient Treatment Probabilities in Design 1



Note: The cumulative distribution functions of patient treatment probabilities by treatment for design 1. The placebo distribution is calculated based on 100,000 draws from the null distribution. For each draw from the null distribution, we sample the number of reads the case receives from the empirical distribution and then draw the number of treatments from a binomial distribution with probability $1/4$.

Table C.1: Covariate Balance in Design 1

	Control	CH	AI	AI x CH	p-value
s_A	0.308	0.299	0.308	0.307	0.410
AIRSPACE OPACITY	0.161	0.142	0.164	0.163	0.222
CARDIOMEDIASTINAL ABNORMALITY	0.130	0.135	0.132	0.131	0.985
SUPPORT DEVICE HARDWARE ABNORMAL	0.173	0.161	0.188	0.195	0.053
WEIGHT	0.183	0.179	0.192	0.191	0.744
TEMP	185.10	186.67	185.46	184.79	0.656
PULSE	99.01	99.04	99.05	99.07	0.057
AGE	92.11	92.68	92.28	93.02	0.012
NUMBER LABS	56.50	56.15	56.31	56.70	0.882
NUMBER FLAGGED LABS	34.59	34.46	34.50	34.27	0.757
FEMALE	5.863	5.914	6.060	5.982	0.646
	0.424	0.412	0.385	0.392	0.080

Note: Balance tests of patient covariates for patients assigned to the four treatments in Design 1. Missing clinical history variables are mean-imputed. The p-values come from the joint test the mean covariates are equal across the four treatments.

Table C.2: Covariate Balance in Design 2

	Session 1	Session 2	Session 3	Session 4
s_A	0.381	0.625	0.381	0.447
AIRSPACE OPACITY	0.243	0.368	0.141	0.483
CARDIOMEDIASTINAL ABNORMALITY	0.164	0.834	0.088	0.716
SUPPORT DEVICE HARDWARE ABNORMAL	0.760	0.770	0.714	0.794
WEIGHT	0.265	0.624	0.722	0.330
TEMP	0.461	0.597	0.878	0.735
PULSE	0.107	0.245	0.437	0.654
AGE	0.242	0.578	0.764	0.772
NUMBER LABS	0.559	0.220	0.082	0.898
NUMBER FLAGGED LABS	0.075	0.348	0.581	0.768
FEMALE	0.297	0.189	0.935	0.738
	0.067	0.052	0.225	0.075

Note: Balance test p-values that the covariate means are equal across the four treatments within each session (column). Missing clinical history variables are mean-imputed.

C.2

C.2 Quality of Ground Truth Reads

Here, we summarize evidence that the ground truth measure we construct is high quality and robust to various decisions an analyst could make. Recall that the preferred ground truth used throughout the paper is defined using the reads of five board-certified radiologists from Mount Sinai, who each read all 324 patient cases in the study. For each pathology, we aggregate these reports into the ground truth for a patient case i as

$$\omega_i = 1 \left[\sum_{r=1}^5 \frac{\pi_r(\omega_i = 1 | s_{i,r}^E)}{5} > \frac{1}{2} \right]$$

where we suppress the pathology index for simplicity and r indexes the radiologist. This method of aggregating reports is robust to certain types of measurement error and dependence across reports as discussed in [Wallsten and Diederich \(2001\)](#). [Table C.3](#) contains summary statistics for the ground truth created using the Mount Sinai radiologists and a leave-one-out internal ground truth calculated using the reads collected during the experiment under the treatment arm with clinical history but no AI assistance. [Table C.4](#) contains additional summary statistics for the five Mount Sinai ground truth labelers, including their average time and number of clicks. We also show the average agreement of the labels with the original radiologist’s read. Taken together, these analyses demonstrate, for the majority of cases, that the ground truth labelers agree with the assessment of the radiologist who originally read the report in a clinical setting and we can reject that the average probability assessment is equal to 0.5 at the 5% level. Moreover, in [Section C.4.2](#) we show that our results are robust to many different methods of calculating ground truth, including using the experiment leave-one-out ground truth and various aggregation methods of the Mount Sinai reports.

Table C.3: Ground Truth Quality

	Prevalence		Share Rejecting 0.5		Average Number of Rads	
	Sinai	Experiment	Sinai	Experiment	Sinai	Experiment
Top-Level with AI	0.147	0.125	0.696	0.775	5.00	14.04
Pooled with AI	0.043	0.031	0.892	0.932	5.00	14.04
Abnormal	0.194	0.525	0.583	0.568	5.00	14.04
All Pathologies	0.013	0.010	0.953	0.977	5.00	14.04

Note: For each of the pre-registered pathology groups, this table shows the average prevalence, the share of cases where we can reject that $\sum_{r=1}^R \frac{\pi_r(\omega_i=1|s_{i,r}^E)}{R} = 0.5$ at the 5% level, and the average number of reads per case for both the Mount Sinai ground truth labels and the experiment leave-one-out ground truth.

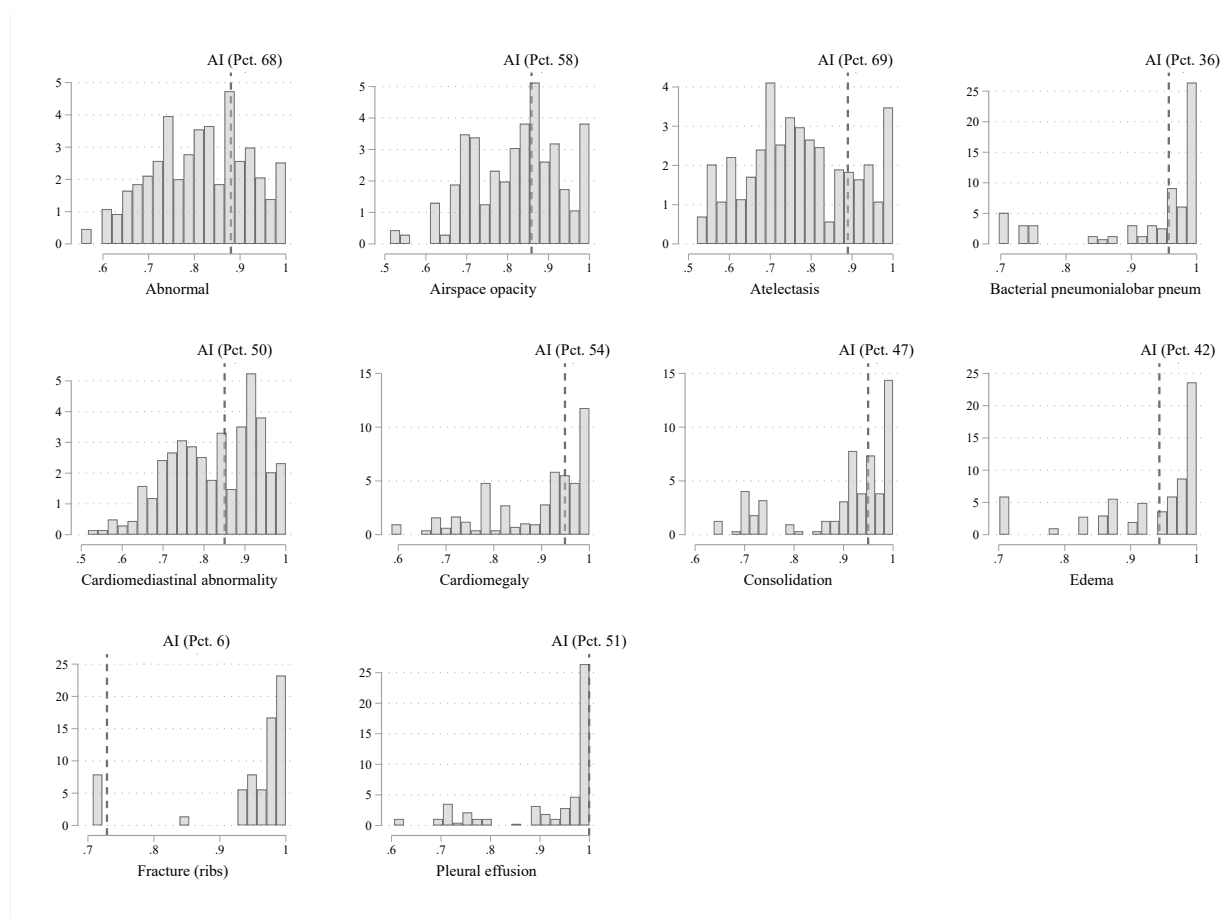
Table C.4: Ground Truth Effort

	Active Time		Clicks		Agreement with Original
	Mean	SD	Mean	SD	
1	77.24	42.78	34.30	17.93	0.868
2	76.44	54.71	32.30	18.24	0.851
3	25.55	30.34	10.84	12.29	0.876
4	79.94	80.22	21.79	20.59	0.866
5	112.96	82.96	26.14	20.12	0.863

Note: For each of the five Mount Sinai radiologists we compute the average and standard deviation of time spent per case and the number of clicks per case. In addition, we compute the average agreement with the original read as labeled by the CheXbert algorithm.

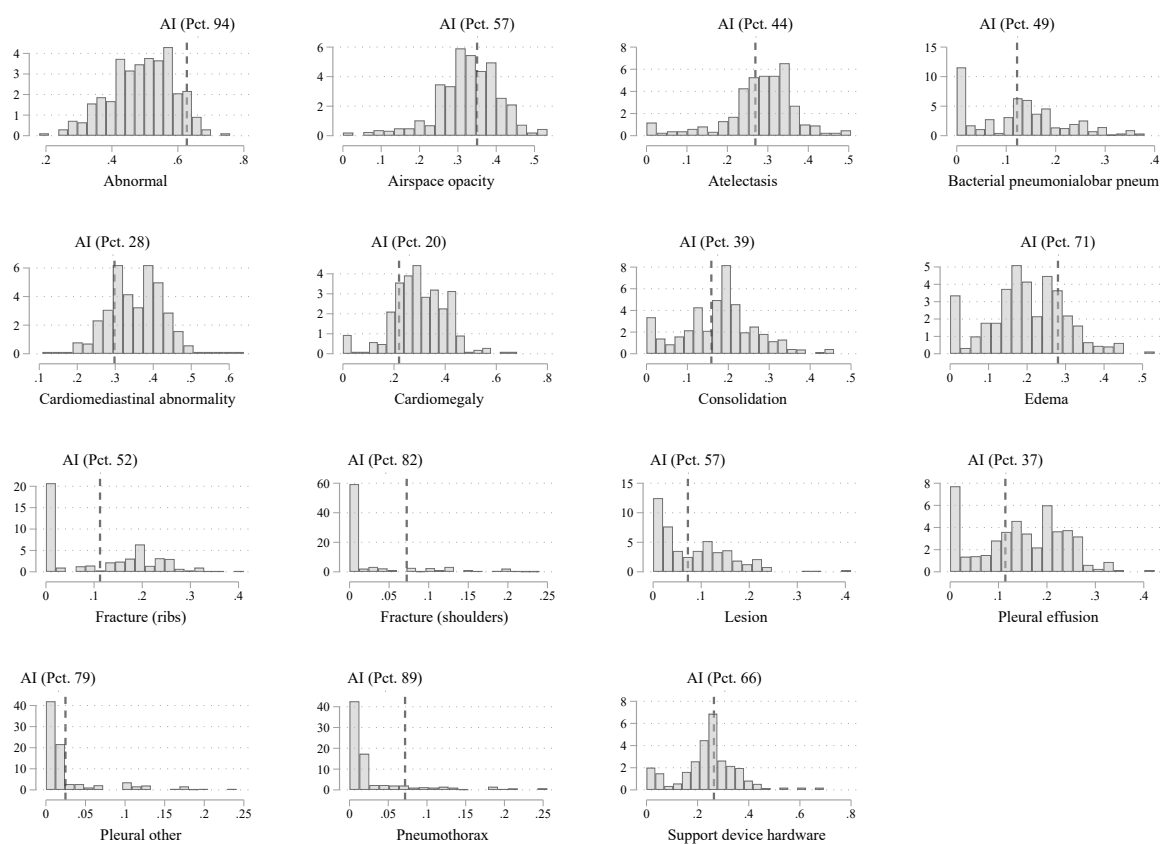
This section presents distributions for two different accuracy measures for radiologists and the AI across different pathology groups. These figures allow for a comparison between the accuracy of the AI relative to the mean radiologist.

Figure C.10: AUROC



Note: This figure summarizes the distribution of radiologist AUROCs across different pathologies, as well as the AUROC of the AI algorithm for the corresponding pathology. Only the cases where contextual history information is available for the radiologist but not the AI prediction were considered.

Figure C.11: RMSE



Note: This figure summarizes the distribution of radiologist RMSE across different pathologies, as well as the RMSE of the AI algorithm for the corresponding pathology. Only the cases where contextual history information is available for the radiologist but not the AI prediction were considered.

C.3 Comparison of Radiologists to Original Reads

The reports from the radiologists who originally read the patient cases included in our sample were classified as positive/negative/uncertain for each pathology using AI predictions generated by the CheXbert algorithm described in [Smit et al. \(2020\)](#). We compare the accuracy of the original reads relative to the ground truth with the radiologists in our sample under the treatment arm with clinical history and no AI assistance. We do this for each pathology by converting the probability reports elicited during the experiment to positive/negative assessments, where positive is defined as having a probability greater than 50%. We convert the CheXbert labels to positive/negative assessments by including the uncertain cases as positive.³² We then calculate the accuracy of the experiment reads and the CheXbert labels for groups of pathologies focused on in this study and test the null hypothesis that the accuracy of the radiologists is the same. The results of this analysis are in [Table C.5](#), and those for when treating uncertain cases negative are in [Table C.6](#).

Table C.5: Comparing Experiment Assessments to Original Reads

	Top-Level with AI (1)	Pooled with AI (2)	Abnormal (3)
EXPERIMENT	-0.004 (0.016)	-0.005 (0.006)	-0.086 (0.025)
CONSTANT	0.194 (0.016)	0.090 (0.006)	0.466 (0.028)
OBSERVATIONS	9718	53449	4859
R-SQUARED	0.000	0.000	0.002

Note: Regression of indicator equal to one if binarized assessment is equal to ground truth from both the original reads and experiment reads onto a constant and an indicator equal to one if the radiologist was in the experiment. Standard errors are clustered at the patient-case level.

³²For all pathologies but bacterial pneumonia and atelectasis, fewer than 5% of patients have uncertain cases. For abnormal and all of the top-level pathologies with AI, there are no cases with uncertain labels.

Table C.6: Comparing Experiment to Original Reads: Uncertain as Not Present

	Top-Level with AI (1)	Pooled with AI (2)	Abnormal (3)
EXPERIMENT	-0.004 (0.016)	0.020 (0.005)	-0.086 (0.025)
CONSTANT	0.194 (0.016)	0.065 (0.005)	0.466 (0.028)
OBSERVATIONS	9718	53449	4859
R-SQUARED	0.000	0.000	0.002

Note: Regression of indicator equal to one if binarized assessment is equal to ground truth from both the original reads and experiment reads onto a constant and an indicator equal to one if the radiologist was in the experiment. Standard errors are clustered at the patient-case level.

C.4 Robustness

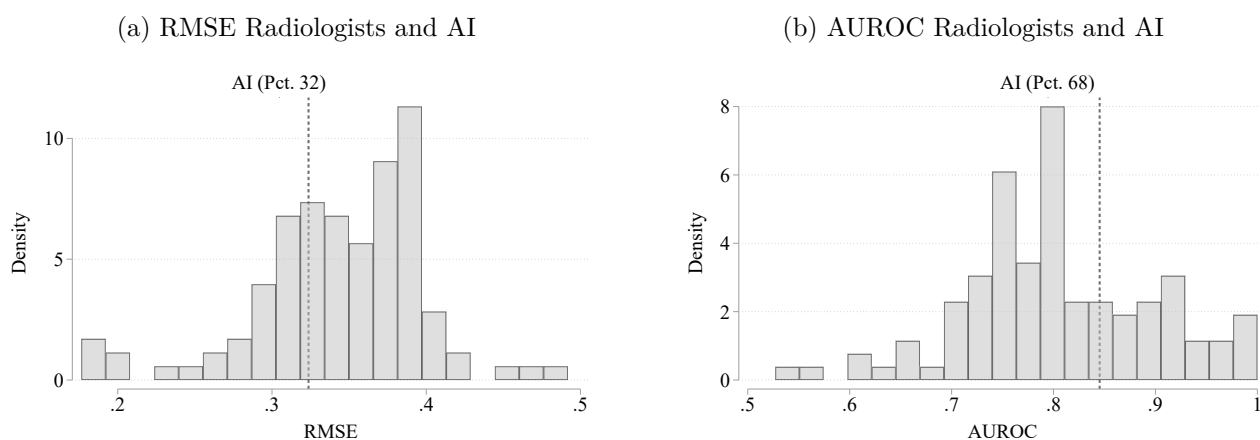
In this section, we show the robustness of the results from Section 4.2.

C.4.1 By Design

Design 1

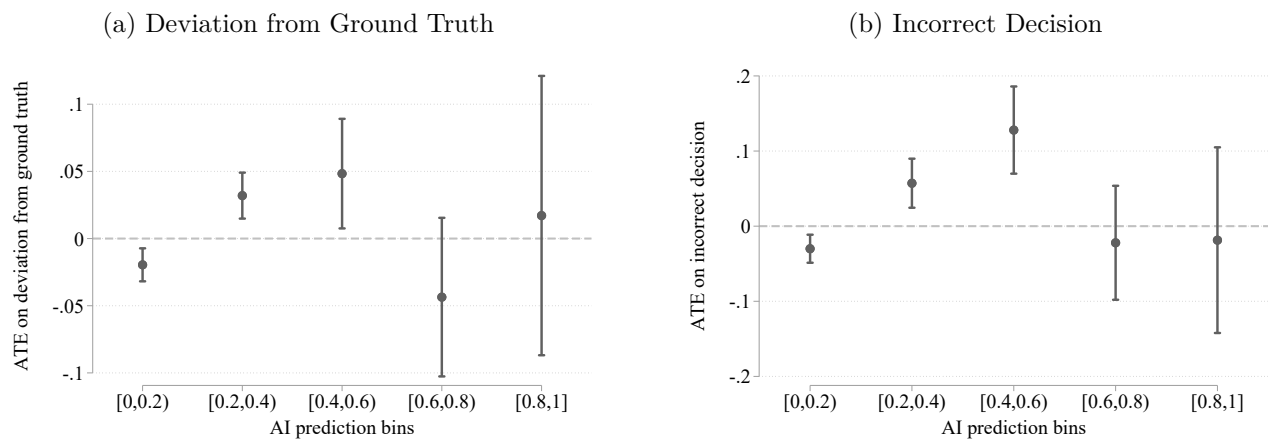
This section presents summaries of radiologist accuracy and treatment effect estimates using data from design 1. We do not present treatment effects conditional on radiologist prediction as some cases are not read in the design.

Figure C.12: Comparing AI performance to Radiologists



Note: Main specifications similar to figure 1 with the exception that observations are from design 1 only.

Figure C.13: Conditional treatment effect given AI prediction



Note: Main specifications similar to figure 3 with the exception that observations are from design 1 only.

Design 2

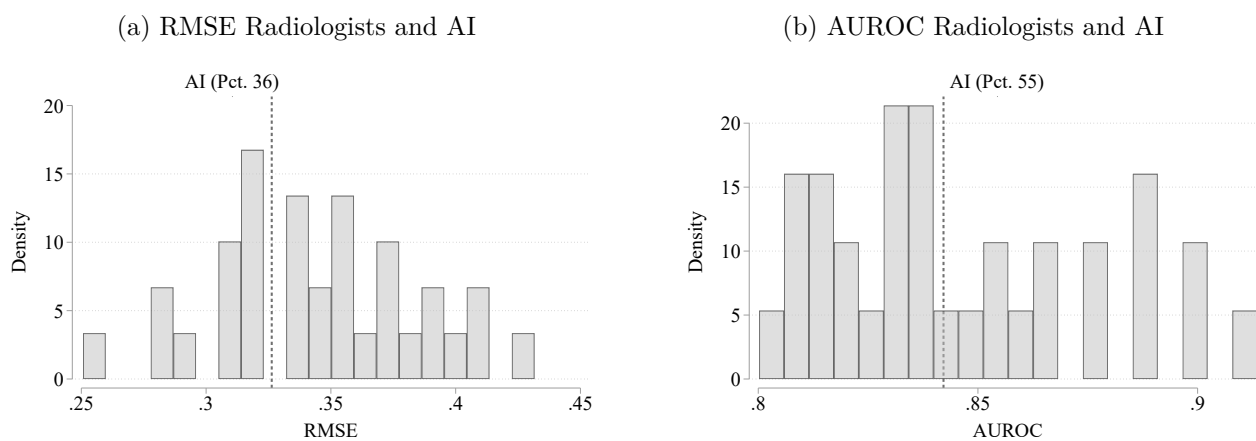
This section presents summaries of key variables, radiologist accuracy and treatment effect estimates using data from design 2.

Table C.7: Summary Statistics

	Mean	SD
	(1)	(2)
Reported Probability	0.245	0.278
Decision	0.400	0.490
Deviation from Ground Truth	0.232	0.265
Deviation from AI	0.172	0.159
Correct Decision	0.620	0.485
Active time	2.76	1.93
Observations	15,840	
Radiologists	33	

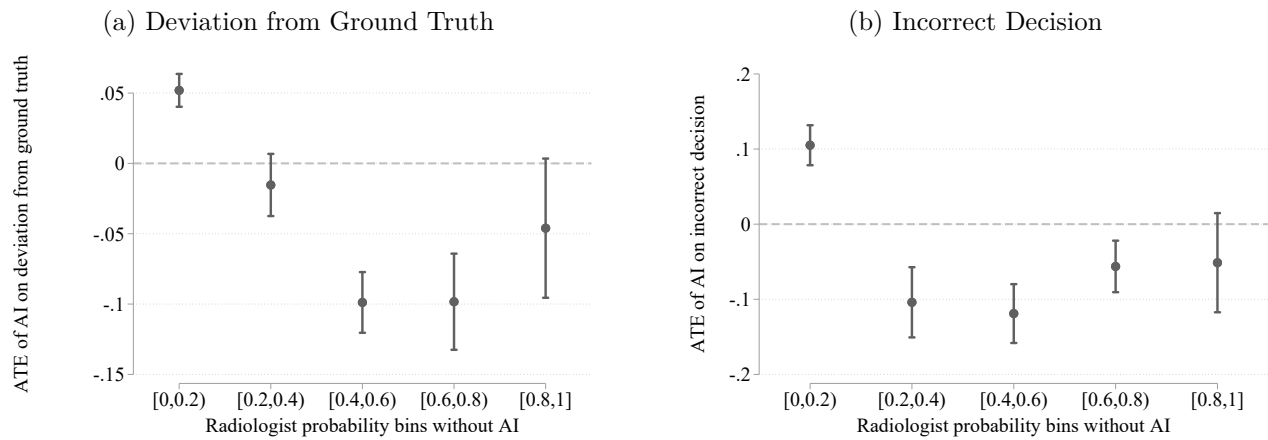
Note: This table presents summary statistics of design 2 similar to table 1.

Figure C.14: Comparing AI performance to Radiologists



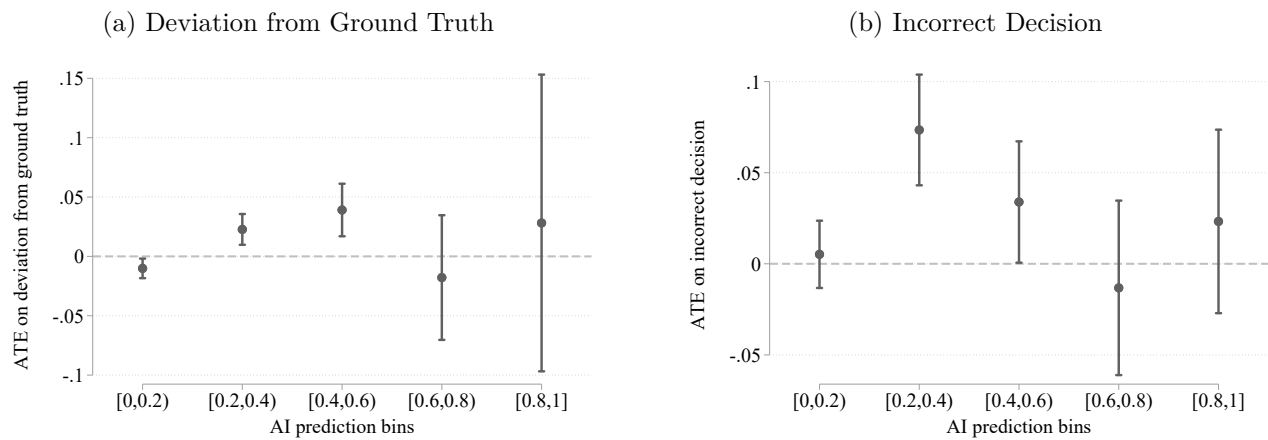
Note: Main specifications similar to figure 1 with the exception that observations are from design 2 only.

Figure C.15: Conditional treatment effect given radiologist prediction



Note: Main specifications similar to figure 2 with the exception that observations are from design 2 only.

Figure C.16: Conditional treatment effect given AI prediction



Note: Main specifications similar to figure 3 with the exception that observations are from design 2 only.

Table C.8: Average Treatment Effects

Treatment	Deviation from AI	Deviation from Ground Truth	Effort Measures	
	(1)	(2)	Active Time	Clicks
AI × CH	−0.001 (0.003)	0.003 (0.004)	−1.63 (3.45)	0.13 (0.64)
AI	−0.034 (0.004)	0.004 (0.004)	7.16 (2.24)	1.17 (0.53)
CH	0.001 (0.002)	−0.008 (0.003)	8.09 (2.36)	0.22 (0.44)
CONTROL MEAN	0.189 (0.009)	0.234 (0.013)	154.19 (5.71)	47.25 (1.75)
PATHOLOGY FE OBSERVATIONS	Yes 15840	Yes 15840	- 7917	- 7917

Note: Main specifications similar to table 2 with the exception that observations are from design 2 only.

Design 3

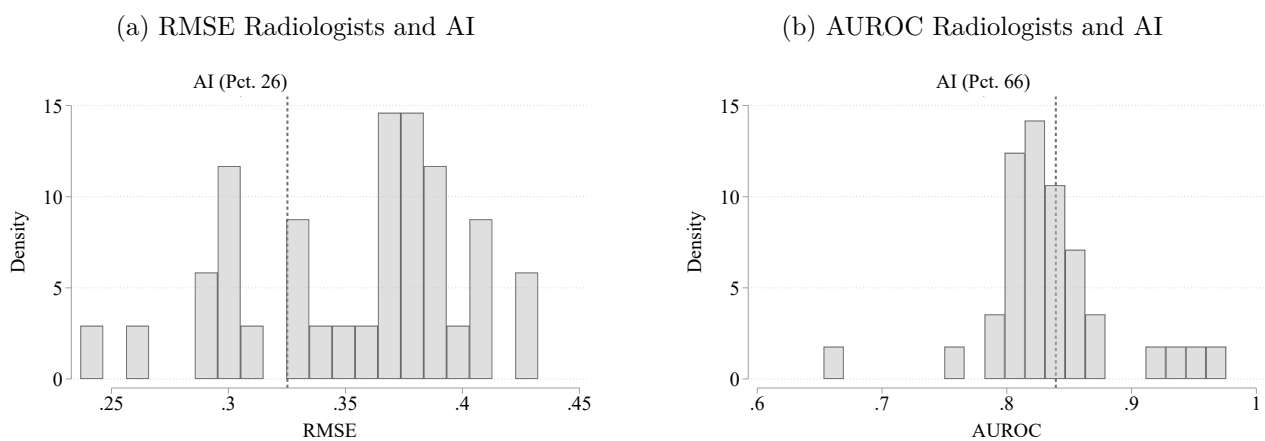
This section presents summaries of key variables, radiologist accuracy and treatment effect estimates using data from design 3.

Table C.9: Summary Statistics

	Mean	SD
	(1)	(2)
Reported Probability	0.240	0.322
Decision	0.231	0.421
Deviation from Ground Truth	0.212	0.297
Deviation from AI	0.216	0.182
Correct Decision	0.785	0.411
Active time	2.58	2.80
Observations	7,000	
Radiologists	35	

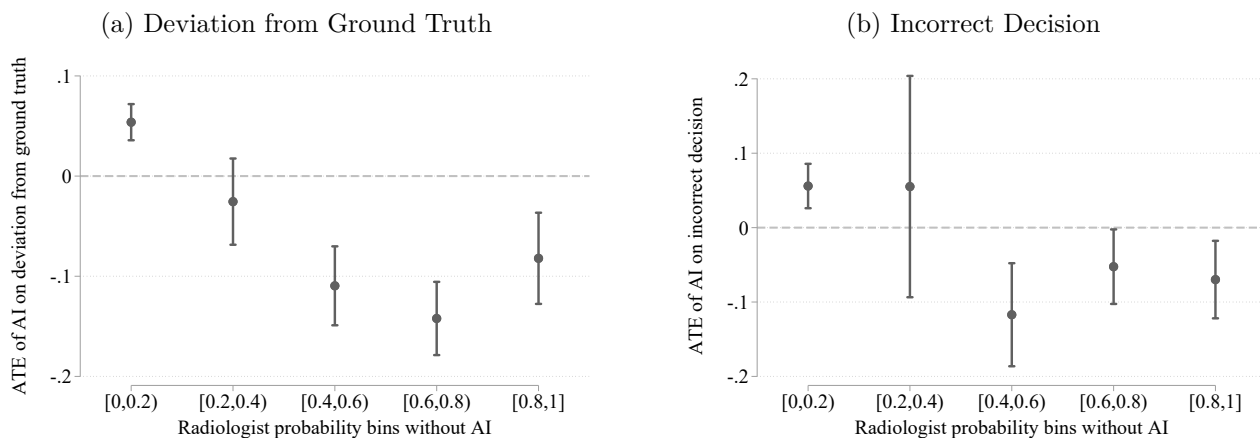
Note: This table presents summary statistics of design 3 similar to table 1.

Figure C.17: Comparing AI performance to Radiologists



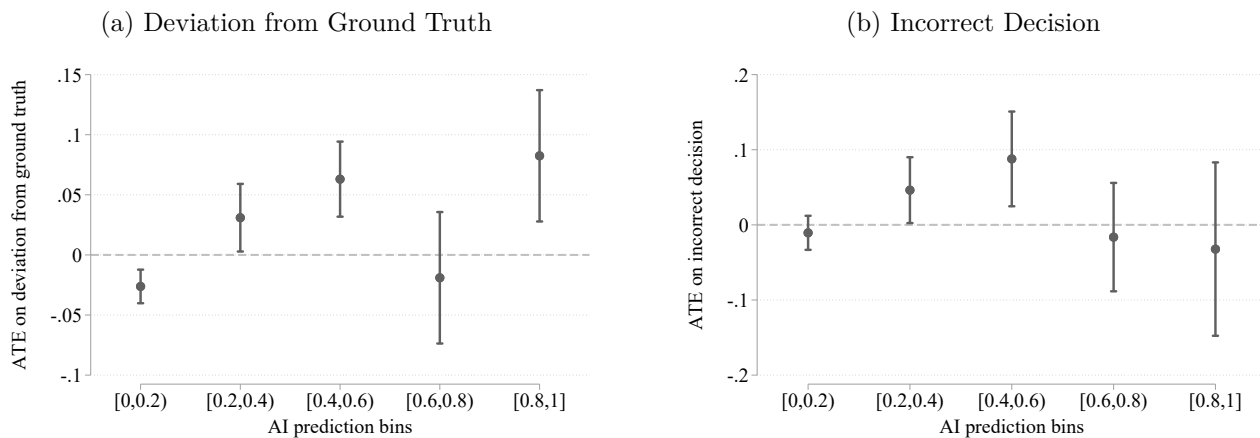
Note: Main specifications similar to figure 1 with the exception that observations are from design 3 only.

Figure C.18: Conditional treatment effect given radiologist prediction



Note: Main specifications similar to figure 2 with the exception that observations are from design 3 only.

Figure C.19: Conditional treatment effect given AI prediction



Note: Main specifications similar to figure 3 with the exception that observations are from design 3 only.

Table C.10: Average Treatment Effects

	Deviation from AI	Deviation from Ground Truth
Treatment	(1)	(2)
AI × CH	0.009 (0.008)	0.010 (0.012)
AI	-0.050 (0.010)	-0.003 (0.008)
CH	-0.003 (0.009)	-0.010 (0.013)
CONTROL MEAN	0.241 (0.011)	0.216 (0.015)
PATHOLOGY FE	Yes	Yes
OBSERVATIONS	7000	7000

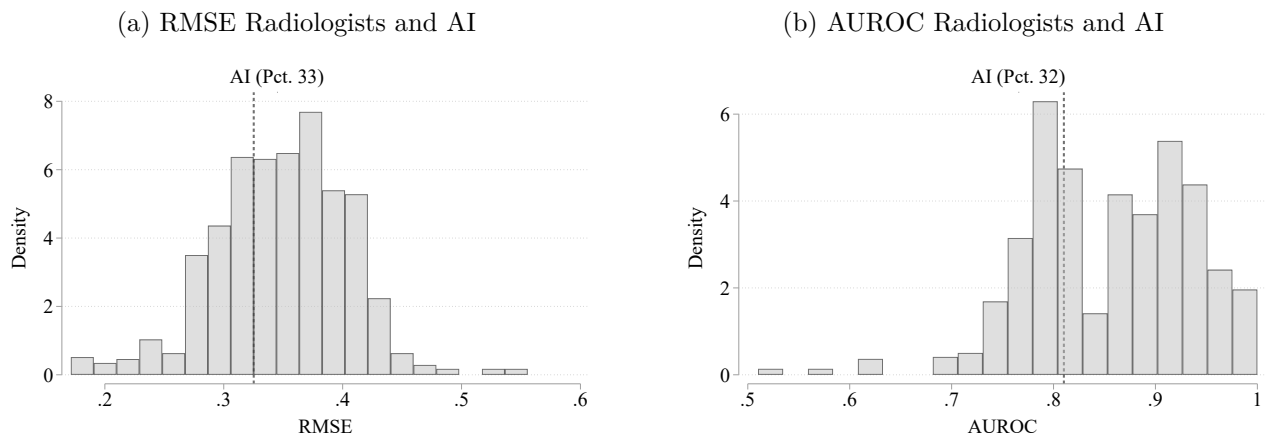
Note: Main specifications similar to table 2 with the exception that observations are from design 3 only.

C.4.2 By Definition of Ground Truths

Experiment leave-one-out Ground Truth

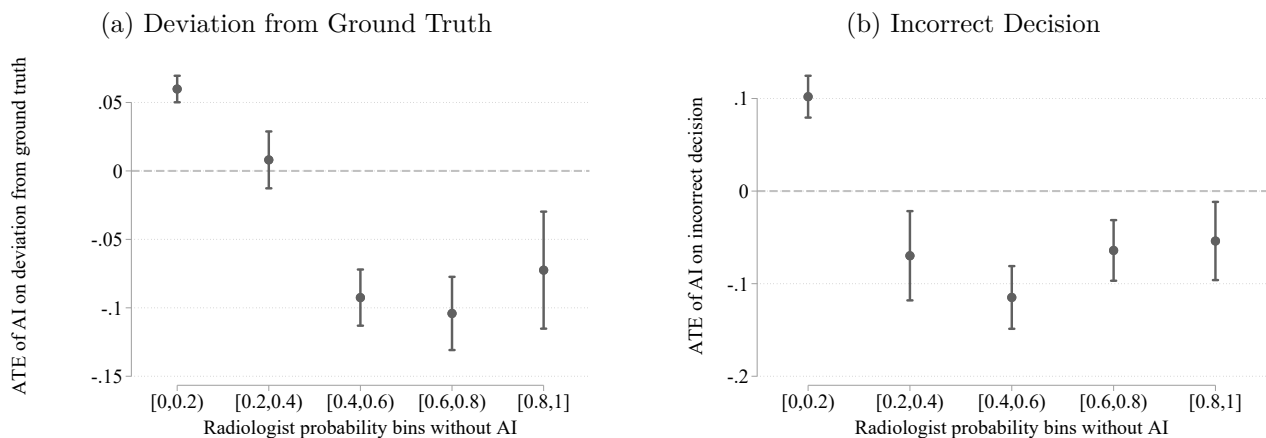
This section computes the main results using a ground truth constructed using a leave-one-out average of assessments by radiologists participating in the experiment in the treatment arm with clinical history but no AI assistance. Specifically, for each radiologist r and patient case i we construct $\omega_{ir} = 1 \left[\sum_{r' \neq r} \frac{\pi(\omega_i=1|s_{ir}^E)}{N_i-1} > 0.5 \right]$.

Figure C.20: Comparing AI performance to Radiologists



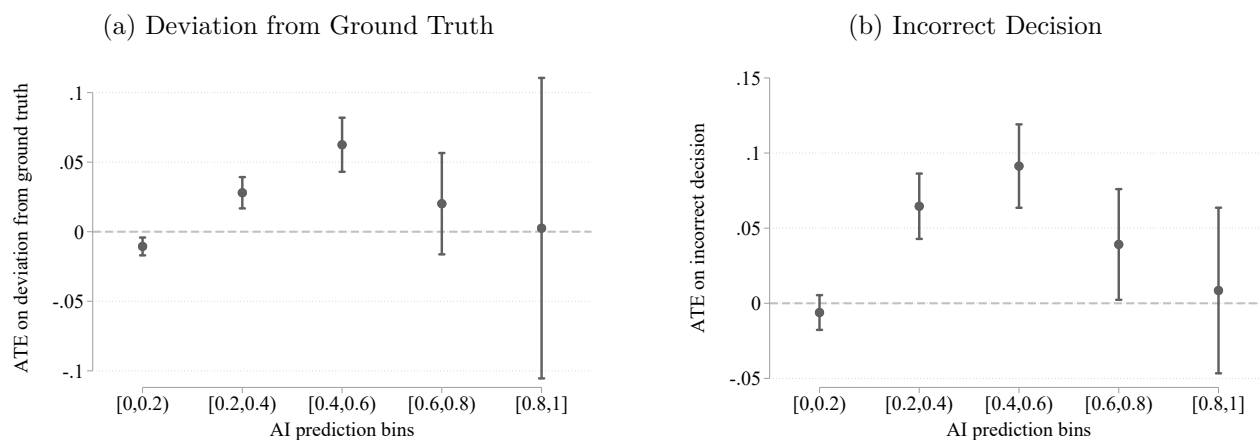
Note: Main specifications similar to figure 1 with the exception that ground truth is constructed using experiment leave-one-out average.

Figure C.21: Conditional treatment effect given radiologist prediction



Note: Main specifications similar to figure 2 with the exception that ground truth is constructed using experiment leave-one-out average.

Figure C.22: Conditional treatment effect given AI prediction



Note: Main specifications similar to figure 3 with the exception that ground truth is constructed using experiment leave-one-out average.

Table C.11: Average Treatment Effects

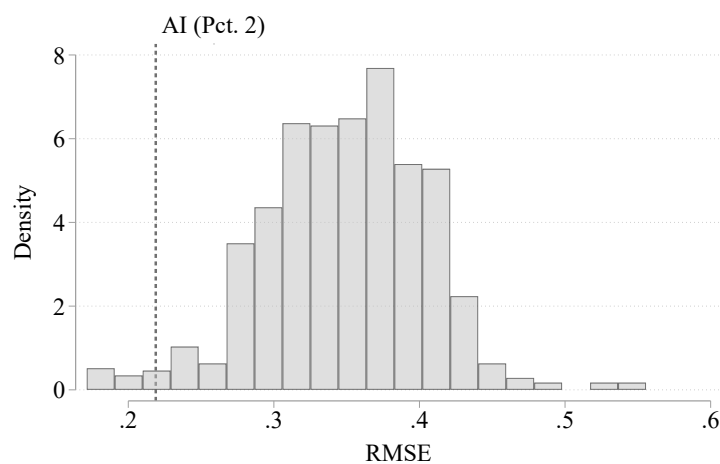
Deviation from Ground Truth	
Treatment	(1)
AI × CH	0.009 (0.005)
AI	0.007 (0.004)
CH	−0.016 (0.004)
CONTROL MEAN	0.222 (0.010)
PATHOLOGY FE	Yes
OBSERVATIONS	36280

Note: Main specifications similar to table 2 with the exception that ground truth is constructed using experiment leave-one-out average.

Continuous Ground Truth

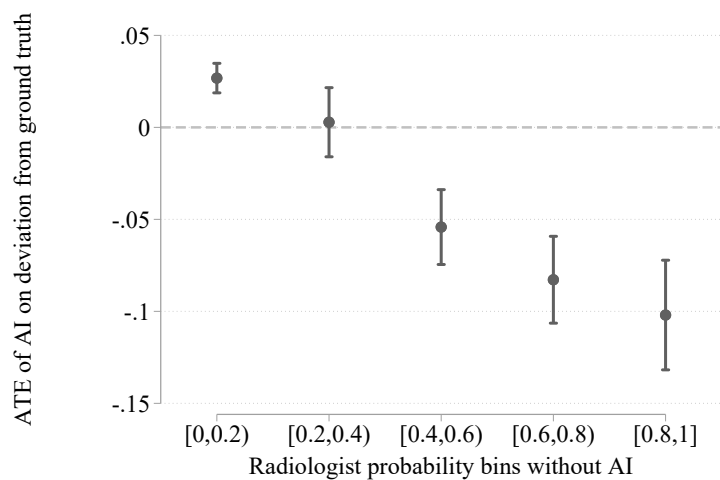
This section computes the main results using a continuous ground truth constructed using a simple average of the ground truth labelers' probability assesment.

Figure C.23: RMSE Radiologists and AI



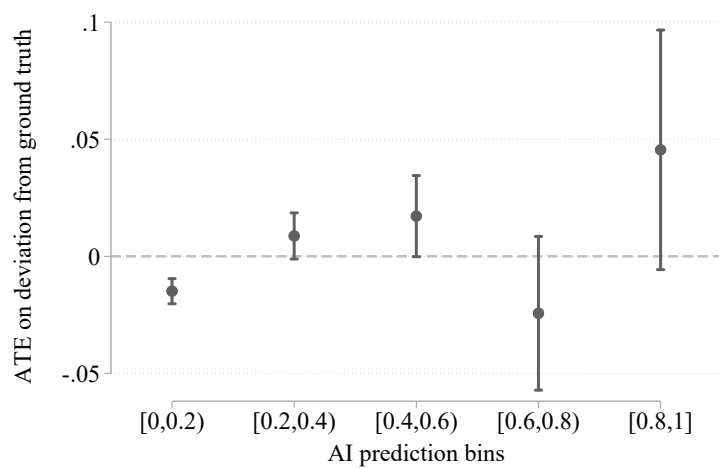
Note: Main specifications similar to figure 1 with the exception that ground truth is constructed using continuous values.

Figure C.24: Conditional treatment effect given radiologist prediction



Note: Main specifications similar to figure 2 with the exception that ground truth is constructed using continuous values.

Figure C.25: Conditional treatment effect given AI prediction



Note: Main specifications similar to figure 3 with the exception that ground truth is constructed using continuous values.

Table C.12: Average Treatment Effects

Deviation from Ground Truth	
Treatment	(1)
AI × CH	0.004 (0.004)
AI	-0.006 (0.003)
CH	-0.009 (0.003)
CONTROL MEAN	0.182 (0.007)
PATHOLOGY FE	Yes
OBSERVATIONS	36280

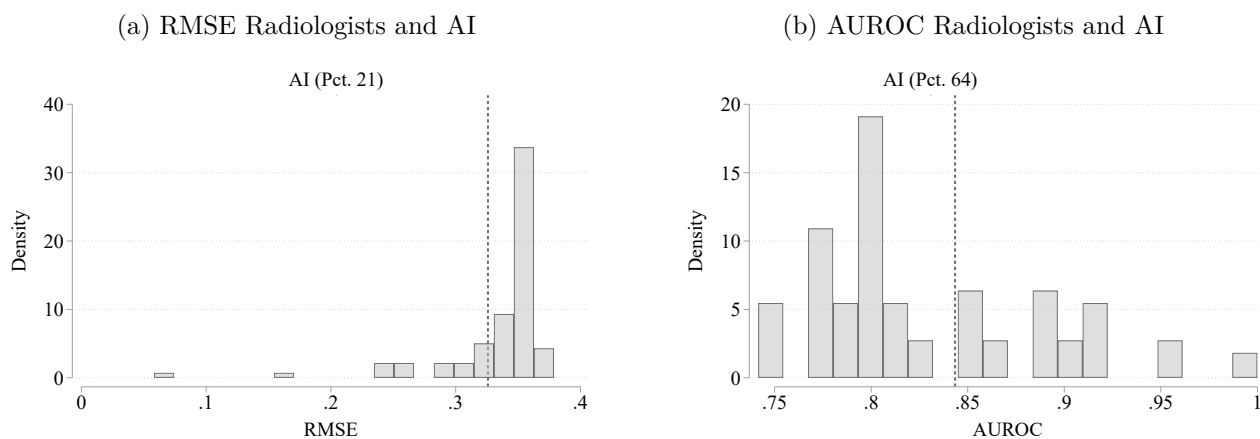
Note: Main specifications similar to table 2 with the exception that ground truth is constructed using continuous values.

C.4.3 Testing for Order Effects

First Treatment (only Design 1 and Design 2)

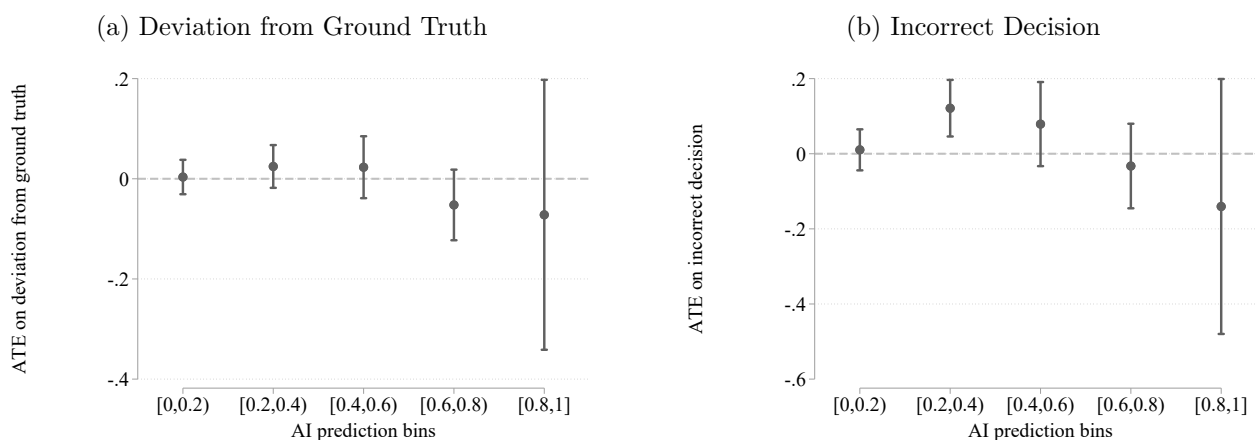
The following graphs contain only those cases from the treatment group that the subjects encountered first. This includes the first 15 reads from design 1 and the first 5 reads from design 2. This exercise is to check if the treatment effects for all the reads is different than for the first reads.

Figure C.26: Comparing AI performance to Radiologists



Note: Main specifications similar to figure 1 with the exception that observations are from the first treatment received in designs 1 and 2 only.

Figure C.27: Conditional treatment effect given AI prediction



Note: Main specifications similar to figure 3 with the exception that observations are from the first treatment received in designs 1 and 2 only.

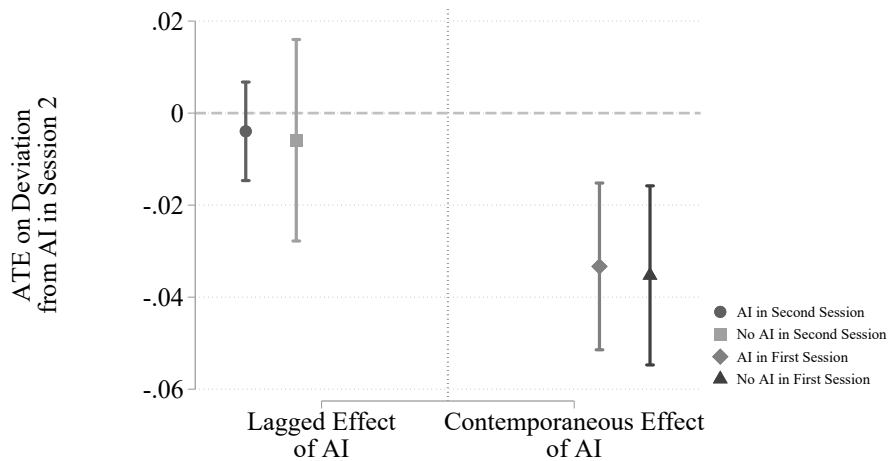
Table C.13: Average Treatment Effects

Treatment	Deviation from AI	Deviation from Ground Truth	Effort Measures	
	(1)	(2)	Active Time	Clicks
AI × CH	-0.027 (0.022)	-0.035 (0.029)	11.15 (28.70)	-0.49 (6.58)
AI	-0.028 (0.017)	0.029 (0.022)	-14.56 (17.94)	1.45 (4.42)
CH	-0.009 (0.016)	-0.010 (0.019)	14.46 (21.96)	0.79 (4.78)
CONTROL MEAN	0.228 (0.010)	0.229 (0.015)	195.90 (14.05)	45.28 (2.93)
PATHOLOGY FE OBSERVATIONS	Yes 3690	Yes 3690	- 1845	- 1845

Note: Main specifications similar to table 2 with the exception that observations are from the first treatment received in designs 1 and 2 only.

Previous Exposure to AI (Design 2)

Figure C.28: Conditional treatment effect given AI prediction



Note: This graph shows the treatment effects of the deviation from AI in the second session because of receiving AI signal in the first session conditional on receiving AI signal in the second session (Lagged Effect). On the other hand, the contemporaneous effects show the deviation from AI in the second session given the participants receive AI in the second session, conditional on receiving AI signal in the second session. These graphs are valid only for design 2 as participants see the same image but in a different information environment.

C.4.4 Incentives

This section tests if incentives for assessment accuracy promote radiologists to make more accurate assessments. We find that the incentives do not play a significant role in getting a correct response. The effect of incentives are estimated using the following regression specification and the results are shown in Table C.14.

$$\begin{aligned}
 Y_{irt} = & \gamma_{h_i} + \gamma_{INC} \cdot d_{INC}(r) \\
 & + \gamma_{CH} \cdot d_{CH}(t) + \gamma_{CH \times INC} \cdot d_{CH}(t) \cdot d_{INC}(r) \\
 & + \gamma_{AI} \cdot d_{AI}(t) + \gamma_{AI \times INC} \cdot d_{AI}(t) \cdot d_{INC}(r) \\
 & + \gamma_{AI \times CH} \cdot d_{CH}(t) \cdot d_{AI}(t) + \gamma_{AI \times CH \times INC} \cdot d_{CH}(t) \cdot d_{AI}(t) \cdot d_{INC}(r) + \varepsilon_{irt}
 \end{aligned}$$

where Y_{irt} is an outcome variable of interest for radiologist r diagnosing patient case-pathology i and treatment t , and γ_{h_i} are pathology fixed effects. Here CH refers to cases with access to clinical history information, AI to cases with AI predictions and INC refers to incentivized cases.

Table C.14: Effect of Incentives

Treatment	Deviation from AI		Deviation from GT		Effort Measures	
	Top-Level with AI (1)	Pooled with AI (2)	Top-Level with AI (3)	Pooled with AI (4)	Active Time (5)	Clicks (6)
AI × CH	−0.002 (0.007)	−0.003 (0.003)	0.002 (0.013)	0.001 (0.004)	−8.71 (8.30)	−1.18 (2.28)
AI	−0.032 (0.007)	−0.013 (0.003)	0.005 (0.009)	0.001 (0.004)	15.46 (6.51)	3.57 (1.66)
CH	0.001 (0.005)	0.001 (0.002)	−0.017 (0.009)	−0.007 (0.004)	10.90 (5.24)	1.01 (1.59)
CONTROL MEAN	0.225 (0.008)	0.113 (0.004)	0.219 (0.012)	0.083 (0.006)	159.47 (9.63)	39.93 (2.07)
AI × CH × INCENTIVES	0.009 (0.010)	0.006 (0.004)	0.006 (0.017)	−0.001 (0.006)	17.51 (13.79)	3.00 (3.26)
AI × INCENTIVES	−0.017 (0.009)	−0.007 (0.004)	−0.009 (0.012)	0.000 (0.005)	−18.42 (9.25)	−4.09 (2.07)
CH × INCENTIVES	−0.008 (0.008)	−0.004 (0.004)	0.007 (0.014)	0.005 (0.005)	−8.75 (9.54)	−1.83 (2.16)
CONTROL MEAN × INCENTIVES	0.005 (0.010)	0.002 (0.004)	0.004 (0.013)	−0.002 (0.005)	4.17 (14.09)	1.56 (3.05)
PATHOLOGY FE	Yes	Yes	Yes	Yes	-	-
OBSERVATIONS	20440	132860	20440	132860	6718	6718
F-STAT	.95	.94	.49	.41	1.09	1.16
P>F-STAT	.44	.44	.74	.80	.36	.33

Note: This table summarizes the average treatment effects (ATE) of different information environments on the (1) absolute value of the difference between the radiologist probability and AI algorithm probability (Columns (1) and (2)), absolute value of the difference between the radiologist probability and the ground truth (Columns (3) and (4)) and radiologists' effort measured in terms of active time and clicks for all and the second-half images (Columns (5) and (6)). The F-statistic tests for the joint significance of the four incentivized groups. Top-level specification includes two pathologies: airspace opacity and cardiomediastinal abnormality while Pooled AI includes all the pathologies with AI predictions excluding abnormality and support device hardware. Only cases in design 1 and design 3 are considered. Two-way clustered standard errors at the radiologist and patient-case level are in parenthesis.

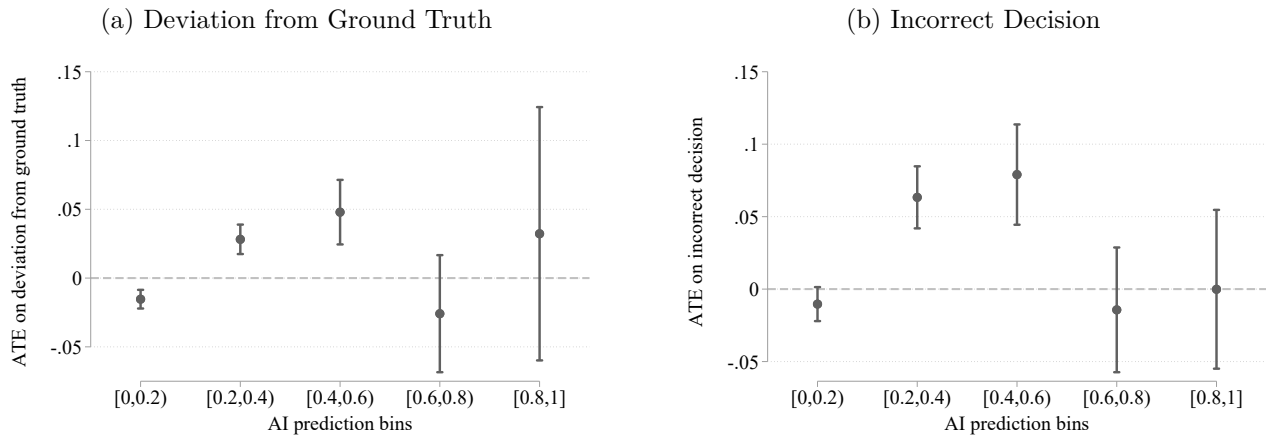
C.4.5 Controlling for sequence number and session

Figure C.29 uses the following specification that controls for the sequence number in which the participants saw a particular case within one experiment session and the session dummies for the different designs and experiment sessions to estimate the heterogeneous treatment effects. There are four sessions in Design 2, whereas Design 1 and 3 have only one session.

$$Y_{irt} = \gamma_{h_i} + \gamma_{AI} \cdot d_{AI}(t) + \sum_g \left[\gamma_g \cdot d_g(s_i^A) + \gamma_{AI \times g} \cdot d_{AI}(t) \cdot d_g(s_i^A) \right] + \gamma_{w_{irt}} + \gamma_{m_{irt}} + \varepsilon_{irt}$$

where Y_{irt} is an outcome variable of interest for radiologist r diagnosing patient case-pathology i and treatment t , γ_{h_i} are pathology fixed effects, $\gamma_{w_{irt}}$ are sequence number dummies and $\gamma_{m_{irt}}$ are session dummies. Here, g is defined as an index for an interval of the AI signal range where $1 \leq g \leq 5$. A case is said to be in an interval g conditional on the signal value for the given patient-case.

Figure C.29: Conditional treatment effect given AI prediction



Note: Main specifications similar to figure 3 with additional controls for rounds and session.

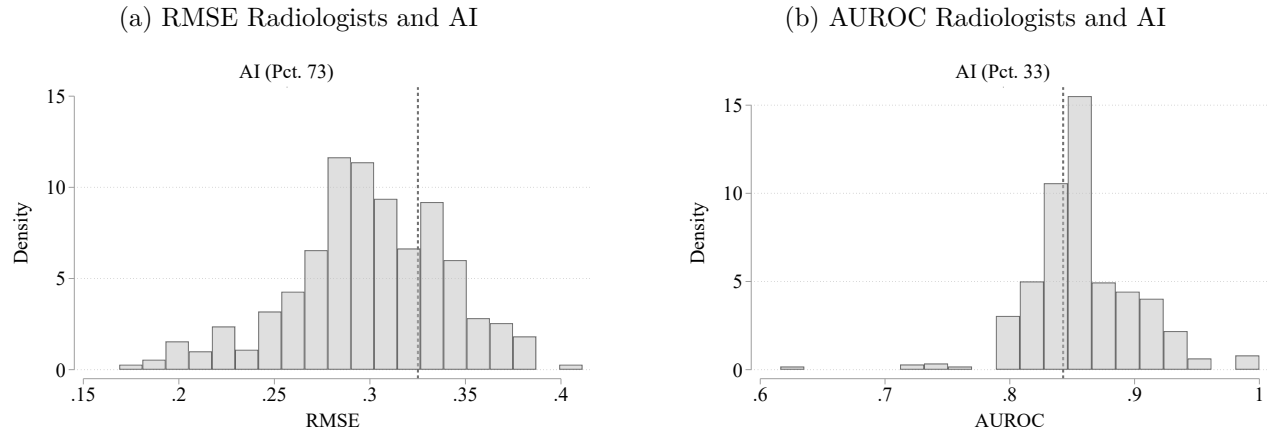
Table C.15: Average Treatment Effects

Sessions	Deviation	Deviation	Effort Measures	
	from AI (1)	from GT (2)	Active Time (3)	Clicks (4)
DESIGN 2: SESSION 1	-0.016 (0.011)	0.029 (0.014)	41.18 (11.17)	14.72 (2.68)
DESIGN 2: SESSION 2	-0.033 (0.010)	0.014 (0.011)	-3.68 (9.91)	6.64 (2.48)
DESIGN 2: SESSION 3	-0.032 (0.011)	0.004 (0.012)	-25.13 (9.77)	3.68 (2.58)
DESIGN 2: SESSION 4	-0.035 (0.010)	0.007 (0.011)	-38.73 (7.87)	1.35 (2.38)
DESIGN 3	0.020 (0.009)	-0.005 (0.012)	- -	- -
CONTROL MEAN	0.219 (0.007)	0.216 (0.010)	164.82 (6.74)	40.76 (1.53)
DESIGN 2: SESSION 1 \times AI	-0.002 (0.007)	0.006 (0.010)	5.09 (6.02)	0.47 (1.30)
DESIGN 2: SESSION 2 \times AI	0.003 (0.008)	-0.005 (0.009)	-1.67 (5.56)	-0.92 (1.26)
DESIGN 2: SESSION 3 \times AI	-0.002 (0.008)	0.001 (0.009)	-1.08 (4.81)	-1.04 (1.29)
DESIGN 2: SESSION 4 \times AI	0.006 (0.007)	0.004 (0.011)	-1.97 (4.86)	-0.28 (1.19)
DESIGN 3 \times AI	-0.009 (0.009)	-0.001 (0.008)	- -	- -
CONTROL MEAN \times AI	-0.036 (0.004)	0.004 (0.005)	6.28 (3.47)	1.69 (0.74)
PATHOLOGY FE	Yes	Yes	-	-
OBSERVATIONS	36280	36280	14635	14635
F-STAT	.63	.26	.46	.42
P>F-STAT	.67	.93	.76	.79

Note: Main specifications similar to table 2 with additional control variables for sequence number of a particular case and the experiment session. Due to the high volume of sequence numbers, we do not show them in this table but account for them. Design 1 session dummy is omitted due to collinearity and is thus the control mean.

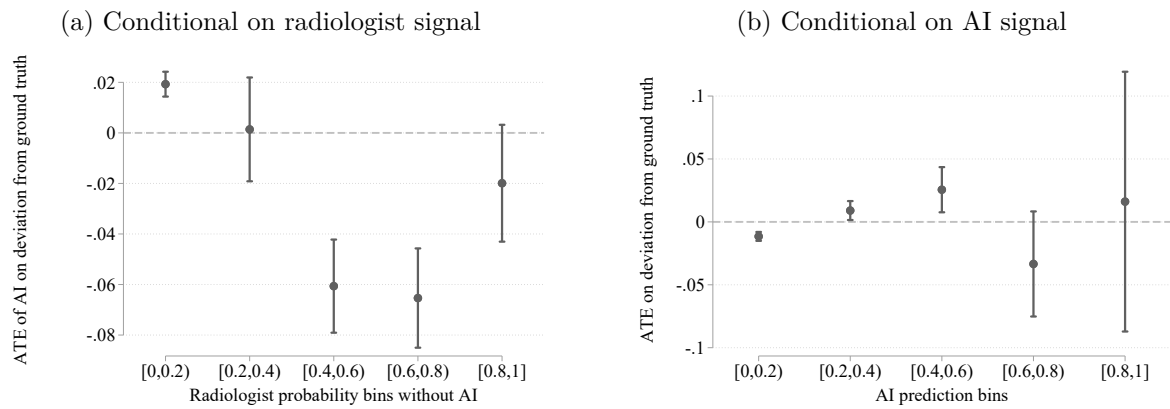
C.4.6 Calibrated radiologist probability

Figure C.30: Comparing AI performance to Radiologists



Note: Main specifications similar to figure 1 with the exception that reported probability of the radiologists is calibrated to the ground truth.

Figure C.31: Deviation from Ground Truth



Note: Main specifications similar to figure 2 and figure 3 with the exception that reported probability of the radiologists is calibrated to the ground truth and there are no separate results for ATE on incorrect decision.

Table C.16: Average Treatment Effects

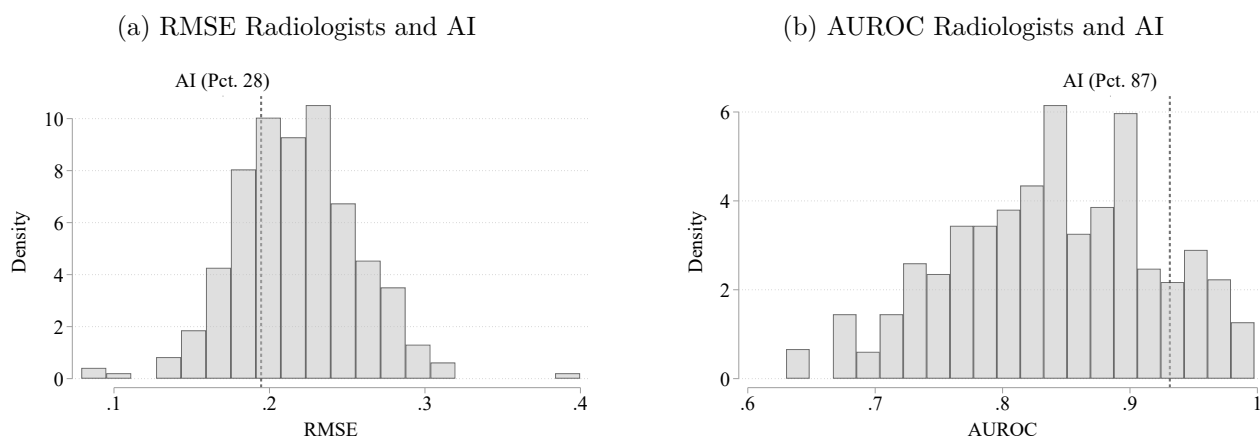
Deviation from GT	
Treatment	(1)
AI × CH	0.000 (0.004)
AI	−0.001 (0.003)
CH	−0.002 (0.003)
CONTROL MEAN	0.184 (0.010)
PATHOLOGY FE	Yes
OBSERVATIONS	36279

Note: Main specifications similar to table 2 with the exception that reported probability of the radiologists is calibrated to the ground truth and hence only the ATE on deviation from ground truth is reported.

C.4.7 All Pathologies and Abnormal with AI

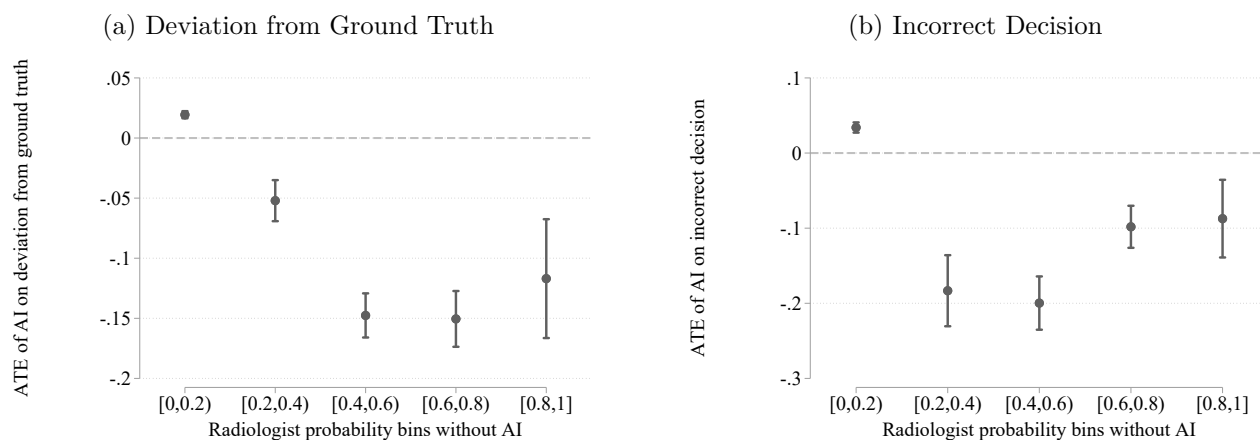
All Pathologies with AI

Figure C.32: Comparing AI performance to Radiologists



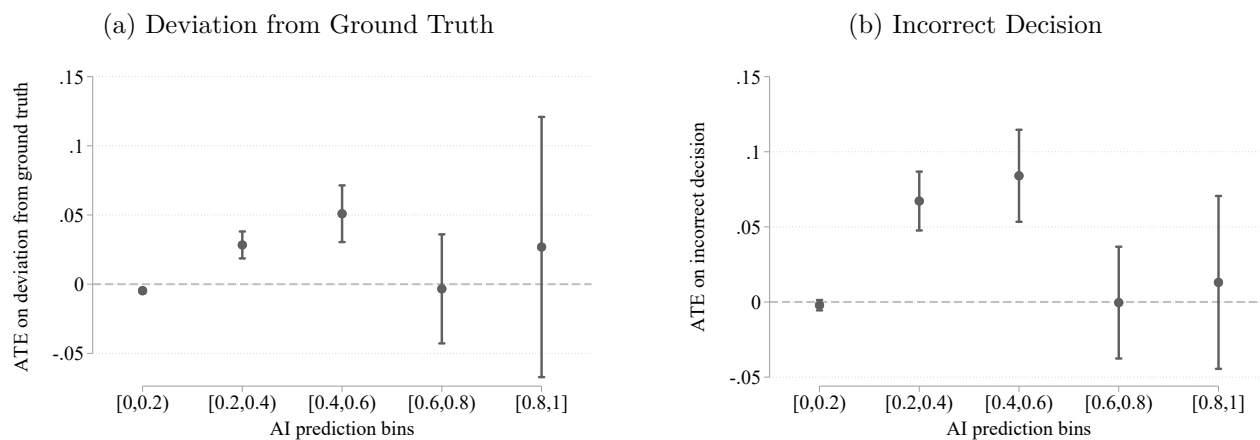
Note: Main specifications similar to figure 1 with the exception that all pathologies with AI are considered.

Figure C.33: Conditional treatment effect given radiologist prediction



Note: Main specifications similar to figure 3 with the exception that all pathologies with AI are considered.

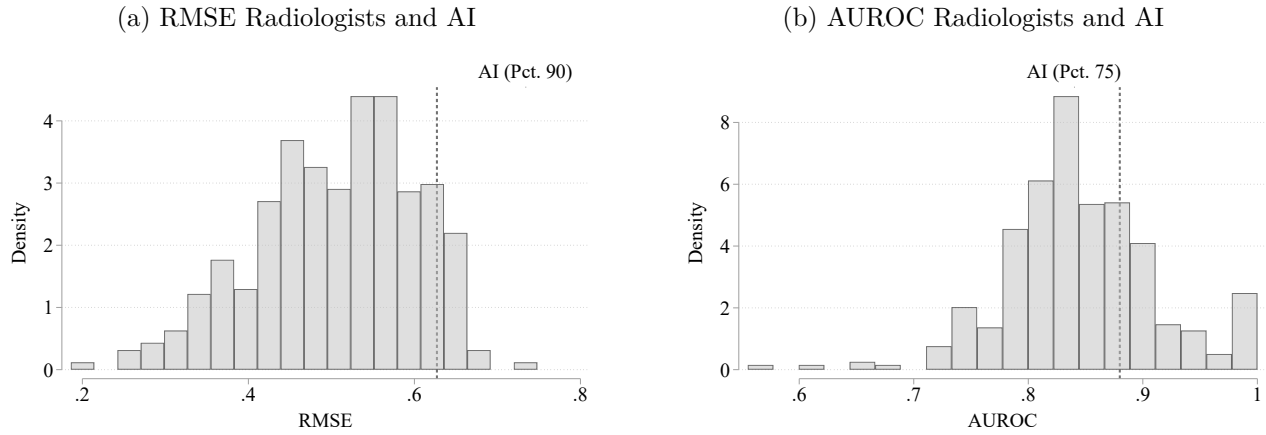
Figure C.34: Conditional treatment effect given AI prediction



Note: Main specifications similar to figure 3 with the exception that all pathologies with AI are considered.

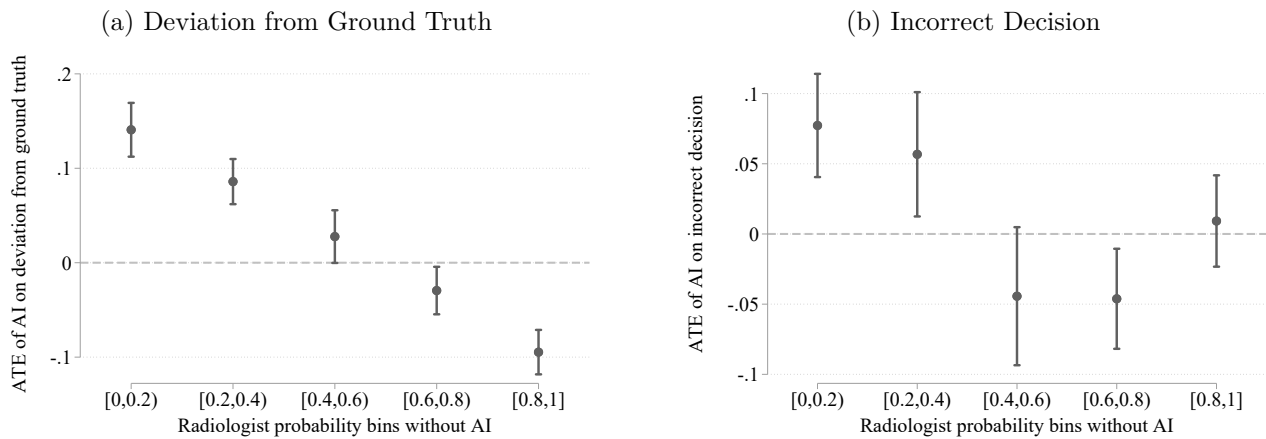
Abnormal

Figure C.35: Comparing AI performance to Radiologists



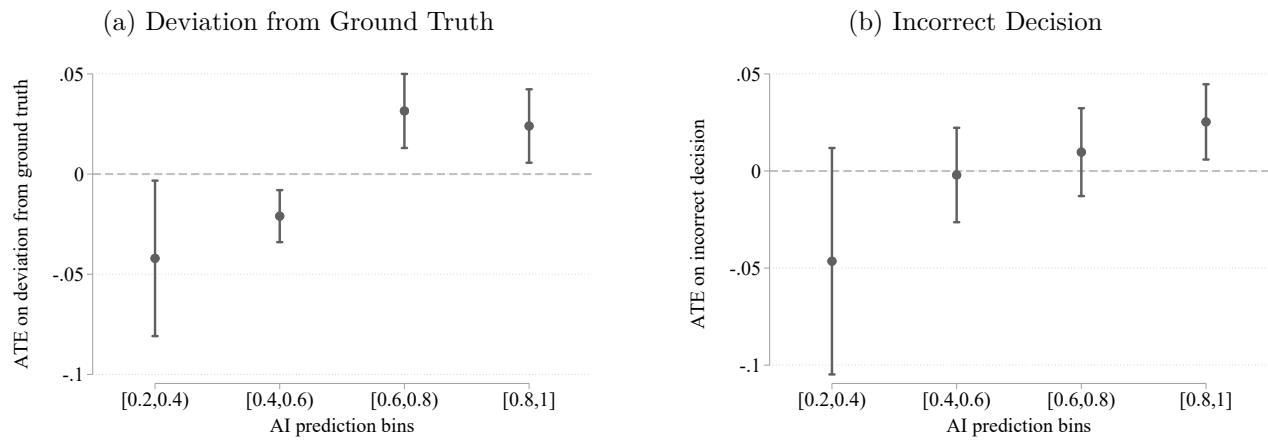
Note: Main specifications similar to figure 1 with the exception that only the abnormal pathology is considered.

Figure C.36: Conditional treatment effect given radiologist prediction



Note: Main specifications similar to figure 3 with the exception that only the abnormal pathology is considered.

Figure C.37: Conditional treatment effect given AI prediction



Note: Main specifications similar to figure 3 with the exception that only the abnormal pathology is considered.

Table C.17: Average Treatment Effects

Treatment	Deviation from AI		Deviation from Ground Truth		
	Pooled with AI	Abnormal	Pooled	Pooled with AI	Abnormal
	(1)	(2)	(3)	(4)	(5)
AI × CH	0.000 (0.001)	0.001 (0.005)	0.001 (0.001)	0.001 (0.002)	0.009 (0.008)
AI	-0.016 (0.001)	-0.054 (0.005)	-0.001 (0.001)	0.001 (0.002)	0.009 (0.007)
CH	-0.000 (0.001)	0.001 (0.004)	-0.001 (0.001)	-0.003 (0.002)	-0.010 (0.006)
CONTROL MEAN	0.108 (0.003)	0.271 (0.010)	0.033 (0.002)	0.085 (0.005)	0.421 (0.013)
PATHOLOGY FE	Yes	No	Yes	Yes	No
OBSERVATIONS	235820	18140	1850280	235820	18140

Note: Main specifications similar to table 2 with the exception that only the abnormal pathology is considered.

C.5 Automation Bias Appendix

C.5.1 Conditional Independence

Table C.18 presents evidence that human and AI signals are not conditionally independent. To test the hypothesis of conditional independence, we regress the human report in the treatment arm without AI assistance on the ground truth, the AI score, and the interaction between ground truth and the AI score. If the signals were conditionally independent, we would observe the AI score to offer no predictive power on the human report after conditioning on the ground truth. As shown in Table C.18 we can reject this null hypothesis.

Table C.18: Test of Conditionally Independent Signals

	Top Level with AI	Pooled with AI	Abnormal
GROUND TRUTH	0.318 (0.042)	0.265 (0.033)	-0.049 (0.078)
AI SCORE	0.536 (0.046)	0.620 (0.035)	0.815 (0.052)
GROUND TRUTH \times AI	-0.244 (0.082)	-0.217 (0.066)	0.205 (0.090)
CONSTANT	0.089 (0.011)	0.044 (0.003)	-0.058 (0.039)
OBSERVATIONS	11420	57100	5710
R-SQUARED	0.260	0.301	0.316

Note: Estimates of a regression of the human report in the treatment without AI assistance on the ground truth interacted with the AI score. Standard errors are two-way clustered at the radiologist and patient case level.

C.5.2 Estimating Bayesian Update Terms

Here, we describe the method we use to estimate the Bayesian benchmark $\pi(\omega_i = 1 | s_{ir}^E, s_i^A)$. This procedure is done separately for each pathology. We train a random forest classifier that predicts the ground truth based on features including the vector of a radiologist’s reported probabilities in the non-AI treatment and the vector of AI predictions. Additional features include radiologist identifiers to allow for heterogeneity in radiologists’ assessments, an indicator equal to one if the case was read with clinical history, and summaries of the patient clinical history. We estimate this quantity for various parameterizations of s_{ir}^E and s_i^A described in Section 5. These are used in the model testing exercise to understand if radiologists account for the joint distribution of signals when forming their posterior beliefs. The hyperparameters of the model are tuned using grouped cross-validation where observations were grouped by patient id to avoid overfitting with five folds. We impose monotonicity constraints on the model to impose that $\pi(\omega_i = 1 | s_{ir}^E, s_i^A)$ is monotonically increasing in all probability inputs. When the model includes clinical history, we provide a summarized patient’s clinical record with their sex, weight, temperature, pulse, age, and the number of available and flagged labs. We mean impute these variables when the radiologist does not have access to the clinical history and include an indicator equal to one if the radiologist had access to the clinical history as an additional feature. Below we summarize the performance of these models and the relative value of increasing the dimension of s_{ir}^E and s_i^A .

Table C.19: Summary of Bayesian Models

		(1)	(2)	(3)	(4)	(5)	(6)	(7)	(8)	(9)	(10)	(11)	(12)
AIRSPACE OPACITY	ACCURACY	0.88	0.91	0.88	0.89	0.90	0.90	0.89	0.90	0.89	0.89	0.91	0.90
	AUC	0.89	0.96	0.91	0.92	0.96	0.96	0.94	0.96	0.93	0.93	0.96	0.96
CARDIOMEDIASTINAL ABNORM.	ACCURACY	0.90	0.92	0.90	0.91	0.93	0.92	0.92	0.92	0.91	0.91	0.93	0.93
	AUC	0.90	0.96	0.91	0.93	0.96	0.96	0.94	0.96	0.94	0.94	0.96	0.96
ABNORMAL	ACCURACY	0.88	0.91	0.88	0.89	0.91	0.91	0.90	0.91	0.90	0.90	0.92	0.91
	AUC	0.91	0.96	0.91	0.93	0.96	0.96	0.95	0.96	0.94	0.94	0.96	0.96
FOCAL s_A		✓	✓	✓	✓	✓	✓	✓	✓	✓	✓	✓	✓
OTHER s_A			✓			✓	✓		✓			✓	✓
FOCAL s_E				✓	✓	✓	✓			✓	✓	✓	✓
OTHER s_E					✓		✓				✓		✓
CLINICAL HISTORY s_E								✓	✓	✓	✓	✓	✓

Note: This table summarizes the models used to estimate the Bayesian benchmark. Each column corresponds to a random forest classification tree with varying signal structures. The rows Focal s^A , Other s^A , Focal s^E , Other s^E , and Clinical History s^E indicate what features are included in the tree. Focal s^A corresponds to the focal pathology's AI score, Other s^A corresponds to vector of AI scores for all pathologies, Focal (Other) s^E includes the radiologist's report without AI assistance on the focal pathology (all pathologies), and Clinical History s^E contains summaries of the patient's clinical history when available to the radiologist.

C.5.3 Model Selection on Additional Pathology Groups

Here, we present the model selection results for the remaining pre-registered pathology groups.

Table C.20: Model Selection: Top Level with AI

	(1)	(2)	(3)	(4)	(5)	(6)	(7)	(8)	(9)	(10)	(11)	(12)
AUTOMATION BIAS (b)	0.29 (0.02)	0.35 (0.03)	0.34 (0.03)	0.31 (0.03)	0.35 (0.03)	0.35 (0.03)	0.19 (0.02)	0.34 (0.03)	0.27 (0.02)	0.25 (0.03)	0.34 (0.03)	0.35 (0.03)
OWN INFO BIAS (d)	1.10 (0.01)	1.06 (0.01)	1.08 (0.01)	1.08 (0.01)	1.06 (0.01)	1.05 (0.01)	1.07 (0.01)	1.06 (0.01)	1.06 (0.01)	1.07 (0.01)	1.06 (0.01)	1.05 (0.01)
CONSTANT	0.40 (0.03)	0.37 (0.04)	0.40 (0.04)	0.38 (0.04)	0.37 (0.04)	0.37 (0.04)	0.31 (0.03)	0.38 (0.04)	0.33 (0.03)	0.34 (0.04)	0.37 (0.04)	0.36 (0.04)
FOCAL s_A	✓	✓	✓	✓	✓	✓	✓	✓	✓	✓	✓	✓
OTHER s_A		✓			✓	✓		✓			✓	✓
FOCAL s_E			✓	✓	✓	✓			✓	✓	✓	✓
OTHER s_E				✓		✓				✓		✓
CLINICAL HISTORY s_E							✓	✓	✓	✓	✓	✓
J-STATISTIC	18.23	0.03	16.86	10.45	0.14	0.17	4.3	0.02	10.7	6.13	0.06	0.09
MMSC-BIC	-23.96	-8.41	-21.12	-10.64	-8.3	-8.27	-12.57	-8.42	-10.39	-10.75	-8.38	-8.35
NUMBER OF MOMENTS	13	5	12	8	5	5	7	5	8	7	5	5
Observations	11420	11420	11420	11420	11420	11420	11420	11420	11420	11420	11420	11420
R-SQUARED	0.50	0.52	0.49	0.49	0.52	0.52	0.46	0.51	0.48	0.46	0.52	0.52

Note: This table presents results of the model selection exercise as described in Table 3, including the full set of models that were included in the selection procedure.

Table C.21: Model Selection: Pooled with AI

	(1)	(2)	(3)	(4)	(5)	(6)	(7)	(8)	(9)	(10)	(11)	(12)
AUTOMATION BIAS (b)	0.16 (0.01)	0.09 (0.01)	0.17 (0.02)	0.14 (0.02)	0.10 (0.01)	0.10 (0.01)	0.12 (0.01)	0.10 (0.01)	0.13 (0.02)	0.14 (0.02)	0.10 (0.01)	0.10 (0.01)
OWN INFO BIAS (d)	1.12 (0.01)	1.10 (0.01)	1.12 (0.01)	1.12 (0.01)	1.10 (0.01)	1.10 (0.01)	1.11 (0.01)	1.10 (0.01)	1.11 (0.01)	1.12 (0.01)	1.10 (0.01)	1.10 (0.01)
CONSTANT	0.37 (0.04)	0.31 (0.04)	0.36 (0.04)	0.37 (0.04)	0.31 (0.04)	0.31 (0.04)	0.34 (0.04)	0.31 (0.04)	0.34 (0.04)	0.36 (0.04)	0.31 (0.04)	0.31 (0.04)
FOCAL s_A	✓	✓	✓	✓	✓	✓	✓	✓	✓	✓	✓	✓
OTHER s_A		✓			✓	✓		✓			✓	✓
FOCAL s_E			✓	✓	✓	✓			✓	✓	✓	✓
OTHER s_E				✓		✓				✓		✓
CLINICAL HISTORY s_E							✓	✓	✓	✓	✓	✓
J-STATISTIC	12.52	3.85	10.53	4.81	2.03	2.71	4.64	3.84	3.98	5.2	2.44	2.4
MMSC-BIC	-12.79	-13.03	-10.57	-12.07	-14.85	-14.17	-12.24	-13.03	-12.9	-11.68	-14.43	-14.48
NUMBER OF MOMENTS	9	7	8	7	7	7	7	7	7	7	7	7
Observations	57100	57100	57100	57100	57100	57100	57100	57100	57100	57100	57100	57100
R-SQUARED	0.45	0.42	0.44	0.43	0.42	0.42	0.43	0.42	0.43	0.43	0.42	0.42

Note: This table presents results of the model selection exercise as described in Table 3, though this table only includes all pathologies with AI assistance.

Table C.22: Model Selection: Abnormal

	(1)	(2)	(3)	(4)	(5)	(6)	(7)	(8)	(9)	(10)	(11)	(12)
AUTOMATION BIAS (b)	0.11 (0.03)	0.06 (0.02)	0.10 (0.03)	0.11 (0.03)	0.06 (0.02)	0.06 (0.02)	0.08 (0.02)	0.06 (0.02)	0.08 (0.03)	0.08 (0.03)	0.06 (0.02)	0.06 (0.02)
OWN INFO BIAS (d)	1.06 (0.02)	1.07 (0.02)	1.06 (0.02)	1.07 (0.02)	1.07 (0.02)	1.07 (0.02)	1.06 (0.02)	1.07 (0.02)	1.06 (0.02)	1.07 (0.02)	1.07 (0.02)	1.07 (0.02)
CONSTANT	0.38 (0.07)	0.29 (0.06)	0.36 (0.07)	0.39 (0.07)	0.30 (0.06)	0.29 (0.06)	0.34 (0.06)	0.29 (0.06)	0.34 (0.07)	0.34 (0.07)	0.29 (0.06)	0.29 (0.06)
FOCAL s_A	✓	✓	✓	✓	✓	✓	✓	✓	✓	✓	✓	✓
OTHER s_A		✓			✓	✓		✓			✓	✓
FOCAL s_E			✓	✓	✓	✓			✓	✓	✓	✓
OTHER s_E				✓		✓				✓		✓
CLINICAL HISTORY s_E							✓	✓	✓	✓	✓	✓
J-STATISTIC	12.65	15.83	13.55	12.74	15.0	15.43	15.8	15.95	16.19	14.87	15.78	15.41
MMSC-BIC	-25.33	-22.14	-24.43	-25.24	-22.98	-22.54	-22.17	-22.03	-21.78	-23.1	-22.2	-22.56
NUMBER OF MOMENTS	12	12	12	12	12	12	12	12	12	12	12	12
Observations	5710	5710	5710	5710	5710	5710	5710	5710	5710	5710	5710	5710
R-SQUARED	0.37	0.32	0.34	0.35	0.32	0.32	0.34	0.32	0.33	0.33	0.32	0.32

Note: This table presents results of the model selection exercise as described in Table 3, though this table only includes Abnormal.

C.5.4 Model Selection Without Adjusting for Measurement Error

This section presents the results of the model selection exercise not accounting for measurement error in the human signal. In these analyses, the instruments are constructed using the radiologist's report on the case in the treatment arm without AI assistance. Note that some time elapses between the reads, so the radiologist likely observes a different draw of s_E introducing measurement error into the right-hand side variables of equation 7. This is why the preferred method uses instruments constructed using a leave-one-out average of reports for the case. Table C.23 presents results for top-level pathologies with AI, Table C.24 presents results for all pathologies with AI, and Table C.25 presents results for abnormal.

Table C.23: Model Selection: Top Level with AI without Accounting for Measurement Error

	(1)	(2)	(3)	(4)	(5)	(6)	(7)	(8)	(9)	(10)	(11)	(12)
AUTOMATION BIAS (b)	0.49 (0.02)	0.37 (0.02)	0.56 (0.03)	0.53 (0.03)	0.37 (0.02)	0.38 (0.02)	0.42 (0.02)	0.37 (0.02)	0.48 (0.03)	0.52 (0.02)	0.36 (0.02)	0.38 (0.02)
OWN INFO BIAS (d)	1.00 (0.02)	0.89 (0.02)	0.95 (0.02)	0.95 (0.02)	0.90 (0.02)	0.90 (0.02)	0.93 (0.02)	0.90 (0.02)	0.91 (0.02)	0.94 (0.02)	0.90 (0.02)	0.89 (0.02)
CONSTANT	0.32 (0.04)	0.13 (0.04)	0.29 (0.04)	0.31 (0.04)	0.12 (0.04)	0.13 (0.04)	0.21 (0.04)	0.14 (0.04)	0.20 (0.04)	0.27 (0.04)	0.14 (0.04)	0.12 (0.04)
FOCAL s_A	✓	✓	✓	✓	✓	✓	✓	✓	✓	✓	✓	✓
OTHER s_A		✓			✓	✓		✓			✓	✓
FOCAL s_E			✓	✓	✓	✓			✓	✓	✓	✓
OTHER s_E				✓		✓				✓		✓
CLINICAL HISTORY s_E							✓	✓	✓	✓	✓	✓
J-STATISTIC	3.47	1.06	2.04	2.94	4.6	1.98	0.01	1.75	0.0	3.7	9.19	0.0
MMSC-BIC	-4.97	-7.38	-2.18	-1.28	-3.84	-6.46	-4.21	-10.91	0.0	-0.52	-7.69	0.0
NUMBER OF MOMENTS	5	5	4	4	5	5	4	6	3	4	7	3
Observations	11420	11420	11420	11420	11420	11420	11420	11420	11420	11420	11420	11420
R-SQUARED	0.58	0.55	0.56	0.56	0.55	0.55	0.56	0.55	0.56	0.56	0.55	0.55

Note: This table presents results of the model selection exercise as described in Table 3 for top-level pathologies with AI assistance without accounting for measurement error in the radiologist reports.

Table C.24: Model Selection: Pooled with AI without Accounting for Measurement Error

	(1)	(2)	(3)	(4)	(5)	(6)	(7)	(8)	(9)	(10)	(11)	(12)
AUTOMATION BIAS (b)	0.45 (0.02)	0.35 (0.01)	0.45 (0.02)	0.46 (0.02)	0.36 (0.01)	0.35 (0.01)	0.39 (0.02)	0.35 (0.01)	0.41 (0.02)	0.45 (0.02)	0.36 (0.01)	0.35 (0.01)
OWN INFO BIAS (d)	1.01 (0.01)	0.93 (0.01)	0.97 (0.01)	0.98 (0.01)	0.93 (0.01)	0.94 (0.01)	0.96 (0.01)	0.93 (0.01)	0.95 (0.01)	0.97 (0.01)	0.94 (0.01)	0.93 (0.01)
CONSTANT	0.21 (0.04)	0.00 (0.04)	0.10 (0.04)	0.14 (0.04)	-0.01 (0.04)	0.01 (0.04)	0.07 (0.04)	0.00 (0.04)	0.04 (0.04)	0.12 (0.04)	0.01 (0.04)	-0.01 (0.04)
FOCAL s_A	✓	✓	✓	✓	✓	✓	✓	✓	✓	✓	✓	✓
OTHER s_A		✓			✓	✓		✓			✓	✓
FOCAL s_E			✓	✓	✓	✓			✓	✓	✓	✓
OTHER s_E				✓		✓				✓		✓
CLINICAL HISTORY s_E							✓	✓	✓	✓	✓	✓
J-STATISTIC	11.7	0.0	0.0	1.18	4.21	7.31	0.0	8.13	0.0	0.0	2.85	8.57
MMSC-BIC	-13.62	0.0	0.0	-3.04	-12.67	-9.57	0.0	-8.75	0.0	0.0	-18.25	-8.31
NUMBER OF MOMENTS	9	3	3	4	7	7	3	7	3	3	8	7
Observations	57100	57100	57100	57100	57100	57100	57100	57100	57100	57100	57100	57100
R-SQUARED	0.58	0.56	0.56	0.56	0.56	0.56	0.57	0.56	0.56	0.56	0.56	0.56

Note: This table presents results of the model selection exercise as described in Table 3 for all pathologies with AI assistance without accounting for measurement error in the radiologist reports.

Table C.25: Model Selection: Abnormal without Accounting for Measurement Error

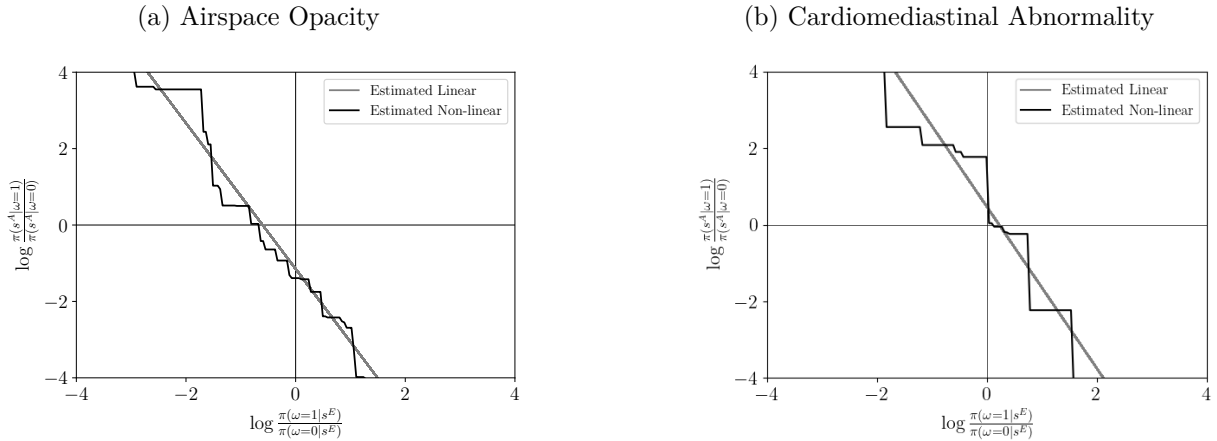
	(1)	(2)	(3)	(4)	(5)	(6)	(7)	(8)	(9)	(10)	(11)	(12)
AUTOMATION BIAS (b)	0.47 (0.02)	0.35 (0.02)	0.44 (0.03)	0.42 (0.02)	0.37 (0.02)	0.37 (0.02)	0.36 (0.02)	0.36 (0.02)	0.36 (0.02)	0.41 (0.02)	0.37 (0.02)	0.36 (0.02)
OWN INFO BIAS (d)	0.92 (0.02)	0.89 (0.02)	0.86 (0.02)	0.90 (0.02)	0.88 (0.02)	0.88 (0.02)	0.85 (0.02)	0.88 (0.02)	0.82 (0.02)	0.87 (0.02)	0.87 (0.02)	0.88 (0.02)
CONSTANT	1.23 (0.07)	0.98 (0.06)	1.16 (0.08)	1.12 (0.07)	1.02 (0.06)	1.05 (0.06)	0.99 (0.06)	1.04 (0.06)	1.01 (0.07)	1.11 (0.07)	1.05 (0.07)	1.00 (0.06)
FOCAL s_A	✓	✓	✓	✓	✓	✓	✓	✓	✓	✓	✓	✓
OTHER s_A		✓			✓	✓		✓			✓	✓
FOCAL s_E			✓	✓	✓	✓			✓	✓	✓	✓
OTHER s_E				✓		✓				✓		✓
CLINICAL HISTORY s_E							✓	✓	✓	✓	✓	✓
J-STATISTIC	12.09	7.1	0.35	4.71	3.06	4.94	0.0	5.79	0.0	0.34	0.0	4.85
MMSC-BIC	-13.23	-5.56	-3.87	-3.73	-1.16	-3.5	0.0	-2.65	0.0	-3.88	0.0	-3.59
NUMBER OF MOMENTS	9	6	4	5	4	5	3	5	3	4	3	5
Observations	5710	5710	5710	5710	5710	5710	5710	5710	5710	5710	5710	5710
R-SQUARED	0.56	0.54	0.53	0.54	0.54	0.54	0.54	0.54	0.53	0.53	0.54	0.54

Note: This table presents results of the model selection exercise as described in Table 3 for abnormal without accounting for measurement error in the radiologist reports.

C.5.5 Linearity of the Update Model

To assess the appropriateness of linear relationship in the model of radiologist updating with AI we estimate non-parametric versions of the model and plot the empirical analog of Figure 5 along with the joint distribution of signals. To do so, we estimate a boosted tree that estimates the radiologist’s reported $\frac{pr(\omega_i=1|s_{ir}^A, s_{ir}^E)}{pr(\omega_i=0|s_{ir}^A, s_{ir}^E)}$ as a non-parametric function of a constant, the update term, and the reported probability without AI assistance. We impose monotonicity constraints on the update term and the reported probability without AI. We then plot the frontier in which radiologists are indifferent between following up on the case-pathology and not following up. We compare this frontier to the cutoff frontier of a Bayesian decision maker, the radiologist without AI assistance, and the radiologist with AI assistance under the linear model.

Figure C.38: Empirical analog of figure 5



Note: For the two top-level pathologies with AI assistance, we plot estimates of the indifference frontier where radiologists are indifferent between following up on a patient-case and not following up on a patient-case for a Bayesian decision maker, the linear model estimated in equation 7, a non-parametric version of equation 7, and the human only without AI assistance. In addition, we plot the joint distribution of the signals log-likelihoods.

C.5.6 Individual Heterogeneity

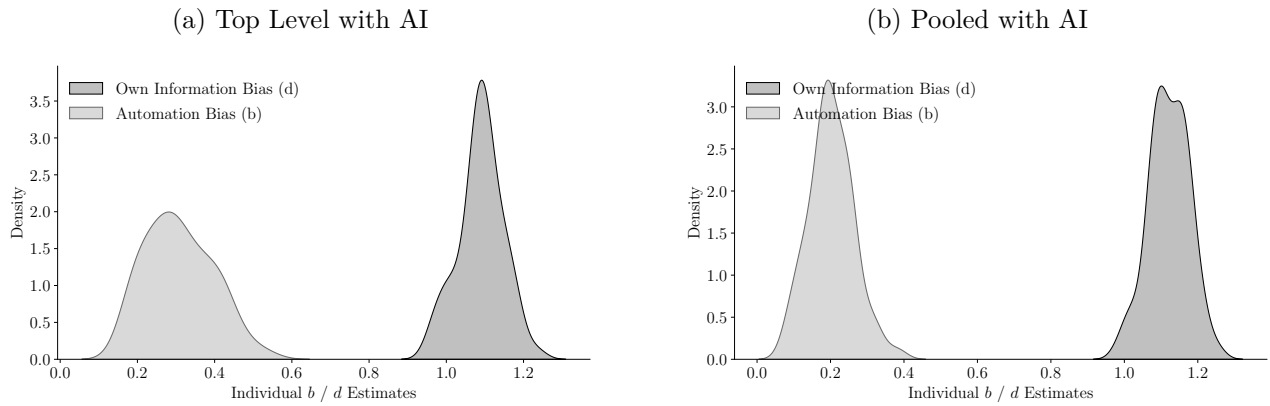
Here we show the distribution of individual estimates of equation (7). Each estimate contains sampling error, as each radiologist is only reading a subset of cases. Therefore, the unadjusted distribution of individual-level estimates is overdispersed as it is a convolution of the true individual-level parameters and the sampling noise. We adjust for this over-dispersion using

a Bayesian hierarchical model, where we model the individual parameter vector θ_r as follows.

$$\begin{aligned}\theta_r &\sim N(\mu, \Sigma) \\ \mu &\sim N(0, 100I) \\ \Sigma &= \text{diag}(\tau) \Omega \text{diag}(\tau) \\ \tau_k &\sim \text{Cauchy}(0, 2.5) \\ \Omega &\sim \text{LKJCorr}(10)\end{aligned}$$

We sample from the posterior of this model and plot the marginal distribution of the posterior means of θ_r below.

Figure C.39: Individual Heterogeneity in b and d



Note: Marginal distributions of individual b and d estimates by radiologist for top level pathologies with AI and all pathologies with AI.

C.6 Preference Estimation

In the experiment we elicit both probability assessment and treatment decisions, allowing us to identify the relative costs of false positives and false negatives the radiologists are using. Recall that radiologist r chooses to treat or follow-up on pathology p in patient case i under treatment t if $a_{ritp} = 1$ where a_{ritp} is given by

$$a_{ritp} = 1 \left[\frac{p_{ritp}}{1 - p_{ritp}} - c_{rel}^{rp} + \varepsilon_{ritp} > 0 \right]$$

where p_{ritp} is the radiologist's probability assessment, c_{rel}^{rp} is the relative cost of false positives and false negatives for radiologist r and pathology p , and ε_{ritp} captures unobserved preference heterogeneity. If ε_{ritp} follows a Logistic distribution, we can estimate c_{rel}^{rp} through a logistic

regression. We impose a low-dimensional structure on c_{rel}^{rp} to improve statistical precision and estimate the following logistic regression

$$\log \frac{P(a_{ritp} = 1)}{1 - P(a_{ritp} = 1)} = \beta_0 + \beta \log \frac{p_{ritp}}{1 - p_{ritp}} + \alpha_p + \gamma_r \quad (9)$$

where α_p are pathology fixed effects and γ_r are radiologist fixed effects. The relative costs of false positives to false negatives for radiologist r and pathology p can then be found as $c_{rel}^{rp} = \exp \left[-\frac{\beta_0 + \gamma_r + \alpha_p}{\beta} \right]$. For each pathology, we winsorize radiologists' relative costs at the 5th and 95th percentile. The results of this exercise are presented in Table C.26.

Table C.26: Preference Estimates

	Mean	Std	Min	25%	50%	75%	Max
All	3.926	5.754	0.233	0.655	1.521	4.040	22.336
Top (with AI)	1.228	1.669	0.149	0.266	0.482	1.259	6.362
AI	2.261	3.312	0.184	0.379	0.867	2.307	13.045
Abnormal	2.459	3.326	0.344	0.537	1.016	2.551	12.604

Note: Distribution of c_{rel}^{rp} for each of the four pre-registered pathology groups calculated from the estimates of equation 9. The distribution of c_{rel}^{rp} is winsorized for each pathology at the 5th and 95th percentile.